

Fracture Behaviour of Hybrid Synthetic Fiber Reinforced Concrete

JAMES JOSE
CE14MTECH11003

A Dissertation Submitted to
Indian Institute of Technology Hyderabad
In Partial Fulfilment of the Requirements for
The Degree of Master of Technology



भारतीय प्रौद्योगिकी संस्थान हैदराबाद
Indian Institute of Technology Hyderabad

Department of Civil Engineering
Indian Institute of Technology Hyderabad

July, 2016

Declaration

I declare that this written submission represents my ideas in my own words, and where other's ideas or words have been included, I have adequately cited and referenced the original sources. I also declare that I have adhered to all principles of academic honesty and integrity and have not misrepresented or fabricated or falsified any idea/data/fact/source in my submission. I understand that any violation of the above will be a cause for disciplinary action by the Institute and can also evoke penal action from the sources that have thus not been properly cited, or from whom proper permission has not been taken when needed.



JAMES JOSE
CE14MTECH11003

Approval Sheet

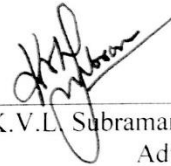
This thesis entitled **Fracture Behaviour of Hybrid Synthetic Fiber Reinforced Concrete** by James Jose is approved for the degree of Master of Technology from IIT Hyderabad.



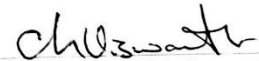
Dr. Anil Agarwal
Examiner



Dr. S. Suriya Prakash
Examiner



Prof K.V.L. Subramaniam
Adviser



Dr. Vishwanath Chinthapenta
Chairman

Acknowledgements

I am thankful to all the people who have guided and supported me throughout my thesis work. First of all, I would like to convey my gratitude to my advisor, Dr. K.V.L.Subramaniam for giving me a chance to work in such an interesting field and believing in me during the research work. I also thank him for his excellent guidance and all time valuable support and encouragement. His suggestions during the three stages of my research, i.e. experimental, analytical and numerical work, have contributed to my knowledge and have vastly improved the quality of this thesis.

I would like to extend my gratitude to my committee members who have made interesting and useful remarks during my thesis work. I wish to thank Dr. S.Suriya Prakash for his feedback on my experiments. I extend my special gratitude to my fellow students, Jayakrishnan Rajendran, K. Chiranjeevi Reddy, G. Sahith Reddy, for their guidance and help in conducting experiments.

Finally, I would like to share this happiness with my parents who rendered me enormous support during the whole tenure of my stay at IIT, Hyderabad. I am also thankful to my IIT Hyderabad friends for the warmth of their friendship and providing a supportive environment, which has made my stay at IIT Hyderabad wonderful. I sincerely acknowledge some of my close friends Dilin Sharaf, Vibin Varghese, Smrithi Hareendran for their role as tension healers and as rich sources of entertainment.

ABSTRACT

Fibers have been used as discrete randomly distributed reinforcement to strengthen a material weak in tension. A concrete beam containing fibers suffers damage by gradual development of single or multiple cracks with increasing deflection, but retains some degree of structural integrity and post-crack resistance even under considerable deflection. A composite can be termed as *hybrid*, if two or more types of fibers are rationally combined to produce a composite that derives benefits from each of the individual fibers and exhibits a synergetic response. In this study, macro polypropylene fibers with micro Polypropylene fibers are been used. Flexural tests are done for Hybrid Synthetic Fiber Reinforced concrete (HFRC) and are compared with Synthetic Fiber Reinforced Concrete (SFRC) of the same fiber volume fraction. It was found that HFRC retains the same toughness as SFRC when the concrete is mature and a better toughness at early age. The strain distribution information obtained from the DIC is used to study the crack growth in the beams. Crack bridging stresses contributed by hybrid-synthetic fibers are determined.

Nomenclature

P₁	First peak load
P_u	Peak load in load deflection response
δ_u	Deflection corresponding to P _u
P_{crit}	Load corresponding to immediate lowest point after peak load
δ_u	Deflection corresponding to P _{crit}
δ_p	Net deflection at peak
δ₁	first-peak loads
F_p	Peak Strength
f₁	First-Peak Strength
P_{D600}	Residual load at net deflection of L/600
f_{D600}	Residual Strength at net deflection of L/600
P_{D150}	Residual load at net deflection of L/150
f_{D150}	Residual Strength at net deflection of L/150
T_{D150}	Area under the load vs. net deflection curve 0 to L/150
R_{T,D150}	Equivalent flexural strength
T_{JSCE}	Toughness
F_{JSCE}	Toughness factor
CMOD	Crack mouth opening displacement
LOP	Limit of proportionality
F_L	load corresponding to LOP
f_{ct,Lf}	Strength corresponding to LOP
F_i	load corresponding to with CMOD = CMOD _j or δ = δ _i (i = 1,2,3,4)
f_{R,j}	Residual flexural Tensile Strength corresponding with CMOD = CMOD _j where (i= 1.5, 2.5, 3.5, 4.5)
CTOD	Crack Tip opening displacement
P_f	First crack load
f_f	First crack strength
SFRC	Synthetic Fiber Reinforced Concrete.
HFRC	Hybrid Fiber Reinforced Concrete.
P	Macro Polypropylene
p	Micro Polypropylene

Table of Contents

List of figures	ix
List of Tables.....	xii
Chapter 1 Introduction.....	1
1.1 General.....	1
1.1 Objectives.....	2
1.3 Scope.....	3
Chapter 2 Review of Standard test methods and Literature.....	4
2.1 Introduction.....	4
2.1.1 Steel Fibers.....	6
2.1.2 Polypropylene Fibers.....	7
2.1.3 Macro-synthetic Polypropylene fiber.....	8
2.2 Hybrid Fiber Reinforced Concrete.....	11
2.3 Standard Test Methods.....	18
2.3.1 ASTM 1609 test procedure.....	18
2.3.2 ASTM 1018 test procedure.....	20
2.3.3 JSCE SF24.....	21
2.3.4 RILEM TC 162 - Test Procedure.....	22
2.3.5 UNI 11039-2 Test Procedure.....	22
2.3.6 EN 14651 Test Procedure.....	24
Chapter 3 Materials and Methods.....	26
3.1 Introduction.....	26
3.1.1 Cement.....	26
3.1.2 Fly Ash.....	26
3.1.3 Aggregates.....	26
3.1.4 Synthetic Fibers.....	26
3.1.5 Admixture.....	26
3.2 Experimental program and Mix Proportions.....	27
3.2.1 Casting and Curing of Specimens.....	28
3.3 Test Methods.....	28
3.3.1 Slump.....	28
3.3.2 Compression Strength Testing.....	29
3.3.3 Four-point-bending test.....	29

3.3.4 Three-point-bending test (For notch beam).....	30
Chapter 4 Result and Discussiona.....	32
4.1 Introduction	32
4.2 Compressive strength	32
4.3 Flexural Testing as per ASTM C1609 (Unnotched Beams)	33
4.3.1 Later Age Results.....	33
4.3.2 Early Age Results.....	37
4.4 Flexure Testing on Notched Specimens (EN 14651).....	39
4.3.1 Later Age Results.....	39
4.3.2 Early Age Results.....	43
4.5 Analysis of Data	45
4.6 Summary of Findings	54
Chapter 5 Digital Image Correlation Results.....	55
5.1 Introduction	55
5.2 Background	55
5.3 Results	56
5.4 Analysis of Results.....	71
5.5 Summary and Findings	72
Chapter 6 Analytical Model.....	73
6.1 Introduction	73
6.2 Load deflection curve from moment curvature analysis	75
6.3 Proposed Analytical Formulation for multi-linear softening.....	76
6.4 Inverse analysis	78
Chapter 7 Summary of findings and Future Works	85
References	86

List of figures

Fig 2.1.1 The composite stress-strain curves for fiber-reinforced brittle matrix.....	5
Fig 2.1.2 Strain hardening response of polypropylene fiber composites.....	6
Fig 2.1.3 Fig 2.1.2 Strain hardening response of polypropylene fiber composites.....	7
Fig 2.1.4 Various types of synthetic fibers tested in the present study.....	9
Fig 2.1.5 Comparison of absorbed energies from pullout tests for various fiber types.....	9
Fig 2.1.6 Load–deflection curves for HE 60 at 30, 40 and 50 kg/m ³ dosage rates and for S4.6 and S 5.3 at 4.6 and 5.3 kg/m ³ dosage rates	10
Fig 2.2.1 Comparison on Flexural behaviour of different HFRCs.....	13
Fig 2.2.2 Load Deflection graph for different mixes.....	14
Fig 2.2.3 Comparison of various HFRCs.....	14
Fig 2.2.4 Stress versus midpoint displacement for different mixes and Stress at first crack for various mixes.....	15
Fig 2.2.5 Toughness determined for small (0.4mm) and large (2mm) deformation.....	15
Fig 2.2.6 Average age at which cracks were first observed and average total crack width at 44 days.....	16
Fig 2.2.7 Comparison of Stress vs Deflection for different HFRCs.....	16
Fig 2.2.8 Comparison of Stress vs Deflection for different HFRCs.....	17
Fig 2.2.9 Comparison of Stress vs Deflection for different HFRCs.....	18
Fig 2.3.1 Diagrammatic View of a Suitable Apparatus for Flexure Test of Concrete by Third-Point Loading Method.....	19
Fig 2.3.2 Example of Parameter Calculations.....	19
Fig 2.3.3 Important Characteristics of the Load-Deflection Curve.....	20
Fig 2.3.4 Definition of Toughness Indices for Elastic-Plastic Material Behaviour.....	21
Fig 2.3.5 Definitions of JSCE Toughness and Toughness Factor	22
Fig 2.3.6 Schematic diagram of the UNI 11309 four-point bending test setup	23
Fig 2.3.7(a) Basic concrete load-CTOD, (b) Load–CTOD	24
Fig 2.3.8 Typical arrangement of measuring CMOD	25
Fig 2.3.9 Load-CMOD and F_j ($j=1.5, 2.5, 3.5, 4.5$).....	26
Fig 3.1.1 FibreTuff™ Monofilament structural polypropylene fiber	27
Fig 3.2 Fibrillated micro polypropylene fiber.....	28
Fig 4.3.1 Load vs Displacement curve for Control and fiber reinforced concrete at different fiber volume fractions.....	34
Fig 4.3.22 Failure of beam (a) Control specimen (b) SPFRC specimen (c) Crack Opening...34	
Fig 4.3.3 Load vs Displacement curve for Hybrid fiber Reinforced concrete on adding 0.2 % and 0.3 % Micro Polypropylene to different Macro fibre volume fractions (a) 0.44 % P (b) 0.66 % P (c) 0.88 % P	34
Fig 4.3.4 Comparison of Load vs Displacement curve for SPFRC and HyFRC (a) 0.66 % (b) 0.88%	37

Fig 4.3.5 Comparison of Load vs Displacement curve for SPFRC and HFRC at 0.66 % volume fraction of fibers (a) 3 days (b) 7 days	38
Fig 4.3.6 Comparison of Load vs Displacement curve at 3, 7, 28 days (a) HFRC (b) SFRC..	39
Fig 4.4.1 Load vs CMOD curve for Control and Synthetic fiber reinforced concrete at different fiber volume fractions	40
Fig 4.4.2 Load vs CMOD curve for Hybrid fiber Reinforced concrete on adding 0.2 % and 0.3 % Micro Polypropylene to different Macro fiber volume fractions (a) 0.44 % P (b) 0.66 % P (c) 0.88 % P	42
Fig 4.4.3 Comparison of Load vs Displacement curve for SPFRC and HyFRC (a) 0.66 % (b) 0.88%	43
Fig 4.4.4 Comparison of Load vs Displacement curve for SPFRC and HFRC at 0.66 % volume fraction of fibers (a) 3 days (b) 7 days	44
Fig 4.4.5 Comparison of Load vs CMOD curve at 3, 7, 28 days (a) HFRC (b) SFRC	45
Fig 4.5.1 Residual Strength for HFRC as per ASTM C 1609 at L/600	45
Fig 4.5.2 Residual Strength for HFRC as per ASTM C 1609 at L/150	46
Fig 4.5.3 Equivalent Flexural strength Ratio for HFRC as per ASTM C 1609	46
Fig 4.5.4 Toughness factor for HFRC as per JSCE 1609	47
Fig 4.5.5 Residual Strength as per ASTM C 1609 (a) L/600 (b) L/150	47
Fig 4.5.6 (a) Equivalent Flexural strength Ratio as per ASTM C 1609 (b) Toughness factor as per JSCE 1609	48
Fig 4.5.7 Residual Strength as per ASTM C 1609 at 3 days (a) L/600 (b) L/150	48
Fig 4.5.8 (a) Equivalent Flexural strength Ratio as per ASTM C 1609 at 3 days (b) Toughness factor as per JSCE 1609	49
Fig 4.5.9 Residual Strength as per ASTM C 1609 at 7 days (a) L/600 (b) L/150	49
Fig 4.5.10 (a) Equivalent Flexural strength Ratio as per ASTM C 1609 at 7 days (b) Toughness factor as per JSCE 1609	49
Fig 4.5.11 Comparison of Toughness factor at different ages	50
Fig 4.5.12 Residual Flexural Strength of FRC as per EN14651 on adding 0.2 % and 0.3 % Micro fibers to a) 0.44 % P b) 0.66% P c) 0.88% P	51
Fig 4.5.13 Residual Flexural Strength of FRC as per EN14651 for 0.66 % Volume fraction of fiber	52
Fig 4.5.14 Residual Flexural Strength of FRC as per EN14651 for 0.66 % Volume fraction of fiber at a) 3 days b) 7days	53
Fig 4.5.15 Residual Flexural Strength of SFRC as per EN14651 at different ages	53

Fig 5. 1: (a) Load-CMOD of plot of HFRC specimen with 0.88 % Macro Polypropylene with 0.2 % Micro Polypropylene fibers. The CMOD measured during the test is also shown in the Figure; (b) ϵ_{xx} at 3.5 kN (pre-peak); (c) ϵ_{xx} at 8.25 kN (prepeak); (d) ϵ_{xx} at 14 (Peak); (e) ϵ_{xx} at 13.07 kN (postpeak); (f) ϵ_{xx} at 11.6 kN (postpeak); and (g) ϵ_{xx} at 9.6 kN (postpeak)	57
Fig 5.2 Horizontal strips for strain computations	58
Fig 5.3: (a) Typical load response of 0.44 P +0.2 %p; (b) displacement profile at line 1; (c) strain profile at line 1 at distinct load points	59
Fig 5.4: (a) Typical load response of 0.44 P +0.3 %p; (b) displacement profile at line 1; (c) strain profile at line 1 at distinct load points	60

Fig 5.5: (a) Typical load response of 0.6 P +0.3 %p fibers (b) displacement profile at line 1; (c) strain profile at line 1 at distinct load points	61
Fig 5.6: (a) Typical load response of 0.88 P +0.2 %p (b) displacement profile at line 1; (c) strain profile at line 1 at distinct load points.....	62
Fig 5.7: (a) Typical load response of 0.44 P +0.2 %p (3day); (b) displacement profile at line 1; (c) strain profile at line 1 at distinct load points	63
Fig 5.8: (a) Typical load response of 0.66P (3day) (b) displacement profile at line 1; (c) strain profile at line 1 at distinct load points.....	64
Fig 5.9: (a) Typical load response of 0.44 P +0.2 %p (7day); (b) displacement profile at line 1; (c) strain profile at line 1 at distinct load points	65
Fig 5.10(a) Typical load response of 0.66P (7 day) (b) displacement profile at line 1; (c) strain profile at line 1 at distinct load points.....	66
Fig 5.11 Variation of Strain value (ϵ_{xx}) on lines along the depth of section at distinct loads for control Specimen at 28 days.	67
Fig 5.12 Variation of Strain value (ϵ_{xx}) on lines along the depth of section at distinct loads for polypropylene with 0.66% volume at 28 days.....	68
Fig 5.13 Variation of Strain value (ϵ_{xx}) on lines along the depth of section at distinct loads for polypropylene with 0.66% volume at 3 days.....	69
Fig 5.14 Variation of Strain value (ϵ_{xx}) on lines along the depth of section at distinct loads for polypropylene with 0.66 % volume at 7 days.....	70
Fig 6.1 Geometry, Loading, and Deformation of Cracked Incremental	73
Fig 6.2 Definition of Parameters of Bilinear Stress-Crack opening relationship	74
Fig 6.3 Distinct Phases of Stress Distribution during propagation of the crack in the section	75
Fig 6.4 Model representation of simply supported beam after cracking	75
Fig 6.5 Definition of Parameters of Multi linear Stress-Crack relationship	77
Fig 6.6 General Stress distribution for multi linear case	77
Fig 6.7. Stress Crack opening relationship of HFRC beams by adding 0.2 and 0.3 % micro fibers to a) 0.44 P b) 0.66% P c) 0.88% P d) 3 day specimens e) 7 day Specimens	82
Fig 6.8 Experimental and matched theoretical curves of HFRC 0.66 P+ 0.3 p beams.....	83
Fig 6.9 Crack depth vs Crack width for mean Crack opening parameters of HFRC.	84
Fig 6.10 Crack depth vs Crack width for mean Crack opening parameters of HFRC (early age).....	84

List of Tables

Table 2.1 Typical Properties of Fibers.....	5
Table 2.2 Table 2.2: Properties of various types of polypropylene fiber.....	8
Table 2.2.1 Physical Properties of the fibre used.....	13
Table 3.1 Summary of weight proportion of the various mixes.....	29
Table 4.1 Mean Compressive strength results.....	32
Table 5.1 Locations of lines.....	58
Table 6.1 Mean Values of crack opening parameters of SPFRC Beam.....	82

Chapter 1

Introduction

1.1 Introduction

Fibers have been used as discrete randomly distributed reinforcement to strengthen a material weak in tension. Fibers have been shown to improve the toughness and the post crack ductility in tension, which is achieved by the reinforcement effect across a crack in the material matrix. Fibers are included in concrete to increase the strength and toughness of the material.

The term fiber reinforced concrete (FRC) is defined by ACI Committee 544 as a concrete made of hydraulic cements containing fine or fine and coarse aggregates and discontinuous discrete fibers. Inherently concrete is brittle under tensile loading. Mechanical properties of concrete can be improved by reinforcement with randomly oriented short discrete fibers, which prevent and control initiation, propagation, or coalescence of cracks. FRC can continue to sustain considerable loads even at deflections exceeding fracture deflections of plain concrete. The character and performance of FRC changes depending on matrix properties as well as the fiber material, fiber concentration, fiber geometry, fiber orientation, and fiber distribution. FRC can be regarded as a composite material with two phases in which concrete represents the matrix phase and the fiber constitutes the inclusion phase. Volume fraction of fiber inclusion is the most commonly used parameter for studying the influence of fibers on the properties of FRC. Fiber count, fiber specific surface area, and fiber spacing are other parameters, which may also be used for this purpose. Another convenient numerical parameter describing a fiber is its aspect ratio, defined as the fiber length divided by its equivalent diameter.

A concrete beam containing fibers suffers damage by gradual development of single or multiple cracks with increasing deflection, but retains some degree of structural integrity and post-crack resistance even under considerable deflection. A similar beam without fibers fails suddenly at a small deflection by separation into two pieces. The toughening effect is the result of several types of fiber/matrix interactions, which leads to energy absorption in the fiber-bridging zone of a fiber-reinforced concrete (FRC). These processes include fiber bridging, fiber debonding, fiber pullout (sliding) and fiber rupture as a crack propagates across a fiber through the matrix [1]. There are many kinds of fibers, both metallic and polymeric, which have been used in concrete to improve specific engineering properties of the material. Steel fibers are used in a wide range of structural applications, in general, when the control of concrete cracking is important such as industrial pavements [2] [3] precast structural elements [4] and tunnel linings [5]. Steel fibers have high elastic modulus and stiffness and produce improvements in compressive strength and toughness of concrete [6]. Improvements in flexural strength of the material are also obtained by the use of steel fibers in concrete. Increase in flexural strength is achieved with increasing fiber aspect ratio (length to diameter ratio) and fiber volume fraction; significant improvements are obtained at high volume fractions [7]. In general, addition of steel fibers influences the compressive strain at ultimate load and ductility in flexure more significantly than the improvements in strength [8]. Steel fibers, however, increase structure weight of concrete and exhibit balling effect during mixing, which lowers the workability of the mix. In addition, steel fibers easily basset and rust, and it also has the problem of conductive electric and magnetic fields.

Synthetic fibres are less stiff than steel fibres and are most typically used in industrial pavements to reduce the cracking induced by shrinkage. Synthetic fibres are mainly effective in reducing crack formation, particularly at an early age after casting and in severe weather conditions (e.g. in dry climatic zones), when hygrometric shrinkage brings along some weak tensile stress which is yet too high for the fresh mixture to withstand. Synthetic fibers made using nylon, polypropylene and acrylic are available commercially. Polypropylene fibers have good ductility, fineness, and dispersion so they can restrain the plastic cracks [9].

A composite can be termed as *hybrid*, if two or more types of fibers are rationally combined to produce a composite that derives benefits from each of the individual fibers and exhibits a synergetic response. Concrete is a complex material with several phases all in different orders of magnitude like products of cement hydration in micron scale, sand in millimeter scale, and gravel in centimeter scale. Reinforcement of concrete with a single type of fiber may improve the properties to a limited level. However by using the concept of hybridization with two or more types of fibers incorporated in a common cement matrix, the hybrid composite can offer more attractive engineering properties because the presence of one fiber enables the more efficient utilization of the potential properties of the other fiber.

Recently, macro-synthetic fibers have been produced with the aim of substituting steel fibers in structural applications. It has been found that macro synthetic fibres along with small volume fraction of micro synthetic fibres has shown better toughness properties than macro fibres alone. Use of hybrid fibers has been shown to reduce permeability, provide better shrinkage resistance and result in increased moment of resistance. The availability of a structural synthetic fiber, capable of contributing to the load carrying capacity of an element while increasing its toughness and durability at a reasonable cost, is an important asset for an improved building technology. The knowledge on the mechanical behaviour of concretes reinforced with these fibers is however still limited.

1.2 Objectives

The broad objective of the work reported in this thesis is to investigate the influence of hybrid synthetic fibers on the mechanical behaviour of concrete. Specific objectives of the thesis include

1. To study the influence of crack bridging on the flexural response of fiber reinforced concrete
2. To evaluate the influence of hybrid-synthetic polypropylene fibers on the toughness and ductility of concrete.
3. To provide an interpretation for the observed tension response of fiber reinforced concrete in flexure in terms of crack propagation and toughening mechanisms in the composite.
4. To determine the crack bridging stresses contributed by hybrid-synthetic fibers.

1.3 Scope

This thesis is organized in four chapters. Description of content of each chapter is given below.

Chapter 2

Introduction to steel, polypropylene, and hybrid fiber reinforced concrete. Effects of steel and polypropylene fiber inclusion on concrete in the hardened and fresh states are overviewed. Durability characteristics of steel fiber reinforced concrete (SFRC) and polypropylene fiber reinforced concrete (PPFRC) are briefly mentioned. Discussion continues with hybrid fiber reinforced concrete (HFRC). Definitions related to HFRC are given and the chapter concludes with a literature review on HyFRC.

Chapter 3

Details of the experimental program to investigate the tensile behaviour of Hybrid fiber reinforced concrete are presented in this chapter. The materials and test methods used in the experimental test program are described.

Chapter 4

Experimental results from flexure tests on notched and unnotched beams for SFRC and HFRC at different volume contents of fibers are presented. The standard test measures available from the different standards for evaluating improvements in toughness, ductility and load carrying capacity are calculated.

Chapter 5

The results of the digital image correlation from the notched beams tested in flexure are analysed. The strain distribution information obtained from the DIC is used to study the crack growth in the beams.

Chapter 6

The results of numerical analysis to obtain the cohesive stress as a function of crack opening within the framework of the hinged crack model are presented. The influence of fibers content on the cohesive crack closing stresses is investigated

Chapter 2

Review of Standard Test methods and Literature

2.1 Introduction

Concrete is a quasi-brittle material with a low strain capacity. Reinforcement of concrete with short randomly distributed fibers can address some of the concerns related to concrete brittleness and poor resistance to crack growth. Fibers, used as reinforcement, can be effective in arresting cracks at both micro- and macro-levels. At the micro-level, fibers inhibit the initiation and growth of cracks, and after the micro-cracks coalesce into macro-cracks, fibers provide mechanisms that abate their unstable propagation, provide effective bridging, and impart sources of strength gain, toughness and ductility. Properties of the different fibers commonly available today are listed in Table 1.1

Table 1.1: Typical Properties of Fibers

Fiber	Diameter (mm)	Specific gravity	Tensile strength (GPa)	Elastic Modulus (Gpa)	Fracture strain (%)
Steel	5-500	7.84	0.5-2.0	210	0.5-3.5
Glass	9-15	2.6	2.0-4.0	70-80	2.0-3.5
Fibrillated Polypropylene	20-200	0.91	0.5-0.75	5-77	8.0
Polyethylene	20-200	0.9	0.7	0.14-0.42	10
Cellulose		1.2	0.3-0.5	10	
Carbon (high strength)	9	1.9	2.6	230	1
Cement matrix (For comparison)		2.5	3.7×10^{-3}	10-45	0.02

Fibers can be classified into 3 categories as per BS EN 14889.

- Class I a : Micro Fibres < 0.3mm in diameter, mono filament
- Class I b: Micro Fibres < 0.3mm in diameter, fibrillated
- Class II: Macro Fibres > 0.3mm in diameter

Fiber volume content is the primary variable which influences the response of the fiber reinforced composite in tension as shown in Fig 2.1.1. For small volume fraction, after first

crack, there is drop in the load. There are a small number of fibers bridging the crack that sustain the load. The capacity provided by the number of fibers crossing the crack is significantly less than the first crack load and load carrying capacity decreases rapidly with increasing deformation. For intermediate volume fraction, after the drop in load associated with the formation of a crack, the load carrying capacity provided by the fibers produces a progressive yet gradual decrease in the load carrying capacity. For high volume fraction, after first crack, there are a large number of fibers bridging the crack and the resistance to crack opening provided by the fibers is larger than the first crack load. As the load increases, more cracks form along the length of specimen.

The observed load response at the different volume fractions is associated with the pullout response of fibers from the concrete matrix averaged over the crack. The mechanical behaviour of the FRC are influenced by reinforcing mechanisms or the ability of the fibers to transfer stress across the crack. In short randomly distributed fibers at low and intermediate fiber volume fractions (typically up to 2%) the contribution of fibers is after strain localization, which occurs close to the peak tensile load. The tensile strength in these cases is comparable to that of the unreinforced matrix. The strain softening is influenced by the cracking closing pressure provided by the fibers as a function of the crack opening displacement. The toughening provided fibers depend upon the pull out resistance of the fibers embedded in the matrix. During crack propagation, debonding and sliding contribute significantly to the pull out resistance of the fibers and hence to the total energy consumption when a large crack develops in the matrix. Fiber breakage has not been considered to contribute significantly to the energy dissipated during crack propagation in FRC [24]. Several fracture based formulations which consider the debonding behaviour of fibers from the cementitious matrix have been proposed [10].

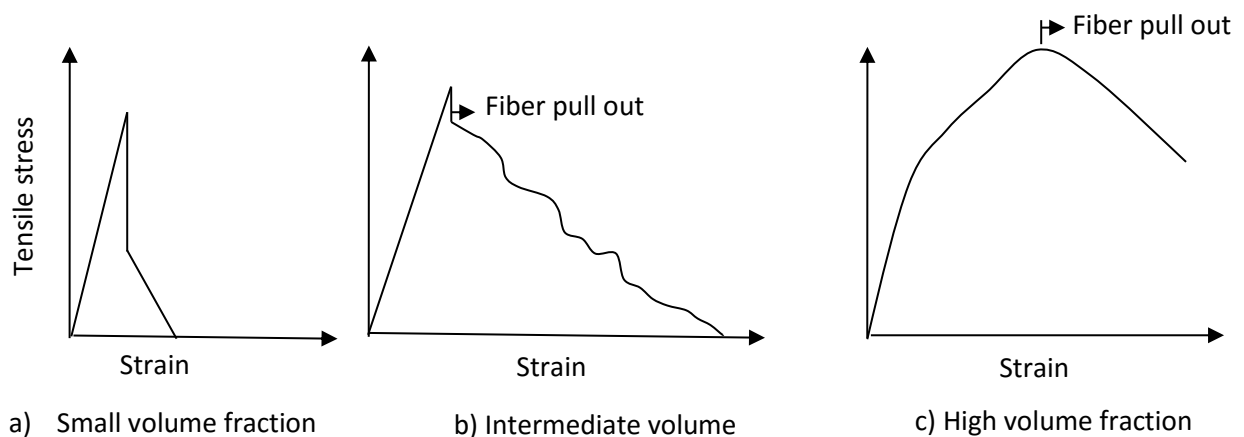


Fig 2.1.1: The composite stress-strain curves for fiber-reinforced brittle matrix

At higher volume fractions, which are usually achieved using special processing techniques, the pre-peak behaviour is fundamentally altered due to stabilization of micro cracking in the matrix. A uniform distribution of micro cracks in the matrix leads to significant enhancement in the strain capacity of the matrix. The load response of such composites exhibits strain hardening response as show in Fig 2.1.2. There is a point in the load response identified as the bend-over-point (BOP) where the matrix contribution to the tensile load response reaches a maximum. The load response following the BOP is characterized by multiple cracking in the

matrix. In this stage the incremental loading of the fibers at the location of the crack is transferred to the matrix through the interfacial bond, which results in a build-up of tensile stress in the matrix. More cracks are produced in the matrix when the tensile stress in matrix reaches the tensile strength of the matrix. Mechanistic and fracture based approaches which consider fiber-matrix interaction in high volume composites where the localization of crack is suppressed is very complex and is still developing.

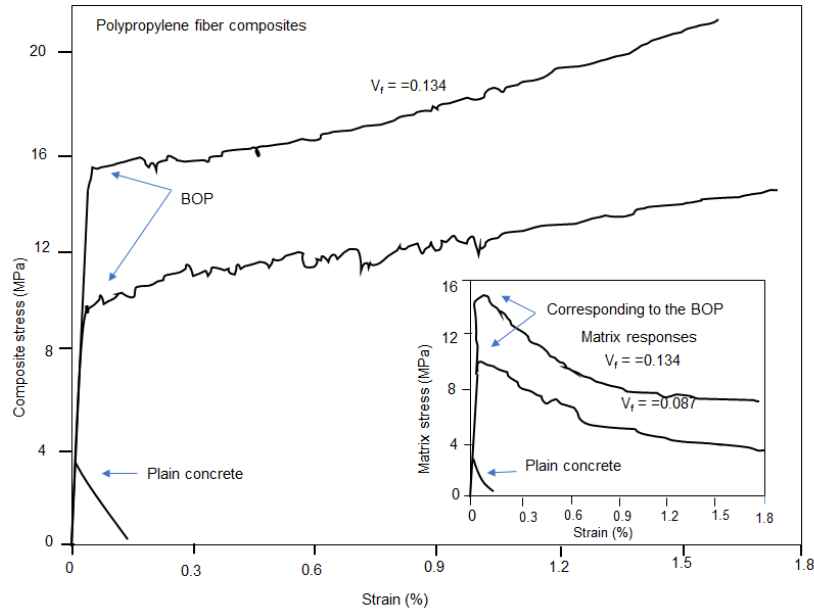


Fig2.1.2: Strain hardening response of polypropylene fiber composites

2.1.1 Steel Fibers

Steel fibers have a relatively high strength and modulus and are available in aspect ratios ranging from 20 to 100 and length ranging from 6.4mm to 75mm. The process of manufacture varies from cut sheets, cold drawn wires or hot melt extraction and are available in different cross-sections and shapes depending on the method of manufacture and use.

While steel fibers improve the strength of concrete under all load actions, their effectiveness in improving strength varies among compression, tension and flexure. There is an insignificant change in the ultimate compressive strength upon the addition of steel fibers; There is an increase of up to 15 percent for volume of fibers up to 1.5 percent by volume [25, 26]. There is a significant improvement in strength in tension with an increase of the order of 30 to 40 percent reported for the addition of 1.5 percent by volume of fibers in mortar or concrete [27]. Strength data [28] shows that the flexural strength of Steel fiber reinforced concrete (SFRC) is about 50 to 70 percent more than that of the unreinforced concrete matrix in the normal third-point bending test [28,29].

The ability of steel fibers to serve as reinforcement is determined by the resistance of the fibers to pullout from the matrix resulting from the breakdown of the fiber-matrix interfacial bond. Improvements in ductility depend on the type and volume percentage of fibers present [30, 31]. In conventionally mixed SFRC, high aspect ratio fibers are more effective in improving the post-peak performance because of their high resistance to pullout from the

matrix. However, at high aspect ratio there is a potential for balling of the fibers during mixing [32]. Techniques such as enlarging or hooking of ends, roughening their surface texture, or crimping to produce a wavy rather than straight fiber profile allow for retaining high pullout resistance while reducing fiber aspect ratio. These types are more effective than equivalent straight uniform fibers of the same length and diameter. Consequently, the amount of these fibers required to achieve a given level of improvement in strength and ductility is usually less than the amount of equivalent straight uniform fibers [32, 33].

The fiber pullout behaviour is influenced by the type of fiber as seen in the load response obtained from steel fiber reinforced concrete with 50 kg/m^3 fibers in Fig2.1.3. For hooked end steel fiber, after first crack, there is drop but that drop is less than the other two fibers, deformed end fiber and corrugated fiber. For deformed end fiber and corrugated fiber, after first crack there is a continuous decrease in the load carrying capacity with increasing deformation. Hooked end fibers, which provide the highest pullout resistance from the matrix provide the highest load carrying capacity with increasing deformation after crack formation.

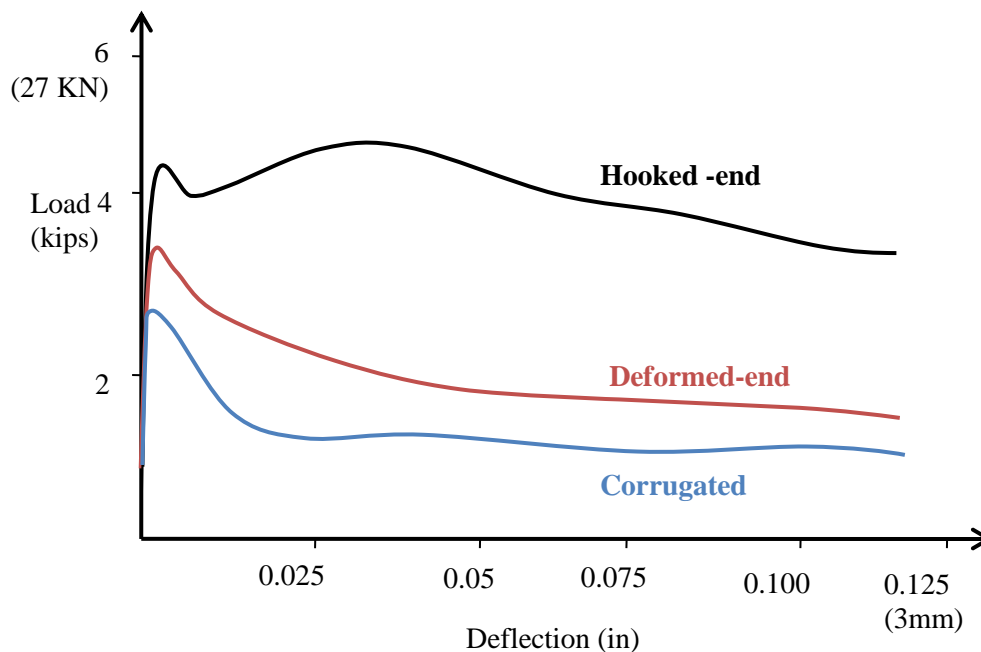


Fig2.1.3: Effect of steel fiber shape on the load response in flexure

Improvements in post-crack ductility under tension result in significant improvements in flexural response. Ductile behaviour of the SFRC on the tension side of a beam alters the normally elastic distribution of stress and strain over the member depth. The altered stress distribution is essentially plastic in the tension zone and elastic in the compression zone, resulting in a shift of the neutral axis toward the compression zone [34].

2.1.2 Polypropylene Fibers

Polypropylene fibers are available in two different forms; Monofilaments and Fibrillated. Monofilament fibers are single strand of fibers having uniform cross-sectional. Fibrillated fibers are manufactured in the form of films or tapes that are slit in such a way that

they have net like physical structure. Most commercial applications of polypropylene fibers have used low volume percentage (0.1 percent), monofilament or fibrillated fibers (in the case of polypropylene). Typical properties of monofilament and fibrillated polypropylene fibers are given in Table 2.1.2.

Table 2.1.2: Properties of various types of polypropylene fiber

Fiber type	Length	Diameter	Tensile strength	Modulus of elasticity	Specific Surface	Density
	(mm)	(mm)	(MPa)	(MPa)	(m²/kg)	(kg/cm³)
Mono filament	30-60	0.30-1	547-658	3.50-7.50	91	0.91
Micro filament	12-20	0.05-0.20	330-414	3.70-5.50	225	0.91
Fibrillated	4-40	0.10-0.30	500-750	5.00-10.00	58	0.91

The use of these fibers has been restricted to non-structural and non-primary load bearing members. At typical dosages usually employed in the construction industry there is a marginal improvement in the mechanical properties of concrete.

At dosages considered by the industry, of 1.2 kg/m³, PP fibers have been shown to influence the fracture behaviour; the influence of the fibres was especially felt in the tail of the P-d curve, showing a wider softening branch in the case of the FRC mixes, which corresponds to a more ductile behaviour of the concrete. The effect of the fibre is more remarkable in the case of the low strength concrete, where the stresses in the cohesive zone are lower, and the bridge effect of the fibre has a greater effect due to the higher level of deformation. It was shown that the fibres with the highest elongation and lowest strength (i.e. the most ductile fibres) presented the highest values of fracture energy. In the case of high strength concrete the higher level of the cohesive stresses mitigates the bridge effect of the fibres. In low- and normal-strength concrete the main mechanism of failure of the fibres was by pull-out while in high strength concrete it was due to fiber breakage [35].

2.1.3 Macro-synthetic Polypropylene fiber

Structural synthetic fibers are available in different geometries and shapes as shown in Fig 2.1.4. The energy absorption capacities from pullout tests on the different shape synthetic fiber obtained from pullout tests are shown in Fig 2.1.5[36]. Test results indicate that the crimped-shape structural synthetic fibers exhibit the highest energy absorption capacity.

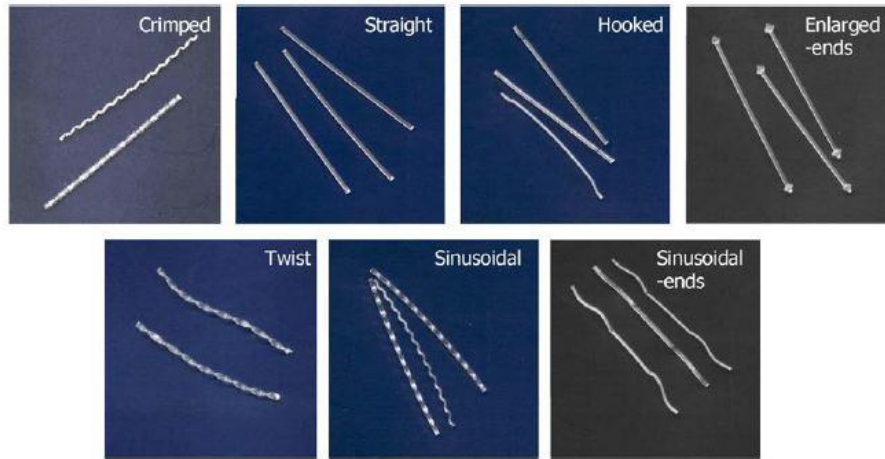


Fig 2.1.4: Various types of synthetic fibers tested in the present study

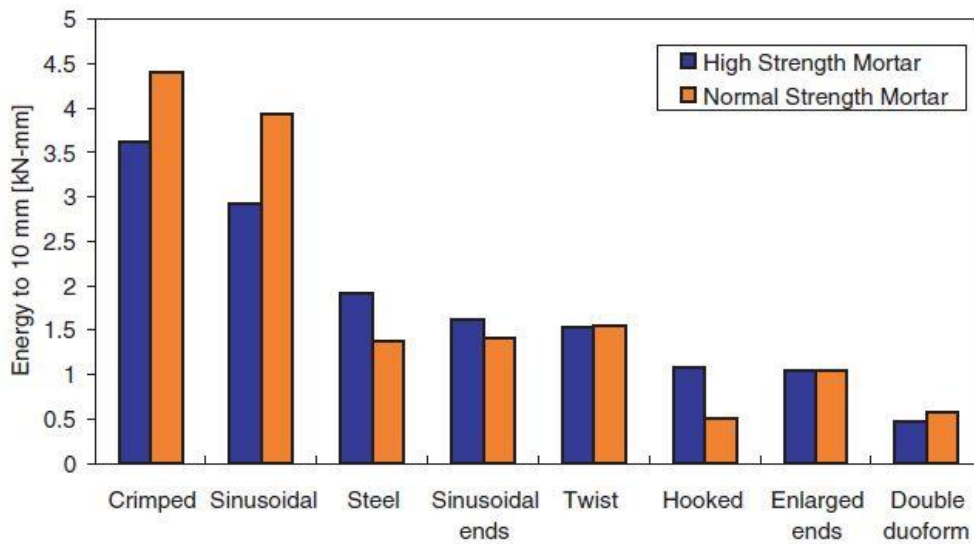


Fig 2.1.5 Comparison of absorbed energies from pullout tests for various fiber types.

A comparison of the load response in flexure between hooked end steel fibers and synthetic fibers is shown in Fig 2.1.6. Data obtained from [37] are plotted in the figure 2.6. Steel fibers at dosages up to 50 kg/m^3 , show in a drop in load immediately after formation of the crack, followed by a gradual decrease in load carrying capacity. In case of synthetic fiber, at fiber dosage rate 4.6 kg/m^3 , there is sudden drop (that drop decrease in fiber dosage rate 5.3 kg/m^3), after first crack, there is continuously decreasing load and increasing the deflection (slowly fiber pull out start from the matrix).

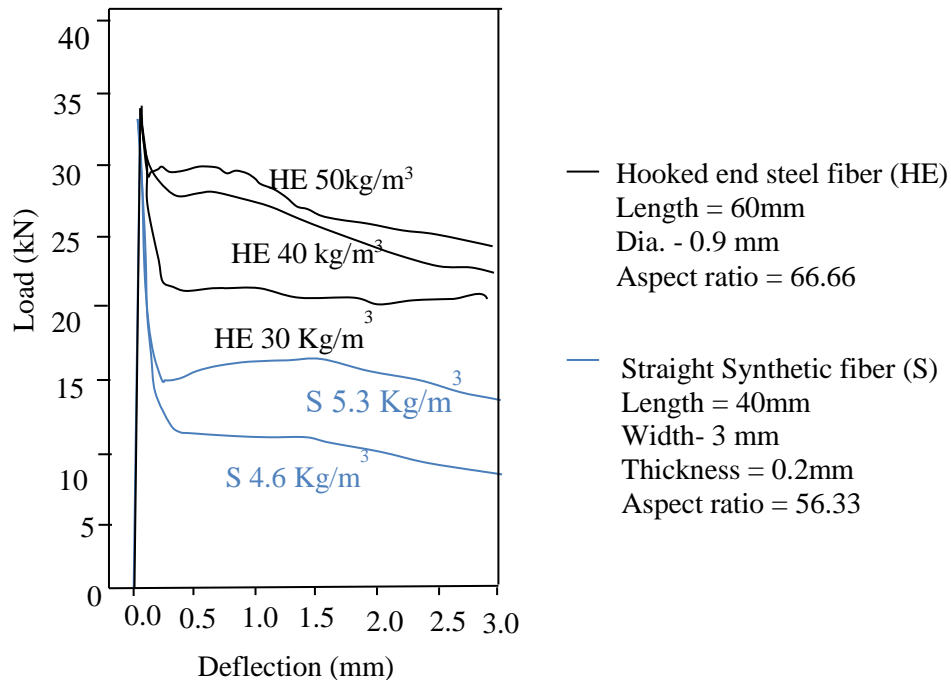


Fig 2.1.6 Load–deflection curves for HE 60 at 30, 40 and 50 kg/m³ dosage rates and for S 4.6 and S 5.3 at 4.6 and 5.3 kg/m³ dosage rates.

A comparative study on the mechanical behaviour and fracture properties and fracture behaviour of concrete containing steel fiber and micro-polypropylene fiber (19mm length) was published by Bencardino et al (1994). It was found that while steel fibers had an insignificant influence on the compressive strength of concrete, Polypropylene fibers reduced the compressive strength about 25% and 35% at 1% and 2% fiber volume contents, respectively. This was attributed to the low modulus of elasticity of the polypropylene fibers and insufficient dispersion of the fibers in the mixture. The elastic modulus of steel fibers were also shown to influence the fracture properties and behaviour obtained using notched beams tested in three-point bending configuration. The equivalent flexural strength values of SFRC are much higher than the strength at the limit of proportionality, while for polypropylene fibers, the reverse is true. Steel fibers produced an increase in the peak load with increase in the steel fiber volume content when compared with ordinary concrete. The polypropylene fiber reinforced concrete specimens were able to retain peak load values similar to those recorded for the control specimens at 1% fiber volume content. However, at the 2% fiber volume content, these specimens showed a substantial decrease in peak flexural loads compared to those of the control. After reaching the peak load, all the PFRC specimens showed sudden drop in load, about 67% and 40% of the peak load for fiber volume contents of 1% and 2%, respectively. The residual loads after the load drop remained constant with increasing deflection, up to the end of the test. Marco synthetic fibers were shown to be significantly less effective than the hooked end steel fibers in increasing the fracture energy. However, the low modulus polypropylene fibers were shown to give as much ductility as the steel fibers.

In their study involving a comparison of hooked end steel fibers and macro synthetic fibers (slightly coiled Polyolefin, hooked Polystyrene, flat polymeric mix), Buratti et al. (2010) also

showed that the residual strength for steel fibers are higher when compare to macro synthetic fibers from notched concrete beams tested in three-point configuration. At volume fractions in the range of 0.2-0.5%, the residual strength was found to increase with an increase the fiber content. The addition of fibres, both steel and macro-synthetic, to the concrete increased its toughness from 5 to 10 times. The results of the experimental investigation revealed that considering the variability of results, the mean values of residual strengths at different CMOD opening normalized to its corresponding flexural strength indicate a significant improvement in the performance of the steel fibres when compared with synthetic fibres. If the characteristic residual strengths, which are obtained as the 5 percentile values are used, the benefit given by the steel fibres is reduced. A direct correlation between the statistical distribution of fibers in the crack plane and the residual strength values is also shown for the macro synthetic fibers.

2.2 Hybrid Fibre Reinforced Concrete

Almost all FRCs used today commercially involve the use of a single fiber type. The main aim of adding fibers to concrete is to increase its fracture energy. Influence of fibers on increasing stiffness and strength are also observed at high volume fractions. Clearly, a given type of fiber can only be effective in a limited range of crack opening and deflection. But instead of going for high volume fraction, including two or more types of fiber that make complementary and additive contributions to performance in a concrete mix is a method for maximizing the improvements possible through fiber reinforcement. That may result in increased load carrying ability and energy dissipation which is result of local crack arrest and resistance to crack opening provided by hybrid fibers.

In well-designed hybrid composites, there is positive interaction between the fibers and the resulting hybrid performance exceeds the sum of individual fiber performances. This phenomenon is often termed “Synergy”.

Hybrids based on fiber constitutive response: One type of fiber is stronger and stiffer and provides reasonable first crack strength and ultimate strength, while the second type of fiber is relatively flexible and leads to improved toughness and strain capacity in the post-crack zone.

Hybrids based on fiber dimensions: One type of fiber is smaller, so that it bridges micro-cracks and therefore controls their growth and delays coalescence. This leads to a higher tensile strength of the composite. The second fiber is larger and is intended to arrest the propagation of macro-cracks and therefore results in a substantial improvement in the fracture toughness of the composite. Fibers of small size (often called micro-fibers) delay crack coalescence in the cement paste and mortar phases and increase the apparent tensile strength of these phases.

Hybrids based on fiber function: One type of fiber is intended to improve the fresh and early age properties such as ease of production and plastic shrinkage, while the second fiber leads to improved mechanical properties. One such hybrid is the combination of a low (0.1%) dosage of polypropylene fiber and a higher (~0.5%) dosage of steel fiber.

Study on Hybrid Fiber reinforced concrete was started in 1990s. Flexural behaviour of concrete containing micro steel fiber and micro-polypropylene fiber was studied by Bantia and Sheng (1991). In hybrids, steel fibers contributed to strengthening and carbon fiber to toughening.

The fracture energy of concrete with macro steel fibres and micro polypropylene was found to increase by approximately 40% [43]. In concrete subjected to 10 years outdoor exposure it was found that hybrid fibre reinforced concrete showed good later strength also. Micro fibers arrest the shrinkage cracks due to its low modulus of elasticity. From studies on flexural behaviour with macro steel fiber and micro-polypropylene fiber by Feldman and Zheng (1993) [44], it was found that stiffer steel fibers improved the ultimate strength and the ductile polypropylene fibers improved post-peak strain capacity. Later in order to study the behaviour of Hybrid fibre reinforced concrete with respect to temperature, Horiguchi and Sakai (1999) [45] investigated using macro steel fiber and micro-polyvinyl alcohol fiber. It was found that HFRC showed greater first crack deflection at -20°C than at 20°C for the same flexural toughness I_{075} .

A good synergy between steel and micro polypropylene fiber in flexural toughness was demonstrated considering different macro steel fibers [46]. Hooked end steel fibers with higher aspect ratio were shown to produce higher values of flexural toughness, which was related to the higher pullout resistance of the hooked end fiber in tension. The flexural behaviour was found to improve by adding small fraction of micro fibres. Hybrid combination of macro steel fiber and micro-polyvinyl alcohol fiber has been shown to provide significant increases to both ultimate load and post-peak ductility [47].

Lawler et al. (2002) [48] showed that the permeability of HyFRC was comparatively decreased when compared to same with macro fibre reinforced concrete. The use of reinforcing fibers is shown to produce a significant reduction in water permeability through a modification of crack topography. This has direct implications for improving durability because many deterioration mechanisms of cement-based materials require the ingress of water. Two different size classifications of fiber, micro- and macrofiber, are combined to modify the cracking mechanisms during the pre- and postpeak response, respectively. Specifically, the combination of steel and polyvinyl alcohol (PVA) microfibers (less than 12 mm in length and $22\ \mu\text{m}$ in diameter) with a larger steel macrofiber in mortar significantly improved resistance to water permeation and displayed additive contributions to mechanical performance.

Flexural behaviour of concrete containing macro steel fiber, micro-polypropylene fiber and micro-carbon fiber was studied by Wu et al. (2003) [49]. Micro and macro fibres with the same aspect ratios were used in the study. It was found that steel fibers contributed to strengthening and carbon fiber to toughening. Carbon with higher elastic modulus than micro polypropylene results in better synergy with macro steel fibre in flexural toughness. The elastic modulus of the micro fibers was also shown to influence the flexural behaviour. The Flexural behaviour of different mixes is shown the Figure. 2.2.1. Banthia and Soleimani (2005) [52] showed that carbon isotropic pitched fibers are better than carbon mesophase pitched in improving flexural strength.

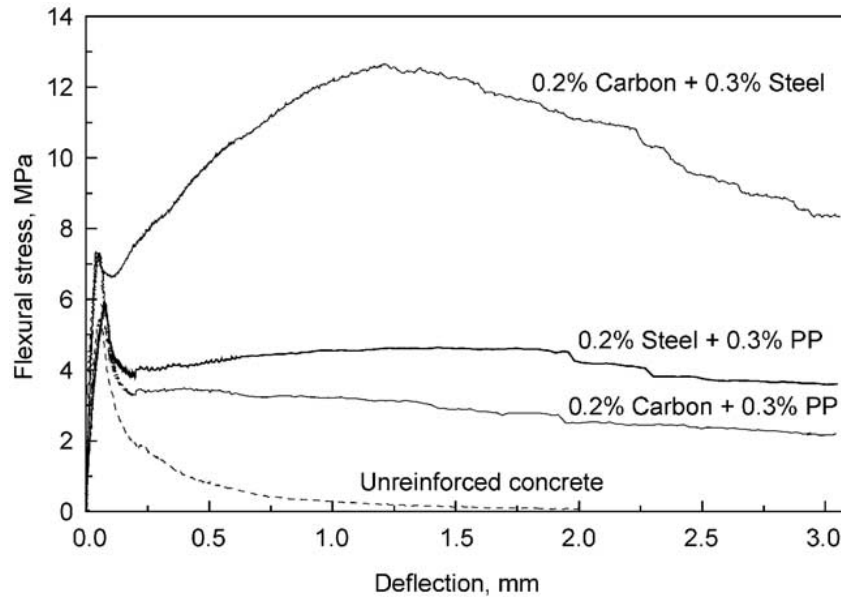


Fig 2.2.1: Comparison on Flexural behaviour of different HyFRCs

Flexural toughness of high strength concrete matrices with Hybrid fibers were studied by Bantia and Gupta (2004) [50]. Macro steel fiber, macro polypropylene fiber and different types of micro- polypropylene fiber (2denier and 3denier) were used in the study. The properties of the fibres are shown in the table 2.2.1. The load responses of the different fiber combinations are shown in Figures 2.2.2 and 2.2.3. It was found that aspect ratio of micro fibers also have an influence on toughness. Significant improvement in the flexural toughness of steel fibers was obtained by adding 0.25 % of micro polypropylene fibers. The matrix strength was not much improved by the fibres as the matrix was of high strength. But the post peak was improved significantly with the help of combining two. High aspect ratio micro fibers when mixed with macro fibers resulted in better toughness (Figure 2.2.3). Pull out resistance will be more when fibers with higher aspect ratio are used. Flexural toughness synergy was comparatively less in high strength matrices. For the same volume fraction there were more number of micro fibres in the mix resulting in more number of fibres across the crack and reinforcing the macro fibres which in effect provides more pull out resistance.

Table 2.2.1: Physical Properties of the fibre used

Fibre Code	Type	Length (mm)	Diameter	Geometry	C/S Shape
S1	Flat ended steel	50	1mm	Flat end	Circular
P1	Macro Polypropylene	50	1mm	Crimped	Rectangular
P2	Self-fibrillating Polypropylene	50	1mm	Straight	Fibrillated
C	Carbon Fibre	12.5	9-11um	Straight	Circular
p1	Micro Polypropylene	12.5	2 denier	Straight	Circular
p2	Micro Polypropylene	12.5	3 denier	Straight	Circular

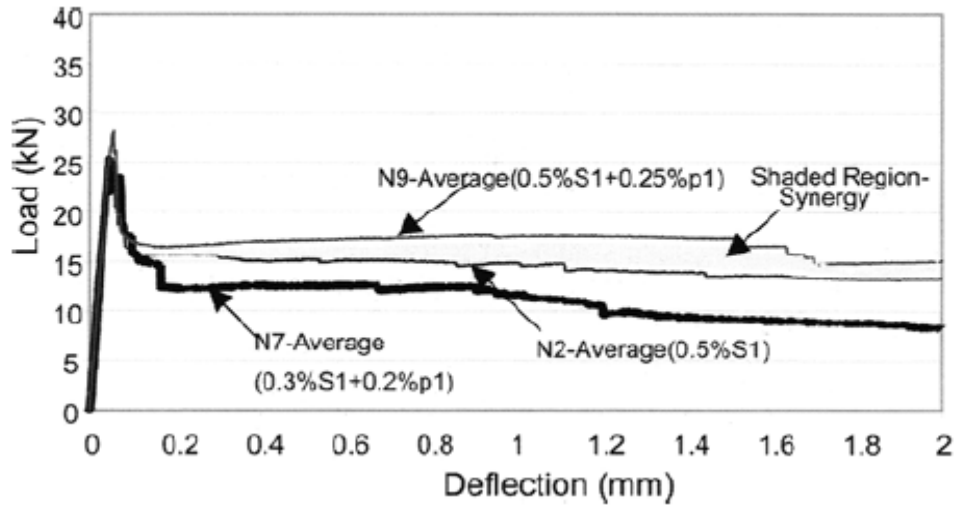


Fig 2.2.2: Load Deflection graph for different mixes.

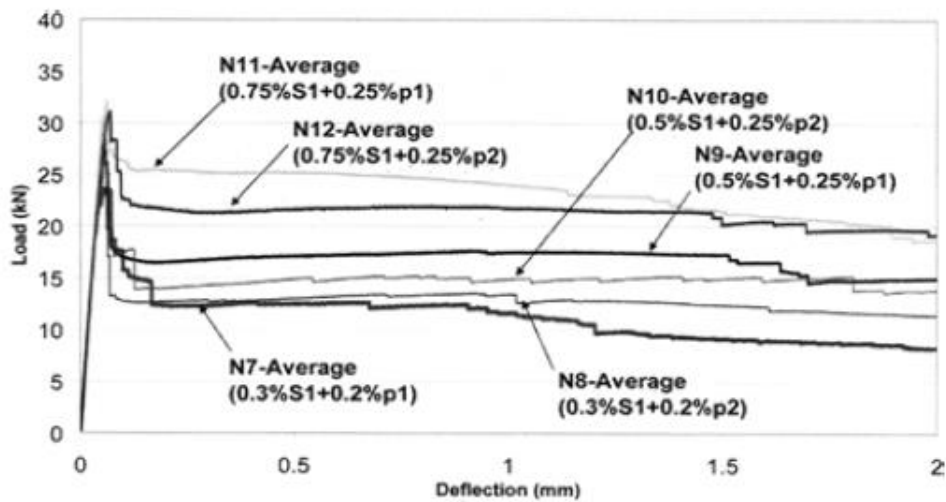


Fig 2.2.3: Comparison of various HyFRC

The benefit of combining macro fibers with micro fibers to cover the different length scales was demonstrated by Bantia and Sappakittipakorn (2007) [54] using hybrid reinforced concrete with two different diameters of macro steel. It was shown that flexural toughness was comparatively less than that with macro steel fiber with micro fiber.

For normal strength concrete matrix, the use of micro-polyvinyl alcohol (PVA) fibers (diameter 14 μm , length 12mm and Modulus = 36 GPa) and micro steel fibers (diameter 14 μm , length 6mm) in combination with hooked end steel fibers resulted in higher modulus of rupture [51]. Micro fibers delayed the development of macro cracks and so the composite demonstrated greater strength and crack resistance than a similar matrix reinforced with macro fibers only. Stress at first crack was found more for hybrid fiber reinforced concrete (Fig 2.2.4). Micro cracks arrest the shrinkage cracks at the early stage and which resulted in higher matrix

strength. It was desirable to have at least 0.1 % of microfibers in the mix to improve the matrix property. HyFRC showed almost same toughness with Macro fibre reinforced concrete at smaller deflections (Fig 2.2.5). However for the same total volume fraction of fibers, Macro fibre reinforced concrete showed better toughness at larger deflections. Macro fibers were also more likely to break since the microfibers reinforced the matrix, increasing the macro fiber pull-out resistance. HyFRC shows cracks at later stage only but the average crack width was found to be almost same after 44 days with FRC (Fig 2.2.6). Crack width test was done using the restrained ring shrinkage cracking setup. It was clear that micro fibers were effective in shrinkage cracking also.

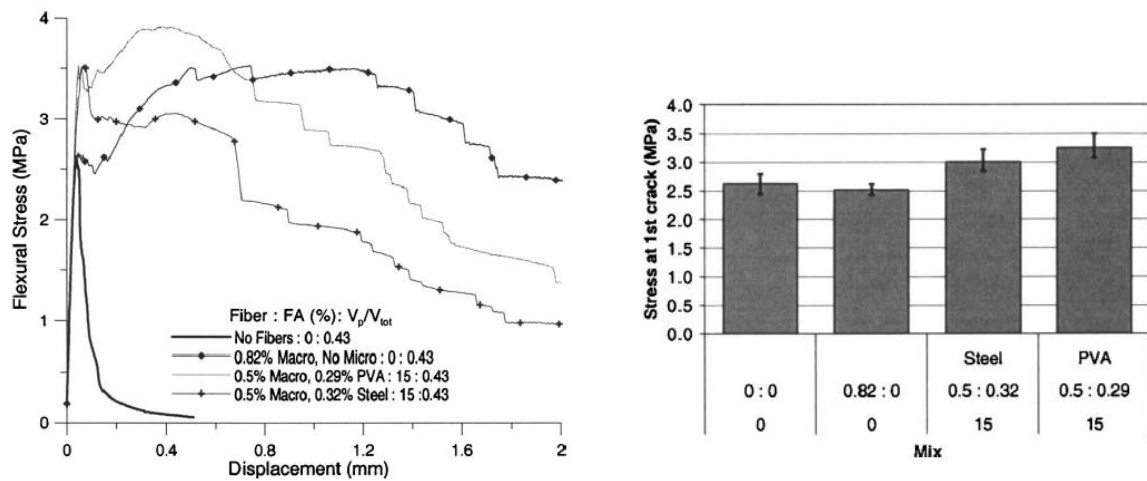


Fig: 2.2.4: Stress versus midpoint displacement for different mixes and Stress at first crack for various mixes.

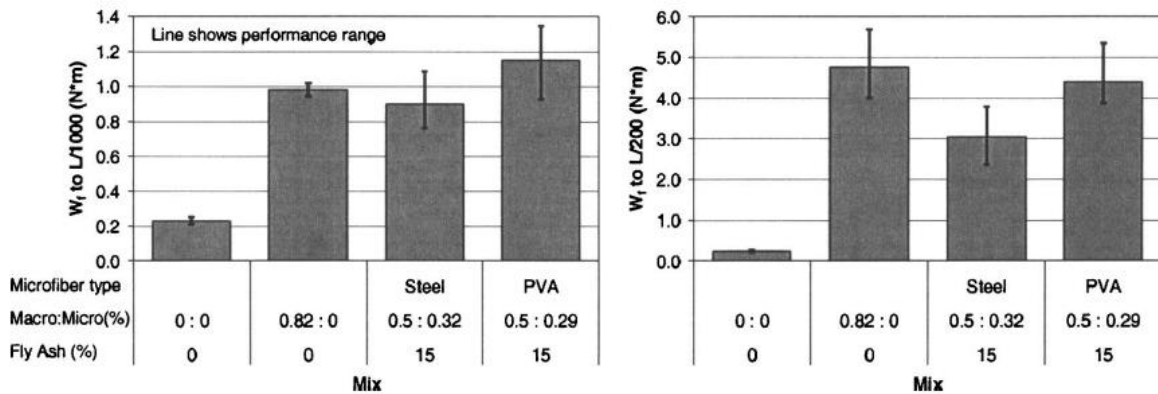


Fig: 2.2.5: Toughness determined for small (0.4mm) and large (2mm) deformation

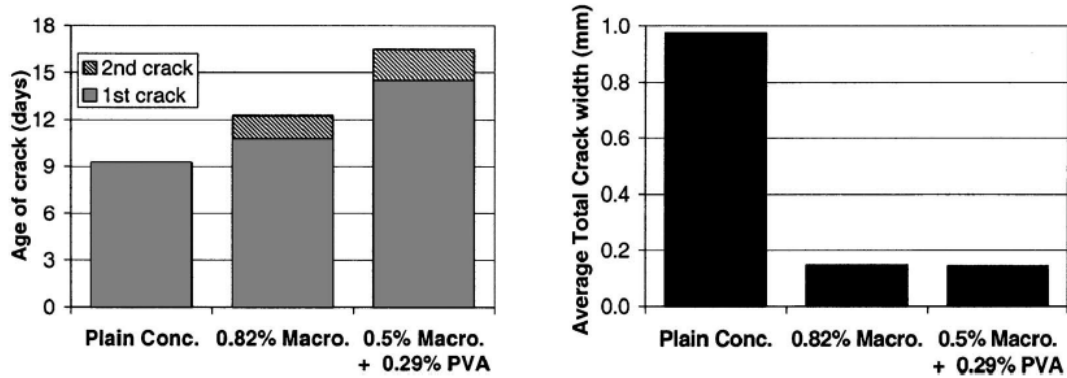


Fig: 2.2.6: Average age at which cracks were first observed (left) and average total crack width at 44 days (right)

Paramasivam (2006) [53] investigated hybrid fiber blends with macro steel (160 μ m diameter, 13mm length), micro- polyethylene (40 μ m diameter, 12 mm length, 44 GPa Modulus) and micro-PVA (39 μ m diameter, 12 mm length, 79 GPa modulus) fibers. Steel with PVA showed better flexural strength due to PVA's better bonding properties and Steel with polyethylene showed better deflection capacity due to polyethylene's better tensile strength. Flexural behaviour has been shown in the fig 2.2.7.

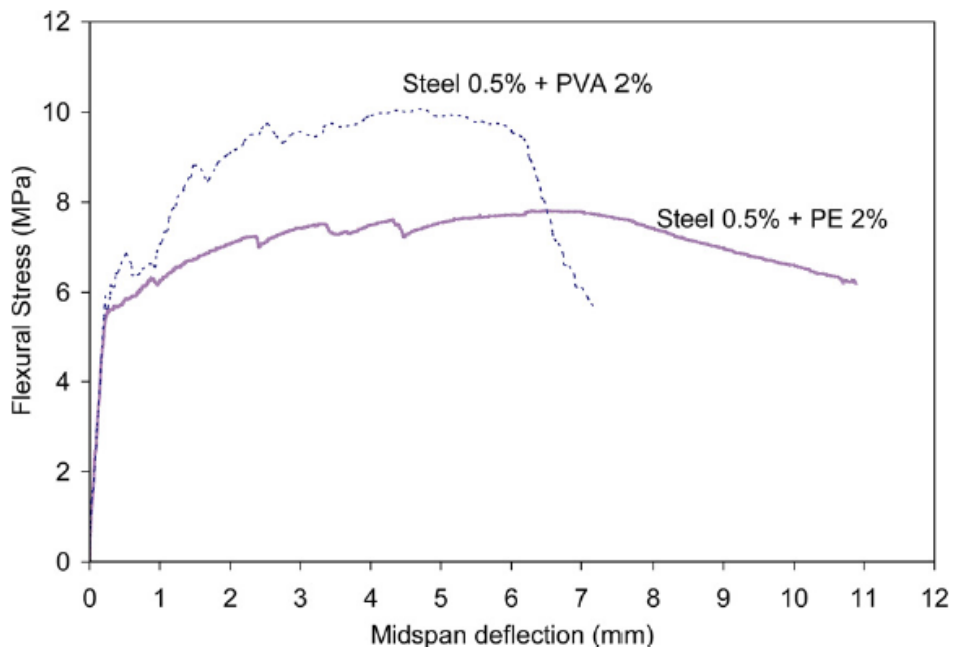


Fig: 2.2.7: Comparison of Stress vs Deflection for different HyFRCs

Blends of mono-filament macro (60 mm length, 1 mm diameter, 5.9 GPa Modulus) and staple micro (10-25 mm length, 20 μm diameter, 4.2 GPa Modulus) polypropylene fibers were investigated for improvements in flexural behaviour of concrete by Hsie et al. (2008) [55]. Adding of micro fibers in lesser volume fraction ($< 0.1\%$) was shown not to produce any improvement in the modulus of rupture. Rather they help in improving the flexural toughness by increasing the pull out resistance of the macro fiber (Fig 2.2.8). Micro fibres reinforce the macro fibre forcing them to break by providing higher pull our resistance. Fibers were distributed properly over the specimen resulting in better shrinkage resistance.

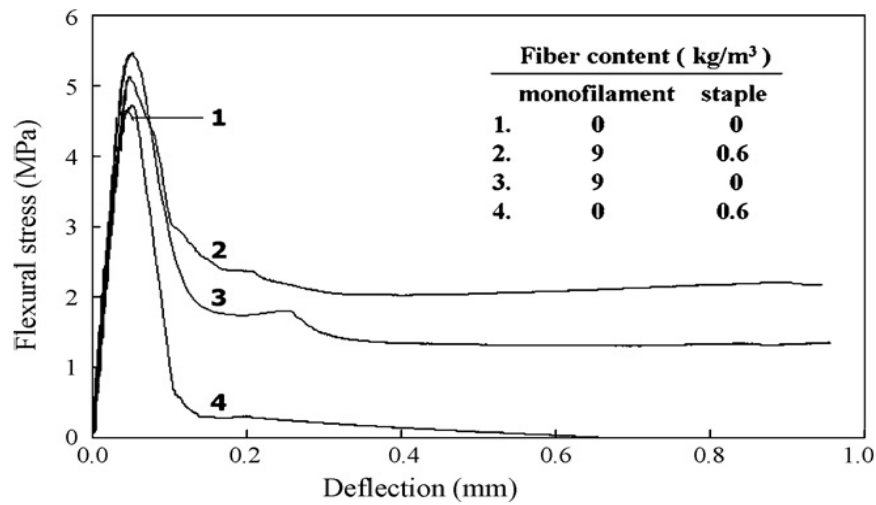


Fig: 2.2.8: Comparison of Stress vs Deflection for different HyFRCs

Banthia et al. (2014) [56] investigated with macro steel hooked end fiber with micro-cellulose fiber and found the combination helped in improving the modulus of rupture (MOR) as well as flexural toughness of the concrete. The cellulose micro fibres reinforce the steel fibres resulting in better flexural toughness (Fig 2.2.9).

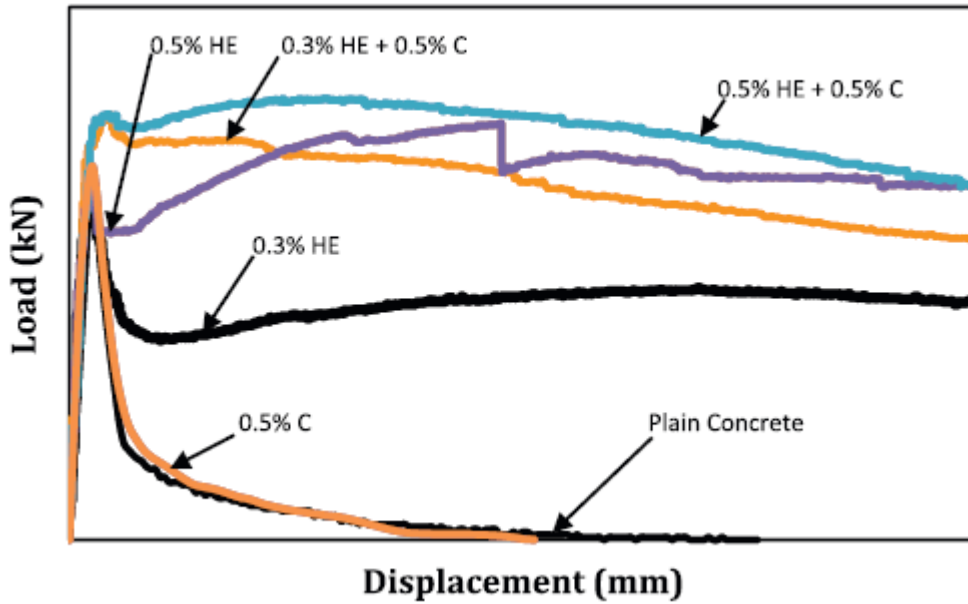


Fig: 2.2.9: Comparison of load vs Deflection for different HyFRCs

2.3 Standard Test Methods

The influence of fibers on overall improvements in ductility and toughness are often interpreted in terms of improvements to fracture behaviour and crack propagation. Quantitative measures which allow for comparison between fibers and assess improvements involve standard test methods and data reduction procedure. The fracture behaviour of fiber reinforced concrete is also investigated using the test configurations and specimens of dimensions specified in standardized test procedures. A review of different standard test is presented first.

Standardized test methods for quantifying improvements in material behaviour and obtaining specific material properties have been developed. In these tests material parameters which quantify ductility and toughness of the material are obtained from measured load response. The quantities derived from these tests allow for comparison of material behaviour. Standard test procedures for evaluating the response of FRC are available in ASTM 1609, UNI 11039-2, ASTM 1018, EN 14651 and JSCE SF 24. Additionally, researchers have proposed methods for obtaining fracture or material parameters from the measured test response from the standardized test procedures. The test procedures and the different data reduction procedures are reviewed in this section

2.3.1 ASTM 1609 test procedure

In ASTM C1609/C1609M-10 a standardized test procedure is available to establish the flexural toughness, the flexural strength and the residual strength factors of the fiber reinforced concrete using beam specimens. The loading and support system capable of applying third point loading the specimen without eccentricity or torque in accordance with ASTM C78-02 [22] is shown in figure 2.3.1. ASTM test is performed measuring the applied load and the beam net deflection (i.e. the absolute mid-span deflection minus the support deflection) at a constant

deflection rate. The beam midpoint deflection between the tension face of the beam is measured in relation to the neutral axis of the beam at its support.

First peak deflection, toughness and Equivalent flexural strength are derived from the measured response. The standard load-displacement behaviours of fiber reinforced concrete beams are shown in figure 2.3.2. The peak load is determined as that value of load corresponding to the point on the load-deflection curve that corresponds to the greatest value of load obtained prior to reaching the end-point deflection. The first-peak load (P_1) is defined as that value of load corresponding to the first point on the load-deflection curve where the slope is zero, that is, the load is a local maximum value. In specimens, which exhibit an increase in load after the load drop produced by cracking, the first peak load is the distinctive point in the load response associated with load drop as shown in Figure 2.3.2.

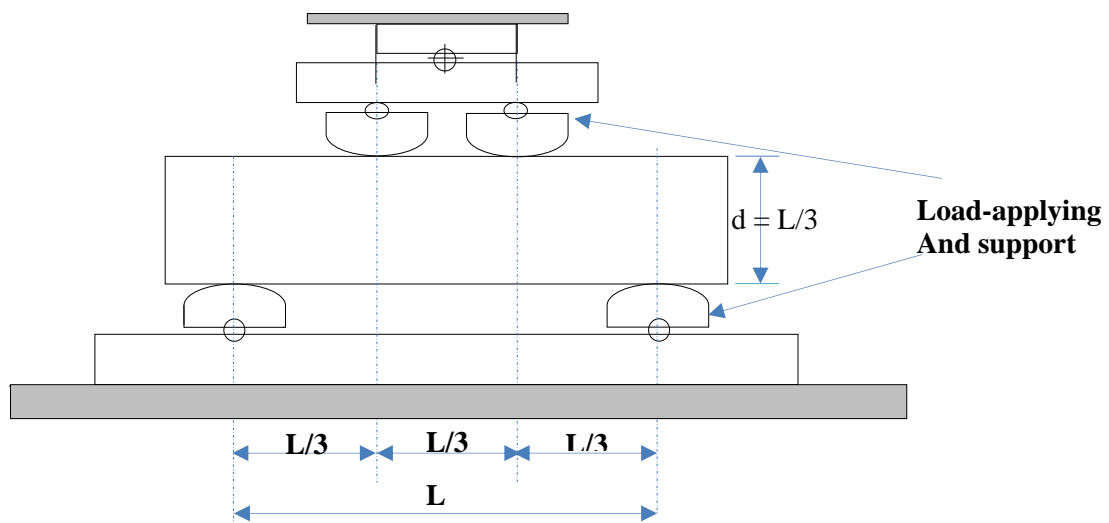


Fig 2.3.1 Diagrammatic View of a Suitable Apparatus for Flexure Test of Concrete by Third-Point Loading Method

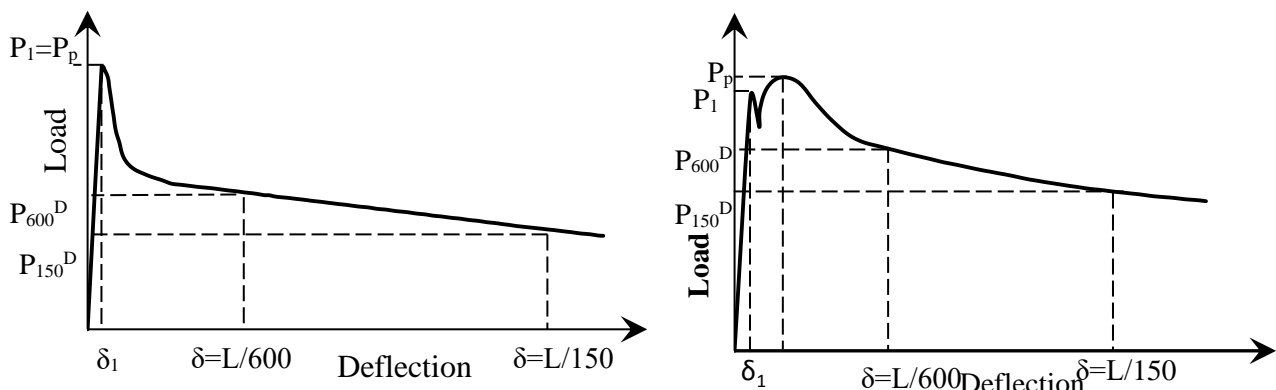


Fig 2.3.2 Example of Parameter Calculations

Strength corresponding to each peak load, f_p is determined following formula for modulus of rupture

$$f = \frac{PL}{bd^2}$$

First-peak deflection for third-point loading is estimated assuming linear-elastic behaviour up to first peak from the equation

$$\delta_1 = \frac{23P_1L^3}{1296EI} \left[1 + \frac{216d^2(1 + \mu)}{115L^2} \right]$$

The residual strengths, f_{600}^D and f_{150}^D are determined from the residual load values, P_{600}^D and P_{150}^D corresponding to net deflection values of 1/600 and 1/150 of the span length.

Toughness T_{150}^D is determined as the total area under the load-deflection curve up to a net deflection of 1/150 of the span length. The equivalent flexural strength ratio, $R_{T,150}^D$ is determined using the first-peak strength determined and the toughness determined. Record the number rounded to the nearest 0.5 % as equivalent flexural strength ratio, as appropriate for the specimen depth.

$$R_{T,150}^D = \frac{150T_{150}^D}{f_1bd^2} 100\%$$

2.3.2 ASTM 1018 test procedure

In ASTM C1018, toughness indices are taken as the area under the load-deflection curve up to certain specified deflection to area under the load-deflection curve up to the first crack as shown in figure 2.3.3. Three level of deflection 3δ , 5.5δ and 10.5δ . Deflection value greater than 10.5δ can also be chosen for composite that can carry considerable loads at large deflection. The three suggested indices called I_5 , I_{10} and I_{20} are defined by following equations.

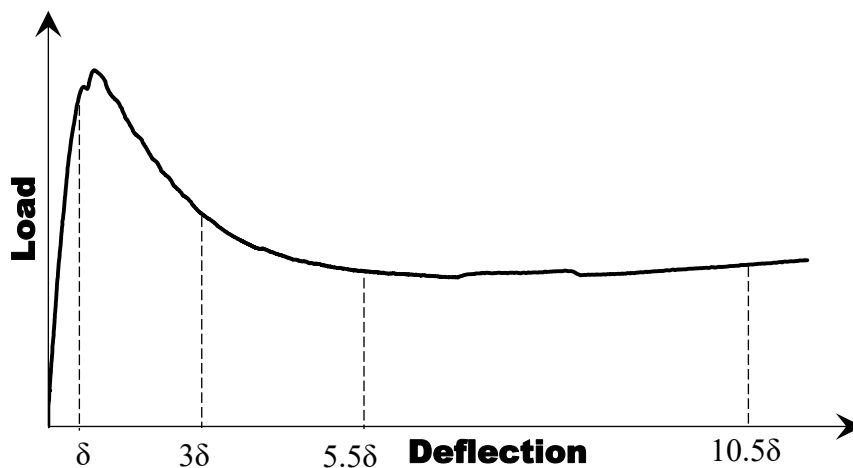


Fig.2.3.3 Important Characteristics of the Load-Deflection Curve

$$I_5 = \frac{\text{Area under the load – deflection curve up to } 3\delta}{\text{Area under the load – deflection curve up to } \delta}$$

$$I_{10} = \frac{\text{Area under the load – deflection curve up to } 5.5\delta}{\text{Area under the load – deflection curve up to } \delta}$$

$$I_{20} = \frac{\text{Area under the load – deflection curve up to } 10.5\delta}{\text{Area under the load – deflection curve up to } \delta}$$

The deflection values of 3δ , 5.5δ and 10.5δ are chosen using elastic perfectly plastic behaviour as the datum as shown in figure 2.3.4. Residual loads at specified deflections, the corresponding residual strengths and determination of specimen toughness based on the area under the load-deflection curve up to a prescribed deflection and the corresponding equivalent flexural strength ratio are also obtained.

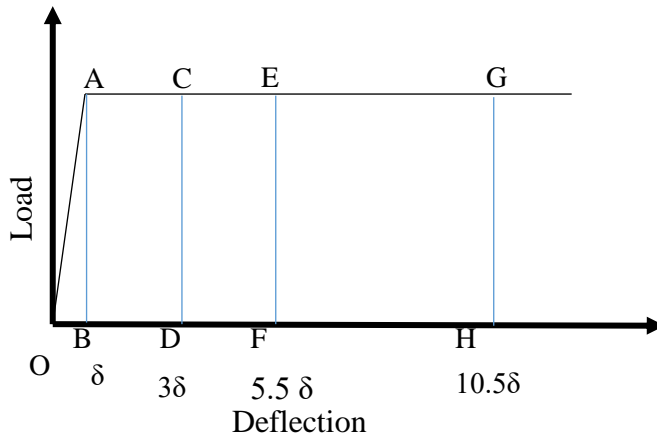


Fig 2.3.4 Definition of Toughness Indices for Elastic-Plastic Material Behaviour

$$I_5 = \frac{OACD}{OAB} \quad I_{10} = \frac{OAEF}{OAB} \quad I_{20} = \frac{OAGH}{OAB}$$

2.3.3 JSCE SF24

Ductility is commonly measured using the Japanese standard test method JSCE-SF4, which used beams in a third-point loading arrangements. The JSCE SF 24 provides a measure of flexural toughness from the measured load-deflection response as shown in figure 2.3.5. The value of toughness, T_{JSCE} is determined as the area under the load-deflection curve up to a deflection equal to $\text{span}/150$. Toughness factor, F_{JSCE} is derived from the value of toughness. F_{JSCE} has the unit of stress such that its value indicates, in a way, the post-matrix cracking residual strength of the material when loaded to a deflection of $\text{span}/150$. The chosen deflection of $\text{span}/150$ for its calculation is purely arbitrary and is not based on serviceability considerations.

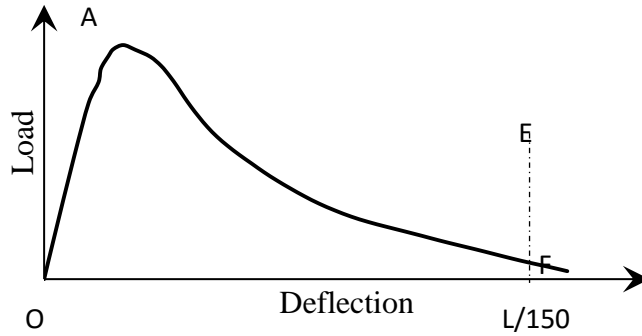


Fig. 2.3.5 Definitions of JSCE Toughness and Toughness Factor

Toughness

$$T_{JSCE} = AREA_{OAEFO}$$

Toughness factor

$$F_{JSCE} = \frac{T_{JSCE} L}{BH^2 w_{tb}}$$

where, F_{JSCE} is Toughness factor or Equivalent flexural strength and w_{tb} is averaged over the prescribed deflection.

The equivalent flexural strength as defined by the JSCE-SF4 for a deflection of 3 mm, the $R_{e,3}$ value, a measure of the ductility, is the average load applied as the beam defects to 3 mm expressed as a ratio of the load to first crack. This measure is also known as the equivalent flexural strength as denoted as $f_{e,3}$ has been calculated as

$$f_{e,3} = \frac{P_{mean,150} \times l}{bd^2}$$

where $P_{mean,150}$ is the area under the load-deflection curve divided by the limit deflection of 3 mm and l , b and d are the span, width and depth of the prism, respectively (i.e. 450 mm, 150 mm and 150 mm, respectively).

2.3.4 RILEM TC 162-Test Procedure

Centre point bend tests are performed on notched specimens with a nominal size (width and depth) of 150 mm and a minimum length of 550 mm. Net deflection at mid-span excluding extraneous deformations is increased at a constant rate of 0.2 mm/min.

This test method is used to determine the limit of proportionality, equivalent flexural tensile strength, residual flexural strength which identify the material behaviour at selected deflection or CMOD.

Limit of proportionality

$$f_{ct,fl} = \frac{3F_L L}{2bh_{sp}^2}$$

where,

$f_{ct,fl}$ is the LOP (N/mm²)

F_L is the load corresponding to LOP (N)

L is span of specimen (mm)

b is the width of specimen (mm)

h_{sp} is the distance between the tip of notch and top of the specimen (mm)

Residual flexural Tensile Strength

$$f_{R,i} = \frac{3F_i L}{2bh_{sp}^2}$$

Where,

$f_{R,i}$ is residual flexural Tensile Strength corresponding with $CMOD = CMOD_j$ or $\delta = \delta_i$ ($i = 1, 2, 3, 4$) (N) and F_i is the load corresponding to with $CMOD = CMOD_j$ or $\delta = \delta_i$ ($i = 1, 2, 3, 4$)

2.3.5 UNI 11039-2 Test Procedure

UNI 11039-2 bending test is a four-point loading test on a prismatic beam. UNI test specifically prescribes the specimen absolute dimensions. The UNI test employs a notched beam with a specimen which is 150 mm deep, 150 mm wide and the span length is 450 mm. It is sawed at mid-span with a depth equal to 0.3 times the overall specimen depth (0.3d). The test is performed measuring the load P and the Crack Tip Opening Displacement (CTOD), at a rate of increase of the Crack Mouth Opening Displacement (CMOD), equal to 0.05 ± 0.01 mm/min. A schematic diagram of the UNI test setup is shown in figure 2.3.6.

The first-crack load which required subtracting the contribution due to matrix cracking is obtained by determining the value of CTOD corresponding to the peak load value obtained by performing four-point bending tests on plain concrete beams is determined ($CTOD_0$). The value of $CTOD_0$ can be assumed equal to $25 \mu\text{m}$.

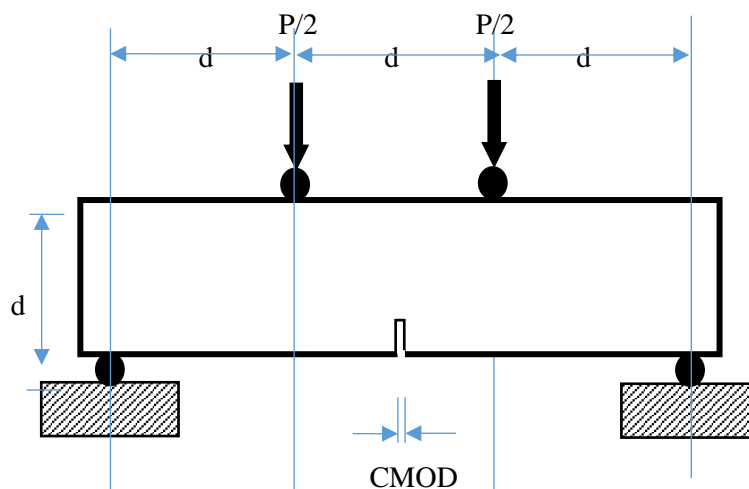


Fig.2.3.6 Schematic diagram of the UNI 11039 four-point bending test setup

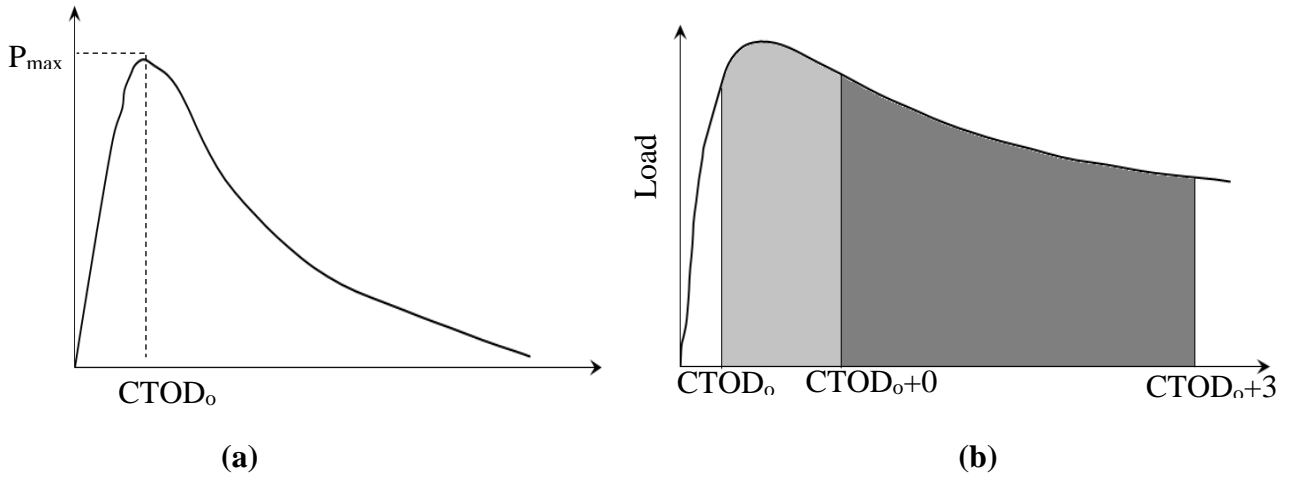


Fig.2.3.7 (a) Basic concrete load-CTOD, (b) Load-CTOD

The first-crack flexural strength is determined, according to UNI 11039, as follows:

$$f_{If} = \frac{P_{If}L}{b(h - a_0)^2}$$

where

L (mm) = span between supports;

b (mm) = specimen width (equal d);

h (mm) = specimen depth (equal d);

a_0 (mm) = notch depth;

P_{If} (N) is the load value corresponding to $CTOD_0$ for the FRC specimen.

The **first** and **second Material's ductility** indexes D_0 and D_1 , according to UNI 1039 [11] by means of the equivalent flexural strengths $f_{eq(0-0.6)}$ and $f_{eq(0.6-3)}$ (MPa), which denote SFRC ductility in a defined range of crack mean opening displacement. Ductility indexes D_0 and D_1 were derived by means of the following equations:

$$D_0 = \frac{f_{eq(0-0.6)}}{f_{If}} \quad D_1 = \frac{f_{eq(0.6-3)}}{f_{eq(0-0.6)}}$$

where $f_{eq(0-0.6)}$ is the equivalent strength (MPa) is calculated when the mean crack opening value is included between 0 and 0.6 mm, $f_{eq(0.6-3)}$ is the equivalent strength (MPa) calculated when the mean crack opening value is included between (0.6 and 3) mm, derived from the following relationships:

$$f_{eq(0-0.6)} = \frac{l}{b(h-a_1)} \cdot \frac{U_1}{0.6} \quad f_{eq(0.6-3)} = \frac{l}{b(h-a_1)} \cdot \frac{U_2}{2.4}$$

where U_2 and U_3 (10^{-3} J) are the area under load - $CTOD_m$ curve for $CTOD_{net}$ intervals equal to 0-0.6 mm and 0.6-3 mm respectively. Such area are approximately proportional to the energy dissipated in the mean crack opening intervals considered.

2.3.6 EN 14651 Test Procedure

Centre point bend tests are performed on notched specimens with a nominal size (width and depth) of 150 mm and a length L so that $550 \text{ mm} < L < 700 \text{ mm}$. Test is performed by increasing the *CMOD* at a constant rate of 0.05 mm/min up to a *CMOD* value of 0.1 mm and at a rate of 0.2 mm/min up to a *CMOD* value of 4 mm. This European standard specifies a method of measuring a flexural tensile strength of metallic fibered concrete on moulded test specimen. The methods provided for the determination of the limit of proportionality (LOP) and of a set residual flexural tensile strength values

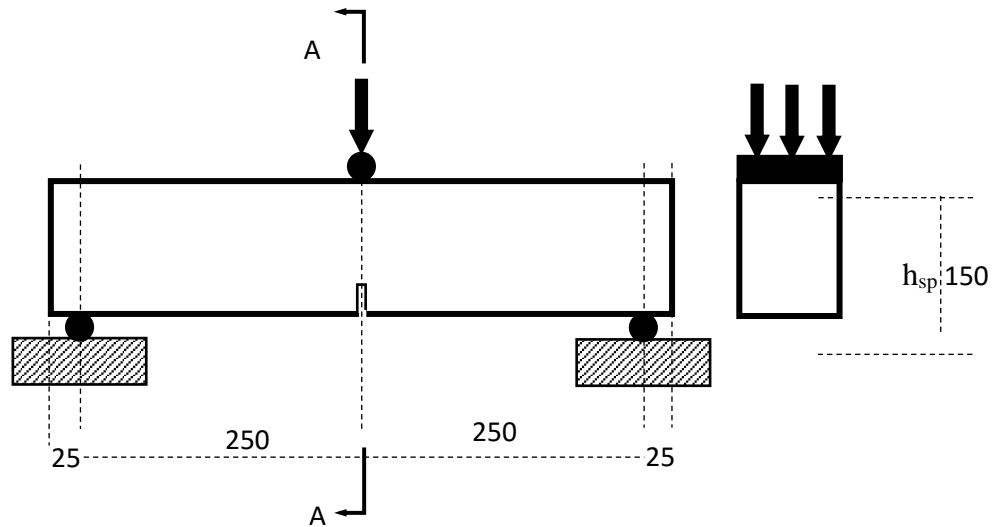


Fig 2.3.8. Typical arrangement of measuring *CMOD*

Limit of proportionality

$$f_{ct,fl} = \frac{3F_L L}{2bh_{sp}^2}$$

Where,

$f_{ct,fl}$ is the LOP (N/mm²)

F_L is the load corresponding to LOP (N)

L is span of specimen (mm)

b is the width of specimen (mm)

h_{sp} is the distance between the tip of notch and top of the specimen (mm)

Residual flexural Tensile Strength

$$f_{R,i} = \frac{3F_i L}{2bh_{sp}^2}$$

Where,

$f_{R,i}$ is Residual flexural Tensile Strength corresponding with $CMOD = CMOD_j$ or $\delta = \delta_i$ ($i = 1, 2, 3, 4$) (N) and F_i is the load corresponding to with $CMOD = CMOD_j$ or $\delta = \delta_i$ ($i = 1, 2, 3, 4$)

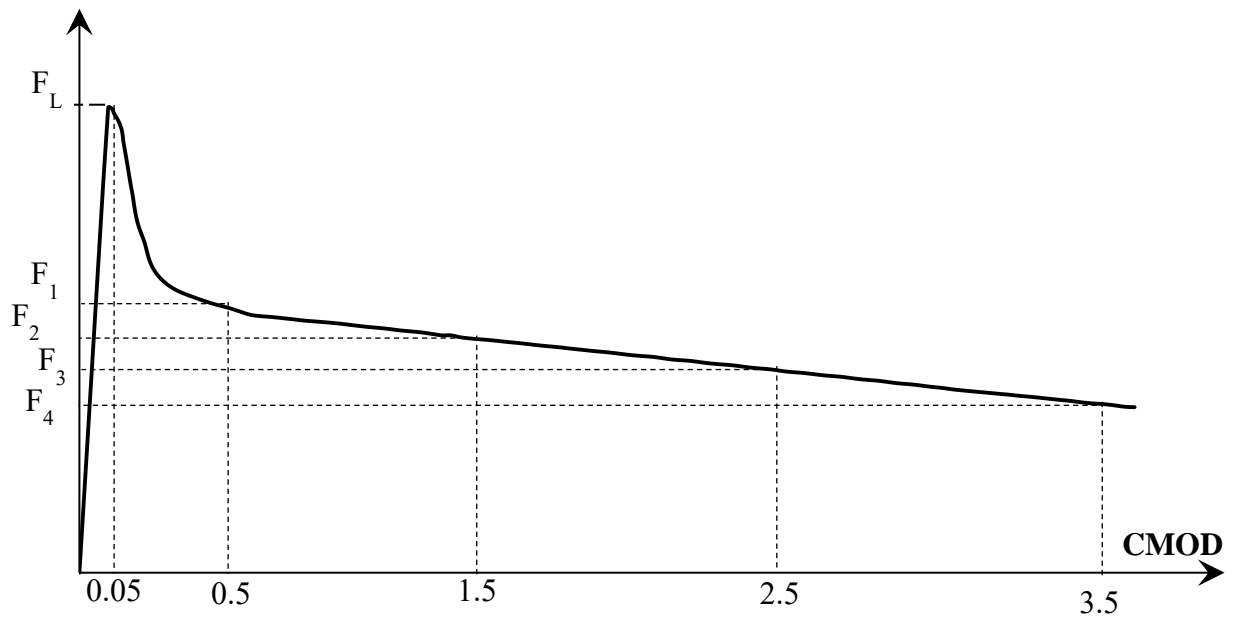


Fig 2.3.9 Load-CMOD and F_j ($j=1,2,3,4$)

Toughness index is used to measure the energy absorbed in deflecting a beam at specified amount, being the area under a load–deflection curve in three-point bending. A measure of toughness index from the results of the EN 14651 test has been proposed as the ratio of the area under the force-CMOD curve up to CMOD of 4 mm for the FRC specimen over that for the plain-concrete specimen

Chapter 3

Materials and Methods

3.1 Introduction

This section presents the details of materials and experimental methods used in the study. The types of specimens, mix proportions and test methods employed are presented.

3.1.1 Cement

In the present investigation, commercially available 53 Grade ordinary Portland cement was supplied by ACC Cement with Specific Gravity of 3.1 and Fineness modulus of 325 m²/kg was used for all concrete mixtures.

3.1.2 Fly Ash

Fly ash conforming to the requirements of IS 3812 and IS 1727 (1967) supplied by NTPC with Specific gravity of 2.5 and fineness modulus of 320 m²/kg was used as supplementary cementitious material in concrete mixtures.

3.1.3 Aggregates

Crushed sand with a specific gravity of 2.67 and fineness modulus of 2.83 was used as fine aggregate and crushed granite of specific gravity of 2.63 was used as coarse aggregate. Two different classes of coarse aggregate fractions were used: 10-4.75 mm and 20-10 mm.

3.1.4 Synthetic Fibers

3.1.4.1 Macro synthetic Fibers

FibreTuffTM Monofilament structural polypropylene fibers of 60 mm length manufactured by Bajaj Reinforcements were used in this study. The fibers are made of a modified polyolefin and have a modulus of elasticity between 6 GPa to 10 GPa and tensile strength between 550 and 640MPa. The fibers are continually embossed surface anchorage mechanism to enhance bond. A photograph of the fibers used in this study is shown in Fig 3.1



Fig 3.1 FibreTuffTM Monofilament structural polypropylene fiber

3.1.4.1 Micro Synthetic Fibers

Fibrillated micro polypropylene fibers of 20 mm length and of 1050 denier manufactured by Bajaj Reinforcements were used in this study. The fibers are made of a modified polyolefin

and have a modulus of elasticity between 6 GPa to 10 GPa and tensile strength between 550 and 640MPa. A photograph of the fibers used in this study is shown in Fig 3.2



Fig 3.2 Fibrillated micro polypropylene fiber

3.1.5 Admixture

Super plasticizer (Glenium) was used to increase the workability of freshly prepared fiber reinforced concrete.

3.2 Experimental program and Mix Proportions

Concrete mix design for the mix design procedure given in IS: 10262 was followed with minor modification for M35 grade. For a target mean strength of 43 MPa, two different water/cement ratios equal to 0.48 was considered (from Fig 2, curve E IS 10262-1982 for 53G). Taking into considerations, the minimum requirements for cement content in kg/m^3 of concrete for M35 as per IS 456-2000 as 300 kg/m^3 , cementitious content was fixed at 340 kg/m^3 . Using this, the water content was determined. In the concrete mixture fine aggregate were taken as 45% of the total aggregate volume fraction. The weights of fine and coarse aggregate were then calculated considering the specific gravities of coarse and fine aggregate.

The Concrete mixtures were produced at a constant water/Cement ratio of 0.48 and one control mixture and three different mixtures with different dosage of fiber were prepared. The control mixture contained no fiber. Concrete mixtures labelled 0.44P, 0.66P and 0.88P were produced with different dosage of polypropylene fiber 4 kg/m^3 , 6 kg/m^3 and 8 kg/m^3 by volume. Micro polypropylene fibres were added at 0.2 % and 0.3% to the above mixtures and were named as 0.44P+0.2p, 0.44P+0.3p, 0.66P+0.2p, 0.66P+0.3p, 0.88P+0.2p, 0.88P+0.3p respectively. The design mixtures are presented in Table 4.8 and the final batch weights of the different mixes for one cubic meter of concrete are presented in Table 3.1.

Table 3.1 Summary of weight proportion of the various mixes

Materials(kg/m^3)	C1	0.44P	0.44P+0.2p	0.44P+0.3p	0.66P	0.66P+0.2p	0.66P+0.3p	0.88P	0.88P+0.2p	0.88P+0.3p
Polypropylene macro fiber	-	4	4	4	6	6	6	8	8	8
Polypropylene micro	-	-	1.82	2.73	-	1.82	2.73	-	1.82	2.73

fiber										
OPC 53 grade cement	200	200	200	200	200	200	200	200	200	200
Fly ash(pozzocrete 60)	140	140	140	140	140	140	140	140	140	140
Water/Cement Ratio	0.48	0.48	0.48	0.48	0.48	0.48	0.48	0.48	0.48	0.48
Admixture (%)	0.65	0.65	0.65	0.65	0.65	0.65	0.65	0.65	0.65	0.65
20 mm aggregates	508	508	508	508	508	508	508	508	508	508
10mm aggregates	508	508	508	508	508	508	508	508	508	508
Fine aggregates(robosand)	823	823	823	823	823	823	823	823	823	823
Water	163	163	163	163	163	163	163	163	163	163

3.2.1 Casting and Curing of Specimens

IS standard 150mm Cubes, 150mm X 300mm cylinder and 150 X 150 X 500 beams were cast from each mixture to evaluate compressive strength and toughness and ductility gain. Concrete was prepared using a drum mixer with a capacity of 0.25 m³. The ingredients were put into the mixer in the decreasing order of their sizes starting from 20mm aggregate to cement. Dry mixing of the aggregates and cement was done for two minutes and then water was added gradually in the rotating mixer and allowed to mix for 15 minutes. During the mixing process, the walls and bottom of mixer were scraped well to avoid sticking of mortar. After mixing, the slump was checked and noted down to ascertain the effects of differently proportioned blends on workability of concrete. Finally the fresh concrete was placed in oiled moulds and compacted properly in three layers, each layer being tamped 35 times using a tamping rod. After the initial setting of concrete, the surface of the specimen was finished smooth using a trowel. Immediately after casting, all specimens were covered with plastic covers to minimize moisture loss. The specimens were stored at room temperature about 25°C. Specimens were demoulded 24 hours after casting and kept in curing water tank.

3.3 Test Methods

An experimental program was designed to study the influence of fiber on the toughness and ductility. Each concrete mixture was evaluated with respect to Slump, compressive strength, and flexural tensile Strength of fiber reinforced concrete.

3.3.1 Slump

Slump was used to find the Workability of fresh concrete where the nominal maximum size of aggregate does not exceed 38 mm. slump cone was used to find the slump of the concrete as per the requirements of IS 1199-1959. Oil was applied on the base plate and interior surface of the slump cone. After that, Slump cone was attached to a base plate with screws and finally kept on the levelled surface. Immediately slump cone was filled with fresh concrete approximately one-quarter of height of the cone, each layer was tampered with the tampered rod 25 times. After compacting the top layer, mould and the base plate was cleaned with the clothes. Slump cone was Unscrewed from the base plate and removed immediately from the concrete by raising it slowly and carefully in a vertical direction. Finally slump cone of the base plate kept reverse position, height between the top of the mould and highest point of the concrete was measured with the scale. This height indicated the slump of the concrete.

3.3.2 Compression Strength Testing

A 2000kN digital compressive testing machine was used for determine the compressive strength of hardened concrete using 150 mm cubes as per the requirements of IS 516-1959. Before starting the test the weight of the sample was recorded. The plates of the machine were cleaned and the specimen was kept centrally between the two plates. Load was applied gradually on the specimen at a load rate of 5.2 kN/s up to failure. Once the sample was failed, the failure pattern was recorded and the compressive strength was calculated from the maximum load recorded in the test.

Cylinders were tested using a servo-hydraulic testing machine to obtain the stress-strain response. The displacements were increased at a rate of 0.05 mm/min. Two LVDTs with a gauge length of 60 mm were used to measure the displacement on the cylindrical specimens. The LVDTs were attached to rings which were mounted 120 mm from the top and the bottom of the specimen. These aluminum ties were able to support the measuring devices, to allow lateral deformations when they occurred, and did not confine the specimens. The data acquisition and signal control were carried out using control unit.

3.3.3 Four-point-bending test

Flexural testing machine with servo hydraulic closed-loop test machine was used to determine the toughness and ductility as per ASTM C1609-M10 and EN 14651.

3.3.3.1 ASTM C 1609 Procedure

This test method utilizes 150 x 150 x 500 mm beams tested on a 450 mm span. The testing was done using a servo-controlled test machine where the net deflection of the centre of the beam is measured and used to control the rate of increase of deflection. Testing was done as per ASTM C1609 to capture the portion of the load-deflection curve immediately after the first-peak. The loading and specimen support system applied third-point loading to the specimen without any eccentricity or torque. The fixtures used in the testing allowed free rotation on their axes. Linear variable displacement transducers (LVDT) were used to ensure accurate determination of the net deflection at the mid-span. Rectangular jig, surrounding the specimen was clamped to it at mid-depth directly over the supports. Two displacement transducers were mounted on the jig at mid-span, one on each side, to measure deflection through contact with appropriate brackets attached to the specimen. The average of the measurements represented the net deflection of the specimen exclusive of the effects of seating or twisting of the specimen on its supports. The loading was applied such that the net deflection of the specimen increased at a constant rate of 0.04 mm/ min up to a net deflection of $L/900$. Thereafter, i.e., beyond $L/900$ and up to a deflection of $L/150$, loading rate was kept constant at 0.08 mm/min. Beyond $L/150$ and up to the end point deflection, the rate of loading was kept constant at 0.16 mm/min. The testing was continued till the specimen failed.

3.3.4 Three-point-bending test (For notch beam)

The test procedure adopted was consistent with the guidelines given by EN 14651:2005 and 150 X 150 X 500 (height X width X length) mm³ prismatic specimens were tested in the

three-point bending configuration. A notch of 25mm depth was introduced at the mid-span using a circular saw as per the guidelines given in EN 14651:2005. The flexure test was conducted in crack mouth opening displacement control by increasing the CMOD at a prescribed rate. The corresponding deflection of the beam was measured using the rectangular jig clamped to the specimen at mid-depth directly over the supports. The testing machine had sufficient stiffness to avoid unstable unloading phenomena in the softening branch of the load-CMOD curve. The notched beam was tested with a span equal to 450 mm during the tests, the rate of increase of the CMOD was controlled in two stages, at 0.05 mm/min for CMOD less than 0.1 mm and at 0.2 mm/min for CMOD greater than 0.1 mm. All the tests were ended when the CMOD reached a value of 3.5 mm.

Chapter 4

Results and Discussions

4.1 Introduction

Improvements in mechanical properties on using fibers are a result of crack closing stresses provided by fibers which have a direct influence on the ductility, load carrying capacity and toughness. The improvements depend upon the crack closing stresses generated by the fibers. The efficiency of fibers depend the ability of fibers to contribute during localization and propagation of a crack. For a given fiber type, fiber volume fraction is a primary variable which controls the properties of the composite.

Preliminary experimental results of compression tests of cube and flexural response of beams reinforced with Hybrid-synthetic fibers at 3, 7, 28 days are presented in this chapter. Influence of the hybrid fibers on the flexural response as a function of age is investigated using un-notched and notched beams. The results of the flexural response are interpreted in terms of the influence of fibers on crack propagation in fiber reinforced concrete.

4.2 Compressive strength

The mean 28 day compressive strength from standard 150 mm cubes for control and synthetic FRC obtained are tabulated in Table 4.1. The observed standard deviation in the compressive strength values from the same batch are the expected variations produced by sample preparation, and due to variations in the actual air contents of the hardened concrete and the differences in their unit weights. While there is an increase in the compressive strength, the variation of compressive strength with fiber content does not show a clear trend with fiber volume fraction. There is a small increase in the compressive strength at 28 days of age on adding micro polypropylene to the macro polypropylene ranging from 0.44 % to 0.88%. While the mean compressive strength at a fiber volume content of 0.66% is higher than the mean compressive strength of the control mix, the associated increase in the standard deviation at this fiber volume fraction does not permit for a making an inference about statistical significance of the observed increase in strength. Thus it may be concluded that there is no statistically significant change in the 28-day compressive strength in HFRC for fibers at quantities up to 0.88 % by volume.

The mean compressive strength along with their standard deviation from standard 150 mm cubes for control and synthetic FRC obtained are tabulated in Table 4.2. It has been clearly observed that the compressive strength of the HFRC has increased by age. But there is no significant finding on the compressive strength with the presence of Synthetic fibres.

Table 4.1 Mean Compressive strength (Mpa) (Standard Deviation) Results

Specimen	Days		
	3 day	7day	28 day
Control			34.6 (1.05)
0.44 % PP			34.4 (0.82)
0.44% PP+ 0.2% p	15.83 (1.06)	21.06 (0.6)	34.9 (1.08)
0.44% PP+ 0.3% p			35.3 (1.76)
0.66% PP	16.06 (1.01)	20.56 (0.38)	38 (2.27)
0.66% PP+ 0.2% p			30.06(0.61)
0.66% PP+ 0.3% p			35.6 (1.2)
0.88% PP			35.6 (0.54)
0.88% PP+ 0.2% p			31.98 (1.00)
0.88% PP+ 0.3% p			32.03 (0.87)

4.3 Flexural test results as per ASTM C 1609 (For Un Notch beam)

4.3.1 Later age studies

The average load-deflection response of the control and Synthetic polypropylene fiber reinforced concrete beams are shown in Figures 4.3.1 (a). All beams, both control and FRC exhibit nonlinearity in the lead response immediately following the initial linear response, before peak load. The failure in both control and FRC beams was due to the formation of a single crack in the constant moment region of the beam. Following the peak load, which is associated with the localization of a single crack, while the control beams failed suddenly in a brittle manner the FRC specimens exhibit significant post-peak response indicating load carrying ability even after the formation of a crack. The brittle failure in a control specimen which resulted in splitting the specimen in two pieces is shown in Figure 4.3.2 (a). A photograph of the FRC specimen with 0.66% fibers taken at a deflection of 4 mm with a visible crack in the constant moment region is shown in Figure 4.3.2 (b) and (c). The fibers crossing the crack are shown in the inset of the figure. Therefore, the fibers are responsible for preventing the brittle failure and providing load carrying capacity. There is also an increase in the post-peak load carrying capacity with the addition of fibers. The beams with 6 kg/m³ show a prominent hardening response following the initial drop after peak load. FRC beams indicate residual load carrying capacity up to a deflection 3 mm and shows a decrease in load carrying capacity after a deflection of 3 mm.

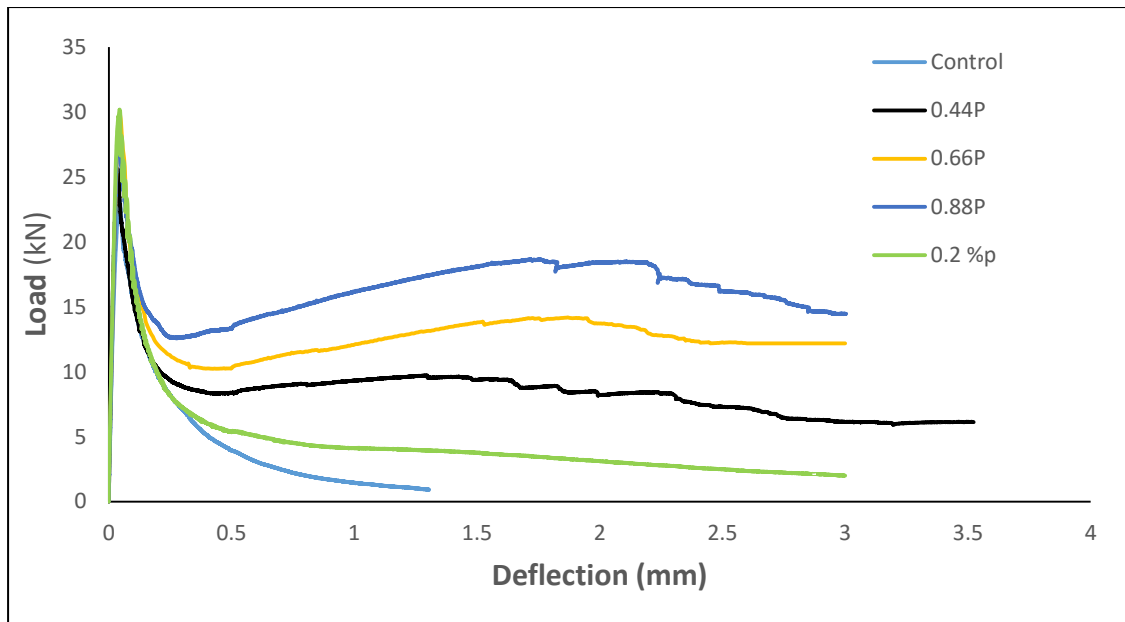


Figure 4.3.1: Load vs Displacement curve for Control and fiber reinforced concrete at different fiber volume fractions

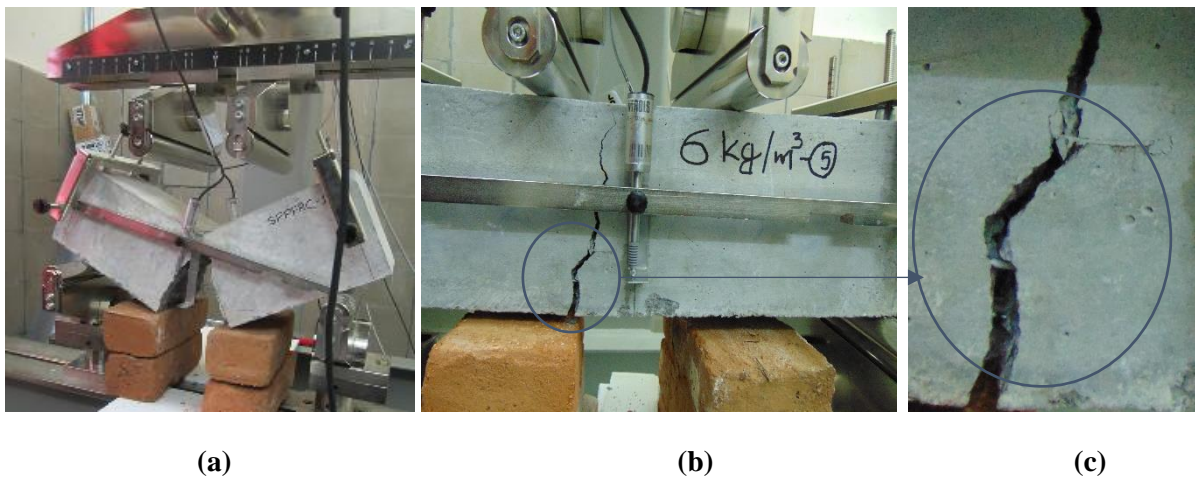
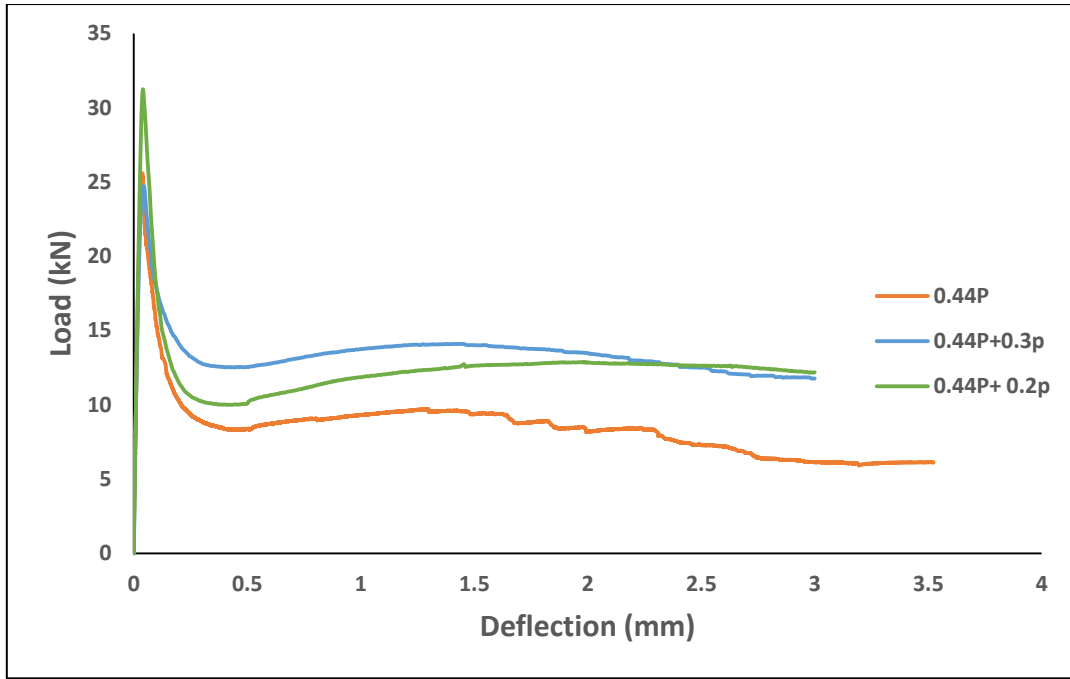
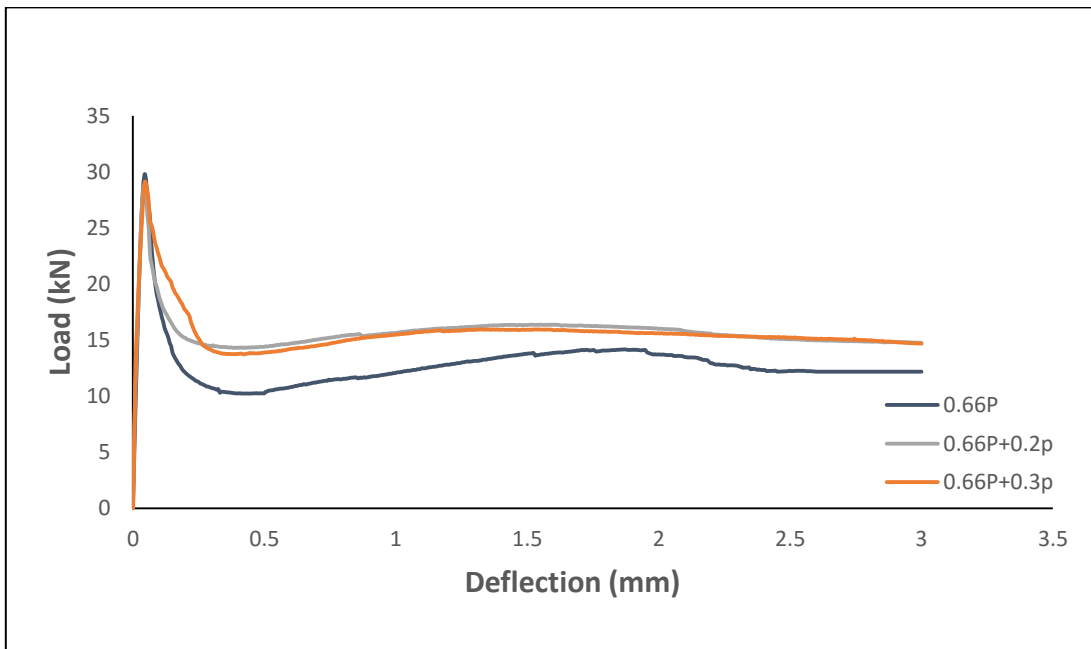


Figure 4.3.2: Failure of beam (a) Control specimen (b) SPFRC specimen (c)

The average load-deflection response of the Hybrid Synthetic fiber reinforced concrete beams are shown in Figures 4.3.3(a) through 4.3.3 (c). Micro Polypropylene fibres at 0.2 % and 0.3 % has been added to the FRC containing macro Polypropylene fibres at 0.44 % , 0.66 % , 0.88 % by volume. There is a clear increase in the post-peak load carrying capacity with the addition of micro synthetic fibers.



(a)



(b)

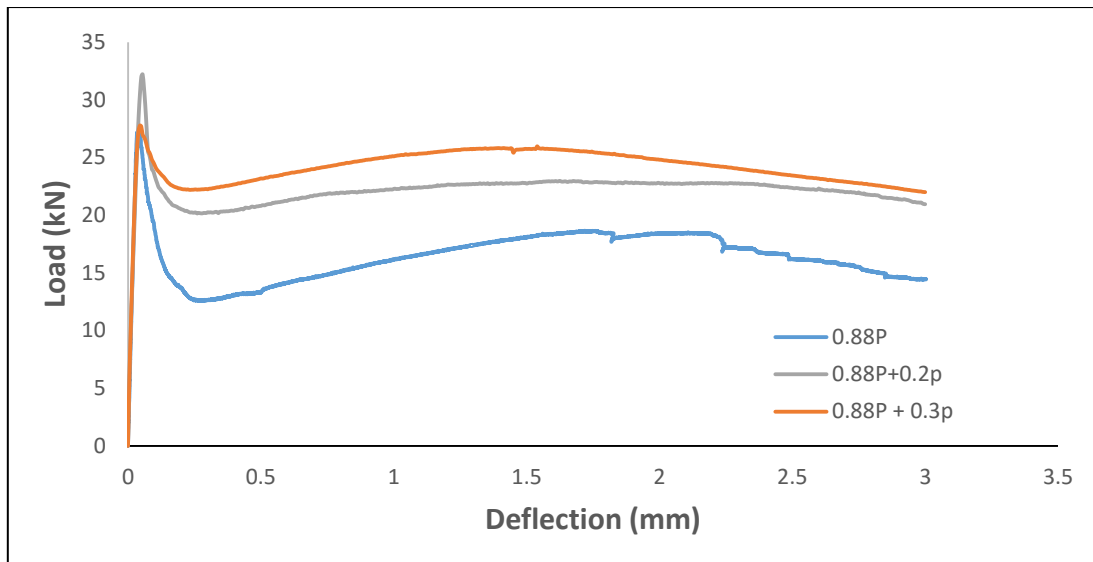
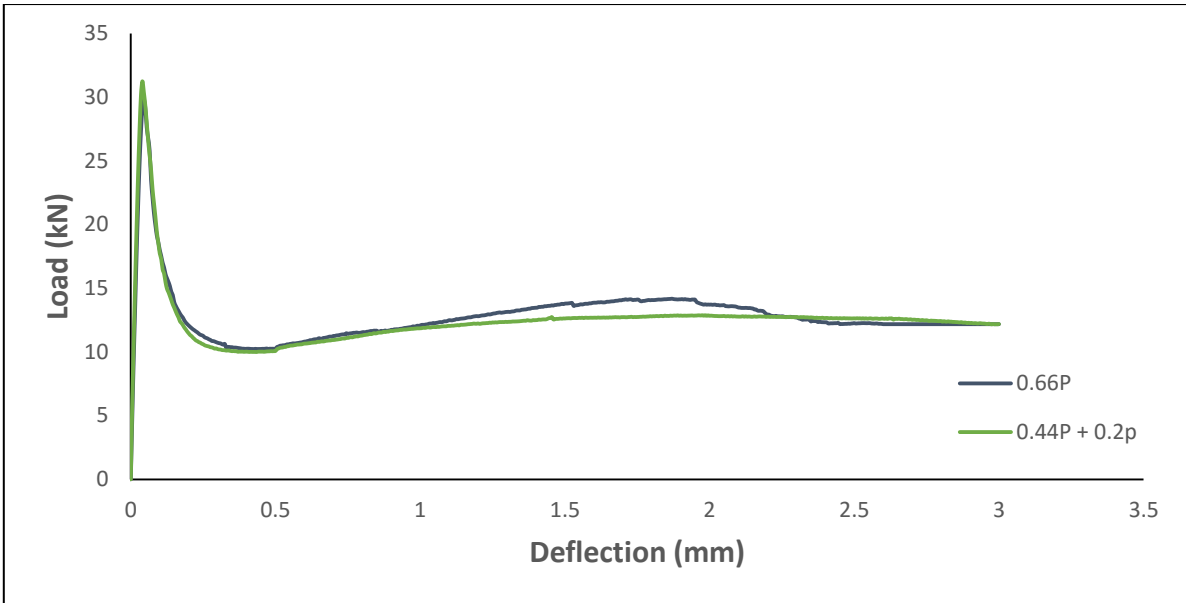


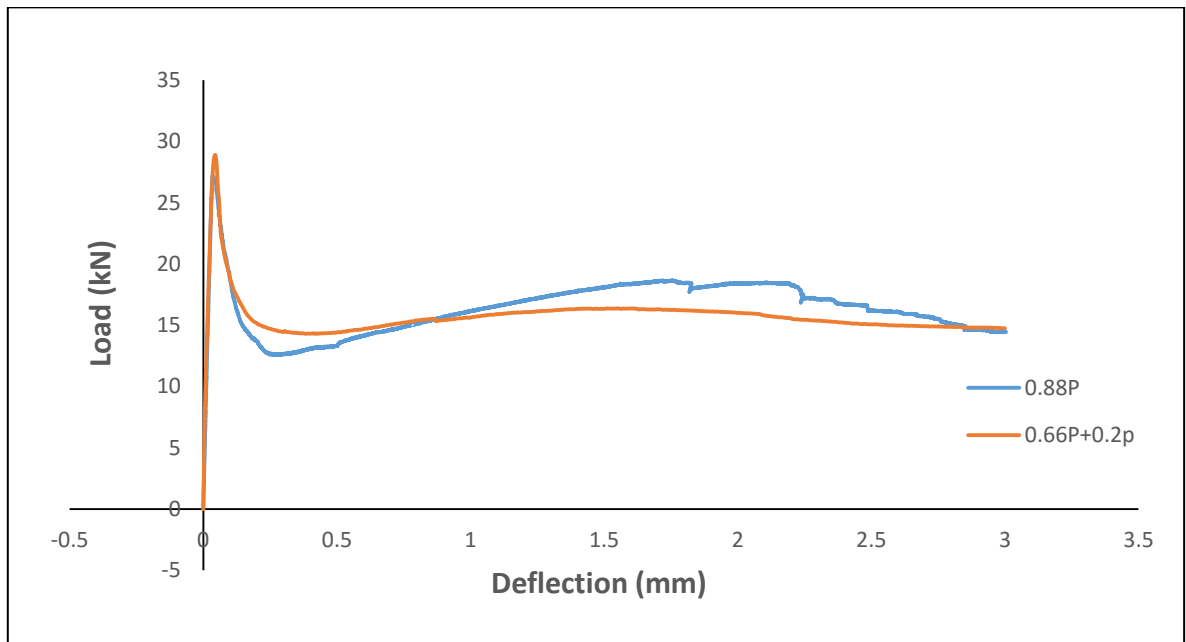
Figure 4.3.3: Load vs Displacement curve for Hybrid fiber Reinforced concrete on adding 0.2 % and 0.3 % Micro Polypropylene fibers to different Macro fibre volume fractions (a) 0.44 % P (b) 0.66 % P (c) 0.88 % P

The load response of FRC in flexure can be delineated in terms of three distinct stages, each associated with a different mechanism of resistance. The first stage consists of the pre-peak load response, where fibers play an insignificant role. Following localization, the initial part of post peak associated with crack propagation in the cementitious matrix is the second stage. The role of fibers becomes significant in determining the end of the second stage, where the local minimum is achieved. The local minimum in the load can be identified as the crack arrest load (CAL). Following CAL, the hardening response associated with the fiber pullout response is the third stage in the flexural response of FRC. From the results presented in Figures 4.3.1, there is an increase in the CAL with an increase in the macro synthetic fiber volume content. The same trend is observed in Figures 4.3.3. There is an increase in the CAL on adding micro synthetic fibres to the macro synthetic fibres.

A comparison of the Load response for the same volume fraction of fibres for HFRC and SFRC is shown in Figure 4.3.4.a and Fig 4.3.4b. The fiber volume content of both mixtures is approximately equal to 0.66 % and 0.88 %. It is observed that for the same total volume fraction of fibers, the load responses from both the Macro Synthetic fibers and hybrid blend of micro and macro fibers are nominally identical at higher deflection. Hybrid FRC shows a higher resistance for a given deflection in the post-peak load response immediately after peak load. This suggests a synergy in the load response of macro polypropylene fibers on using micro polypropylene fibers.



(a)



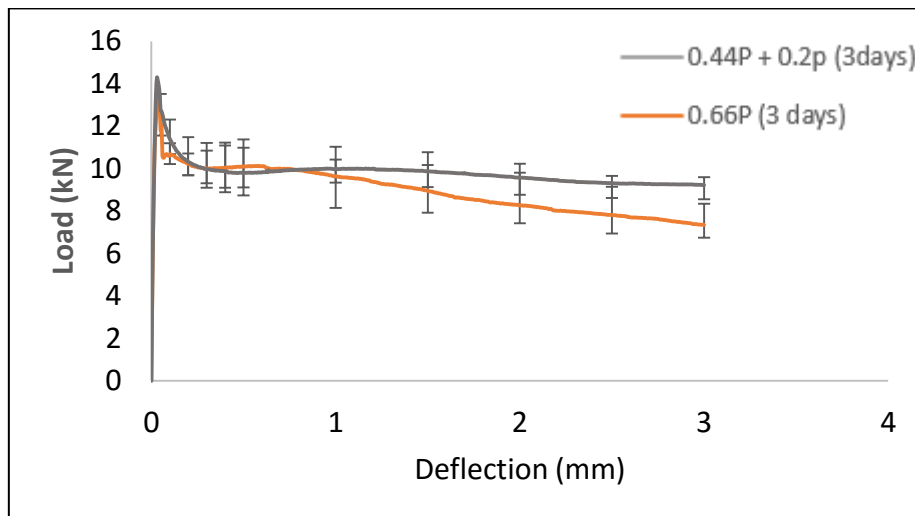
(b)

Figure 4.3.4: Comparison of Load vs Displacement curve for SPFRC and HyFRC (a) 0.66 % (b) 0.88%

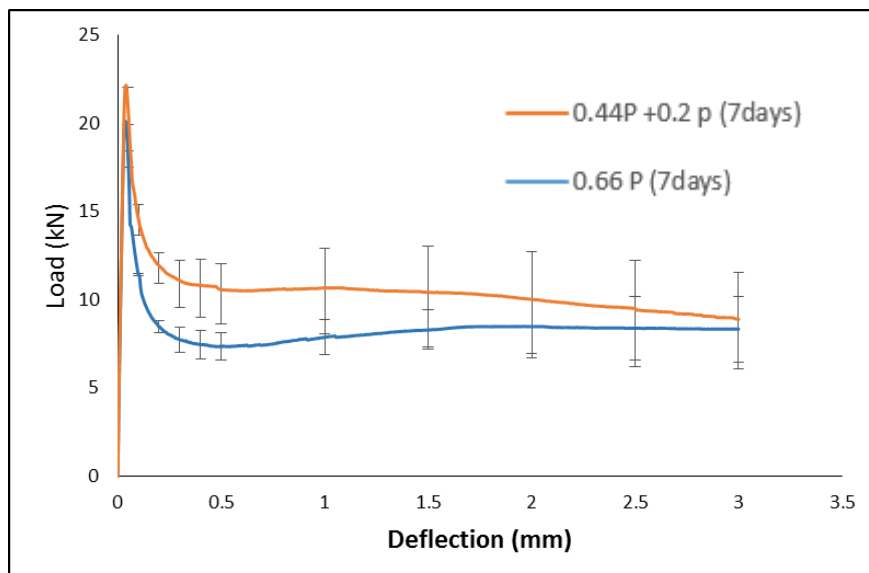
4.3.2 Early age Studies

A comparison of the Load response for the same volume fraction of fibres for HFRC and SFRC at 3 days and 7 days of age is shown in Figure 4.3.5.a and Fig 4.3.5b. It is observed that the matrix strength also increases by the presence of micro fibres at early age resulting in the higher Modulus of Rupture (MOR). A clear increase in the first peak (MOR) which is mainly due to the matrix strength is observed in the flexural test at 3 days as well as 7 days. HFRC shows a better flexural response for all the deflections. This suggests synergy is more in the load response of

macro polypropylene fibers on using micro polypropylene fibers at early age than the later age.



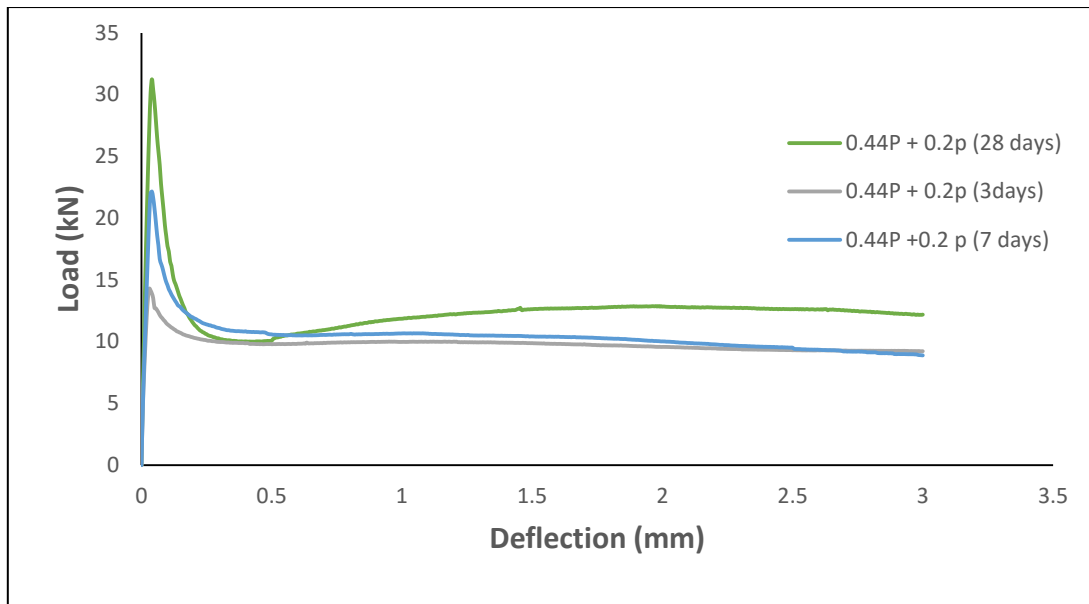
(a)



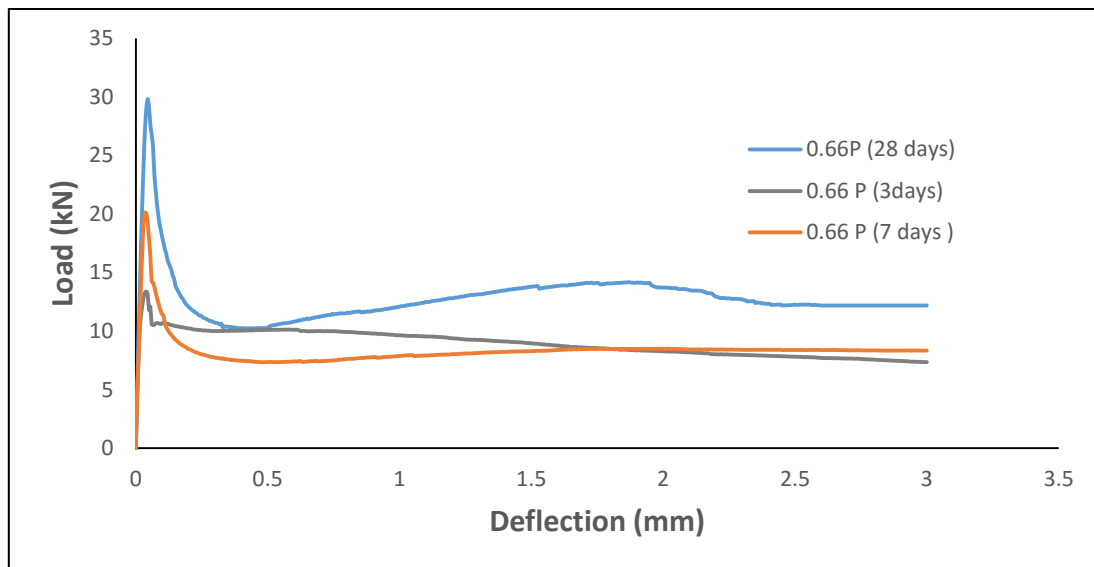
(b)

Figure 4.3.5: Comparison of Load vs Displacement curve for SPFRC and HFRC at 0.66 % volume fraction of fibers (a) 3 days (b) 7 days

Flexural response of the HFRC and SPFRC at different age is shown in the Fig 4.3.6 a and Fig 4.3.6b respectively. It is clearly observed that matrix strength is increasing by age resulting in better MOR and pull out resistance of the fibres.



(a)



(b)

Figure 4.3.6: Comparison of Load vs Displacement curve at 3, 7, 28 days (a) HFRC (b) SFRC

4.4 Flexural test results as per EN 14651-2005 (notched beam)

4.4.1 Later Age Studies

The average load-CMOD response for the control and the SPFRC specimens are shown in Figure 4.4.1. The behaviour from the notched beams is nominally similar to the observed response from unnotched beams. The control specimens exhibit a steady decrease in the post-peak load carrying capacity with an increase in CMOD following a non-linear pre-peak response up to peak load. Use of CMOD control allowed for obtaining the entire post peak response in a controlled manner. The post-peak softening response is associated with unstable crack growth following localization. The initiation and propagation of crack from the notch in

SPFRC leads to a 3-stage response observed earlier in the case of unnotched specimens. The variations in the peak load are found to be within the range of experimental scatter for each suggesting that the fibers do not influence the peak load. Further, immediate post-peak softening response after peak load is also identical for control and SPFRC. After peak load, the decrease in the load with increasing CMOD is produced by the increasing compliance associated with cracking in the matrix. The initial drop in the load in the post-peak softening is not influenced by the presence of fibers. The influence of larger number of fibers across the crack results in a significant deviation from the load response with increasing CMOD for the SFRC when compared with the control. At any CMOD, the SFRC supports a higher load when compared with control. The CMOD response indicates the contribution of fibers in the post-peak softening more sensitively than evident in the load deflection response of un-notched specimens. The distinctive crack arrest loads for SPFC and the hardening responses associated with increased resistance provided by pullout of fibers is clearly identified in the responses. The load-CMOD responses for control and different SFRC specimens are shown in Figure 4.4.1.

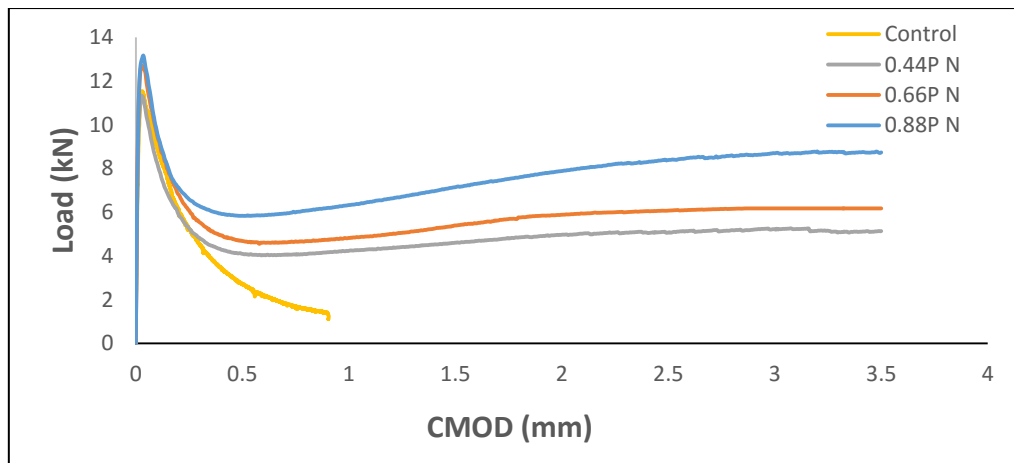
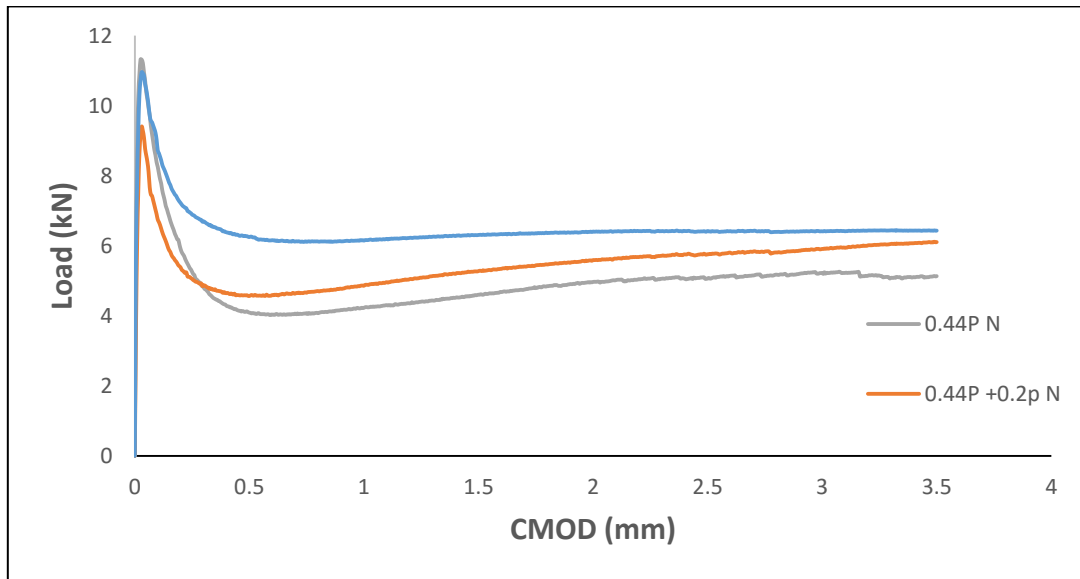


Figure 4.4.1: Load vs CMOD curve for Control and Synthetic fiber reinforced concrete at different fiber volume fractions

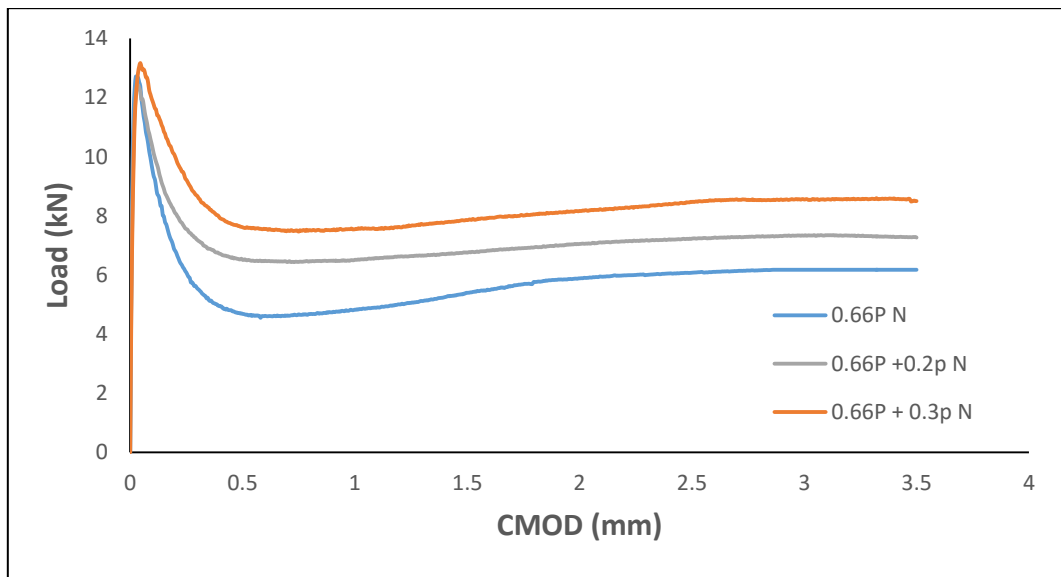
The presence of fibers results in an increase in the load carrying capacity with increasing crack opening after an initial load drop in the immediate post-peak load response following the peak load. While the fiber volume content does not appear to influence the peak and the immediate post-peak load response on increasing crack opening, the influence of the fiber volume is evident at a smaller value of crack opening displacement where the load recovery starts. The larger fiber volume produces a load recovery at a smaller value of crack opening. There is also a higher load achieved during the load recovery on increasing the fiber volume.

The average load-CMOD response of the Hybrid Synthetic fiber reinforced concrete beams are shown in Figures 4.4.2(a) through 4.3.3 (c). Micro Polypropylene fibres at 0.2 % and 0.3 % has been added to the SFRC having macro Polypropylene fibres at 0.44 % , 0.66 % , 0.88 % by volume. There is a clear increase in the post-peak load carrying capacity with the addition of micro synthetic fibers. Micro fibers has increased the pull out resistance of the macro fibres there by increasing the flexural strength of the concrete. The post peak response has been

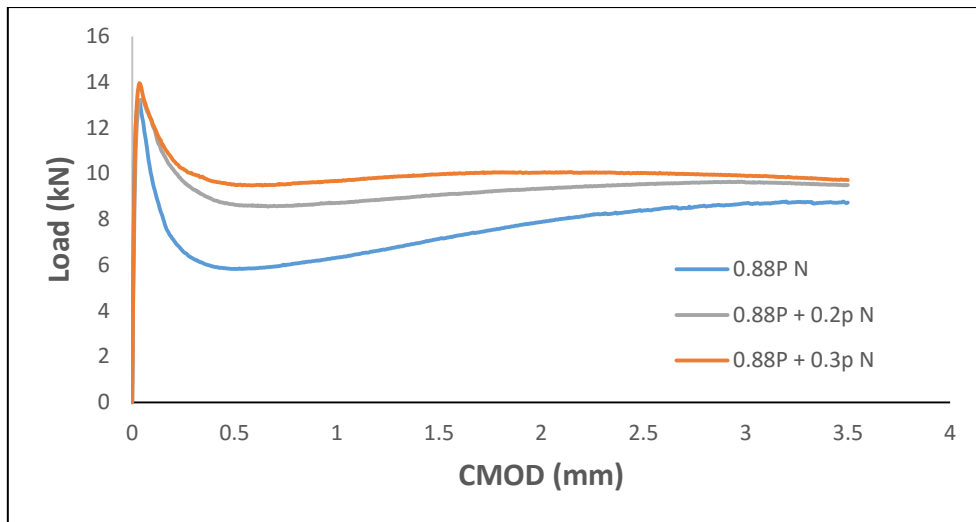
significantly improved on adding micro fibres to the macro fibres. This is the same trend which has been found with Un Notched specimens



(a)



(b)

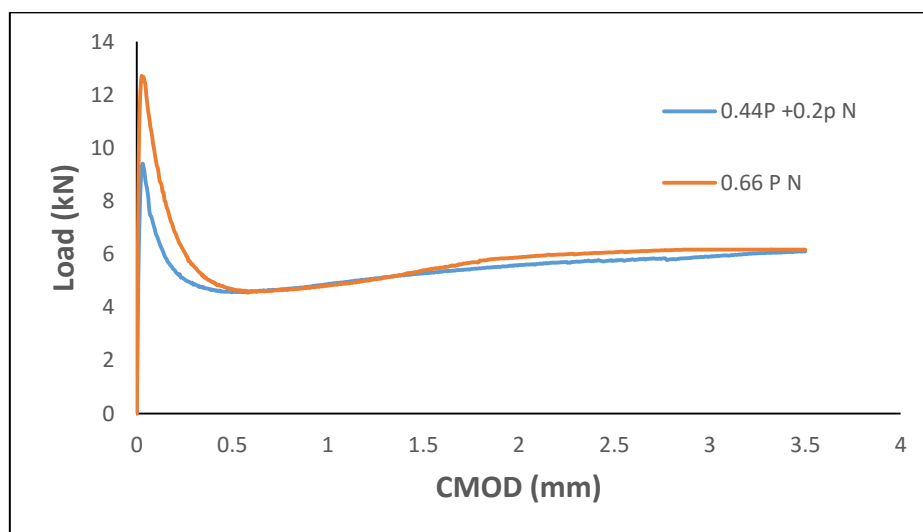


(c)

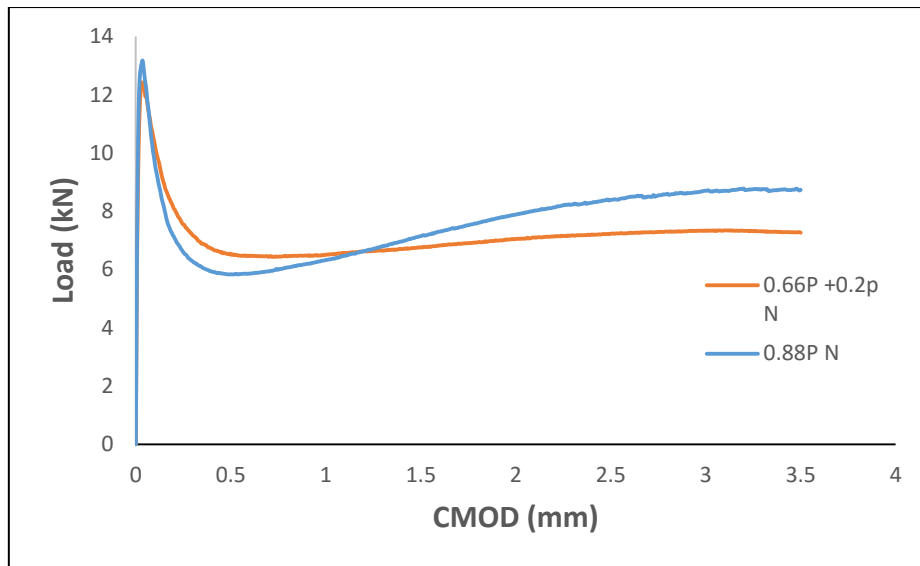
Figure 4.4.2: Load vs CMOD curve for Hybrid fiber Reinforced concrete on adding 0.2 % and 0.3 % Micro Polypropylene to different Macro fiber volume fractions (a) 0.44 % P (b) 0.66 % P (c) 0.88 % P

So on increasing the fiber volume, increases the resistance to crack opening, and thereby provides an earlier deviation from the descending portion of the load response seen in control specimens. Thus at larger volume fractions, the fibers are effective at a smaller crack opening.

It has been observed that for the same volume fraction of fibres, HFRC has shown more resistance to crack opening than SFRC at smaller deflections. A comparison of the Load response for the same volume fraction of fibres for HFRC and SFRC is shown in Figure 4.4.3.a and Fig 4.3.4b. The fiber volume content of both mixtures is approximately equal to 0.66 % and 0.88 %. It is observed that for the same total volume fraction of fibers, the load responses from both the macro synthetic fibers and hybrid blend of micro and macro fibers are nominally identical for smaller volume fraction (0.66%).HFRC has shown a better load carrying capacity at small crack opening and SFRC at larger crack openings. (Fig 4.3.3 b).



(a)

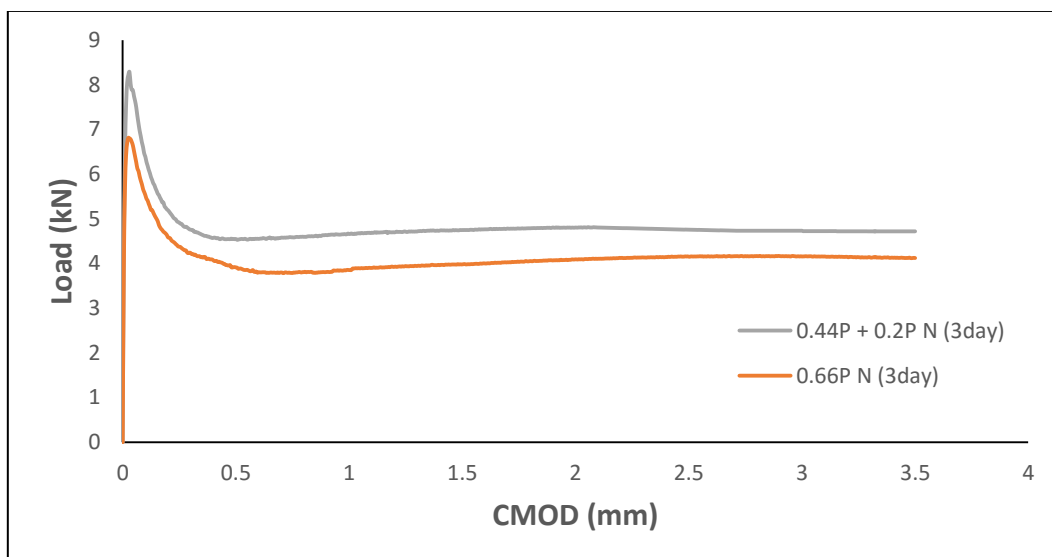


(b)

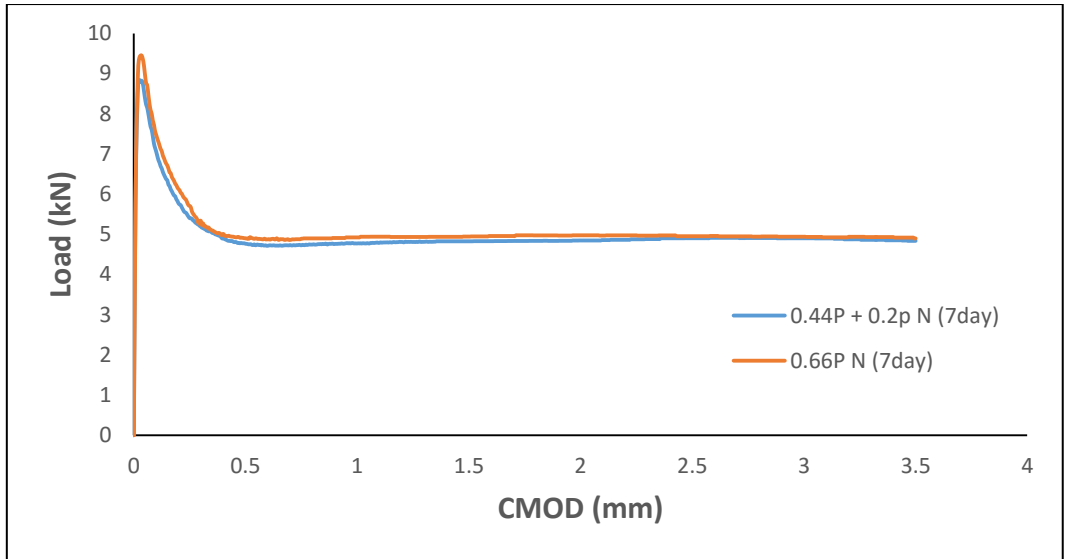
Figure 4.4.3: Comparison of Load vs CMOD responses for SPFRC and HyFRC (a) 0.66 % (b) 0.88%

4.4.2 Early Age Studies

A comparison of the Load CMOD response for the same volume fraction of fibres for HFRC and SFRC at 3 days and 7 days is shown in Figure 4.3.5.a and Fig 4.3.5b. We cannot infer any from the first peak in case of notched specimens HFRC has shown a better post peak response for all crack opening. This suggests synergy is more in the load response of macro polypropylene fibers on using micro polypropylene fibers at early age than the later age.



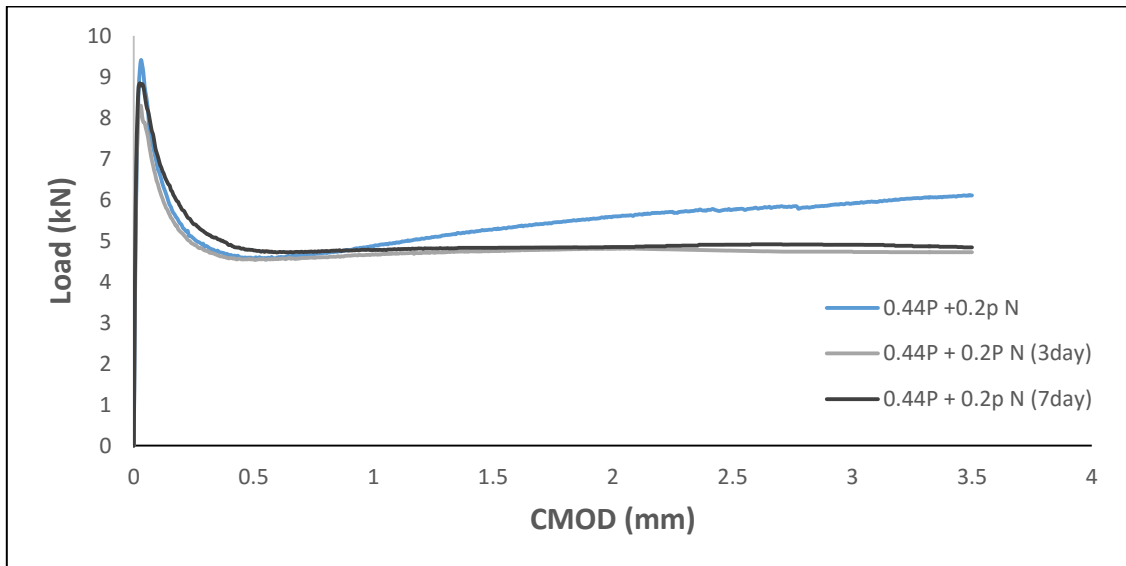
(a)



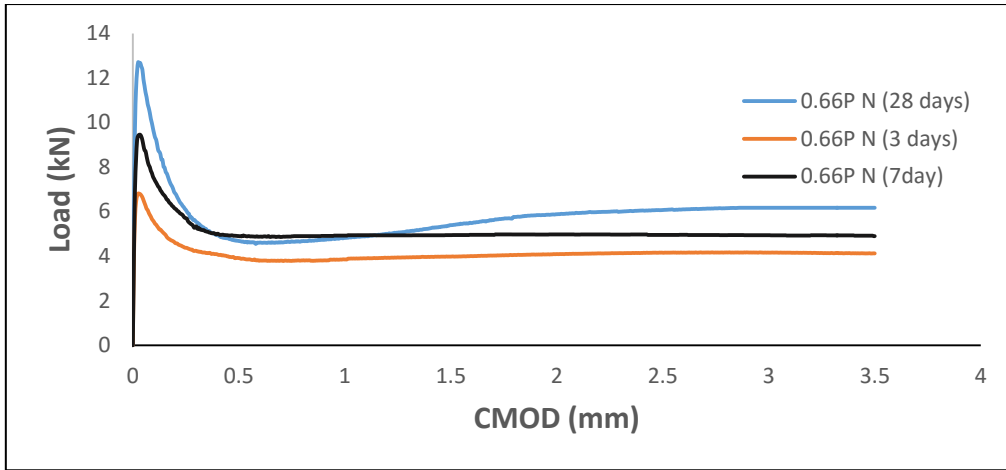
(b)

Figure 4.4.4: Comparison of Load vs Displacement curve for SPFRC and HFRC at 0.66 % volume fraction of fibers (a) 3 days (b) 7 days

Flexural response of the HFRC and SPFRC at different age is shown in the Fig 4.3.5a and Fig 4.3.6b respectively. It is clearly observed that matrix strength is increasing by age resulting in better MOR and pull out resistance of the fibres.



(a)



(b)

Figure 4.4.5: Comparison of Load vs CMOD curve at 3, 7, 28 days (a) HFRC (b) SFRC

4.5 Analysis of Data

The response of the SFRC and HFRC beams under flexure were analyzed in compliance with ASTM C1609, ASTM C1018, JSCE SF4 for unnotched beams and EN14651 for notched beams and corresponding parameters are graphically shown in Fig 4.5.1 through Fig 4.5.16. The variation of residual flexural strength at L/600 and L/150 on adding 0.2 % and 0.3 % micro fibers onto 0.44 % , 0.66 % , 0.88 % macro polypropylene fibers are shown in Fig 4.5.1 and Fig 4.5.2 respectively. The residual strength at span/600 (0.75 mm deflection) and span /150 (3 mm deflection) is observed to increase on adding micro fibers to SPFRC. However HFRC with micro fibers added to 0.66 % of macro fibers did not show much improvement on flexural strength. (Fig 4.5.2) There is clear increase in the residual strength on increasing the volume of macro fibers. (0.44 % to 0.88%). All beams exhibit considerable amount of residual strength even at 3 mm deflection. There is however considerable improvement in the residual flexural strength on adding micro fibers at span/150 deflection in all the specimens.

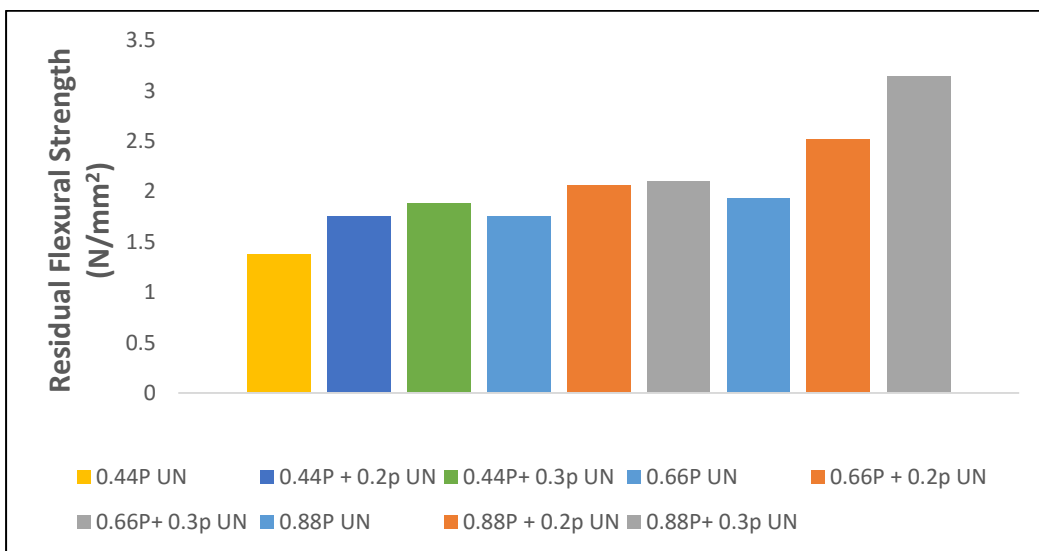


Fig 4.5.1 Residual Strength for HFRC as per ASTM C 1609 at L/600

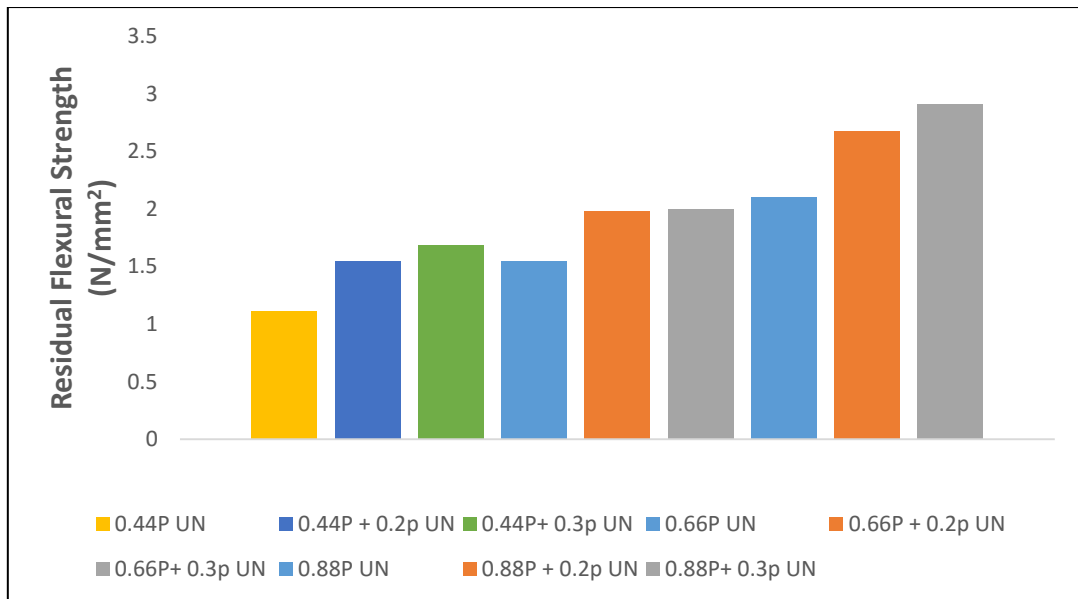


Fig 4.5.2 Residual Strength for HFRC as per ASTM C 1609 at L/150

Equivalent flexural strength ratio calculated as per ASTM C1609 is shown in Fig 4.5.3. Equivalent flexural strength ratio increases with an increase in the fiber volume indicating that more energy is required to break the specimen with higher fiber volume. It is observed that there is 20% enhancement in flexural strength ratio in SFRC beams on increasing macrosynthetic fibers from 0.44 to 0.88 % and 15-20 % increase on adding 0.2 % of micro fibers to the macro polypropylene fibers.

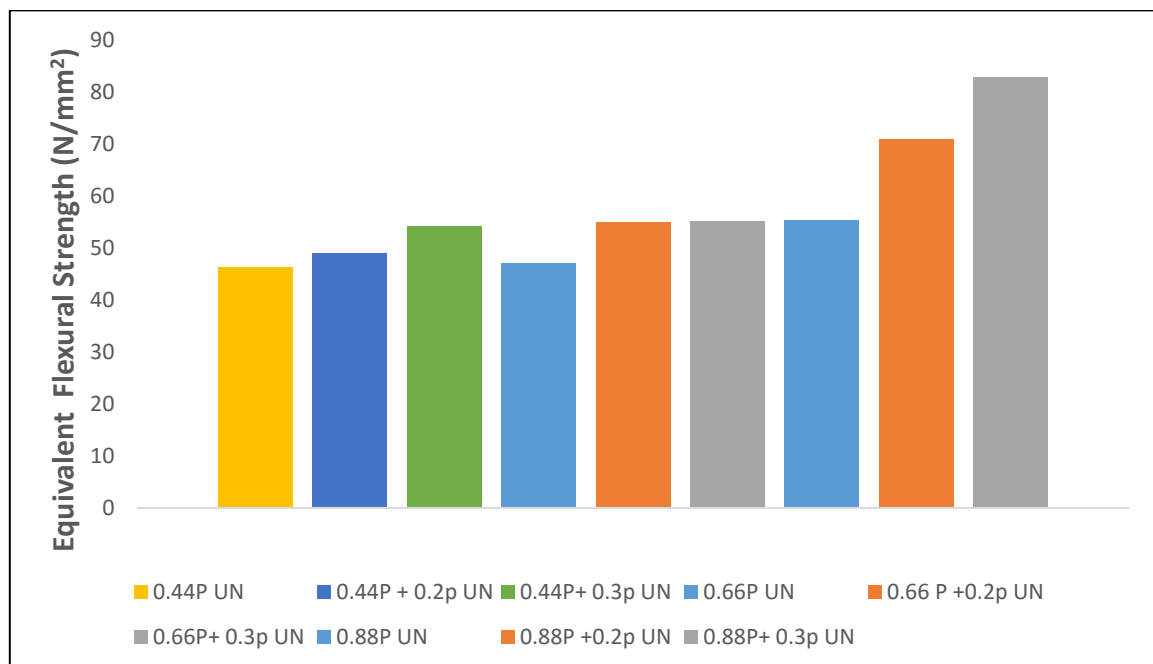


Fig 4.5.3 Equivalent Flexural strength Ratio for HFRC as per ASTM C 1609

Toughness factor calculated as per JSCE standard 4 is shown in Fig 4.5.4. The toughness factor is observed to increase with fiber volume indicating the enhancement in energy absorption capacity of beam. The increase in toughness factor is 60 to 70 percent when the macro fiber volume is increased from 0.44 to 0.88 % by weight. Toughness factor increased by 30 -35 percent just by adding 0.2 % of micro fibers.

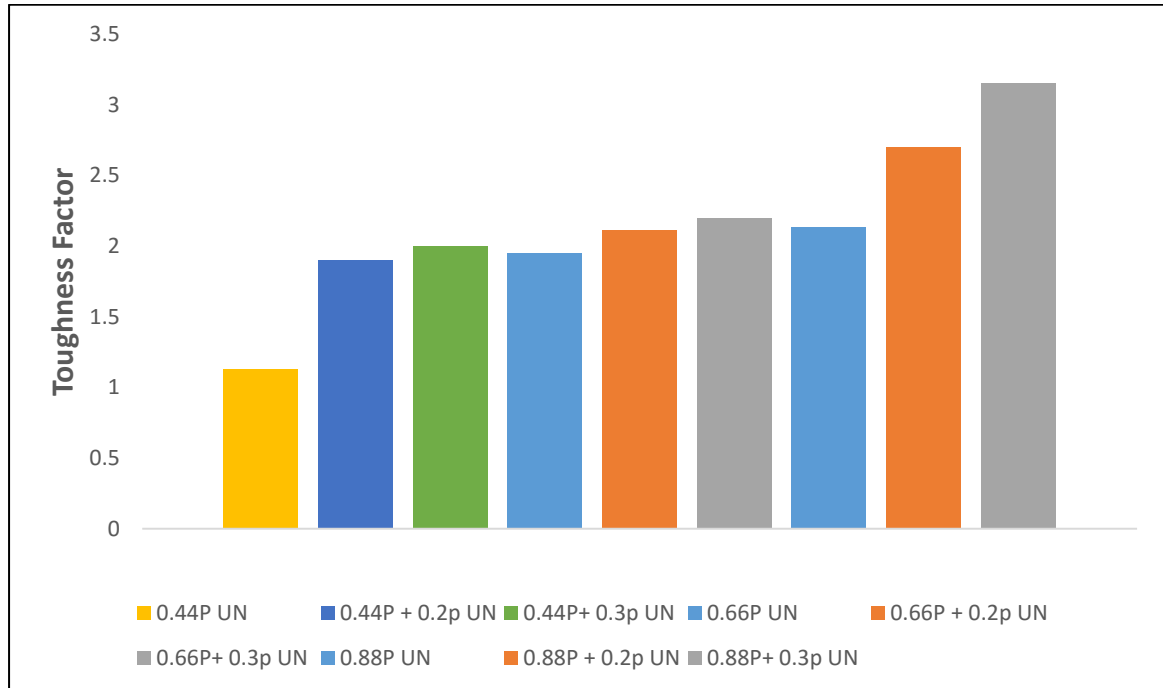


Fig 4.5.4 Toughness factor for HFRC as per JSCE 1609

Fig 4.5.5 and Fig 4.5.6 show a comparison of the flexural properties of SFRC and HFRC with comparable volume fractions of fibers. It is seen that for the same volume fraction of fiber (0.66%) Hybrid fiber reinforced concrete (HFRC) has comparable Residual flexural strength at both the deflections (0.75 mm and 3 mm) and toughness factor when compared with Synthetic Fiber reinforced Concrete (SFRC) at 28 days.

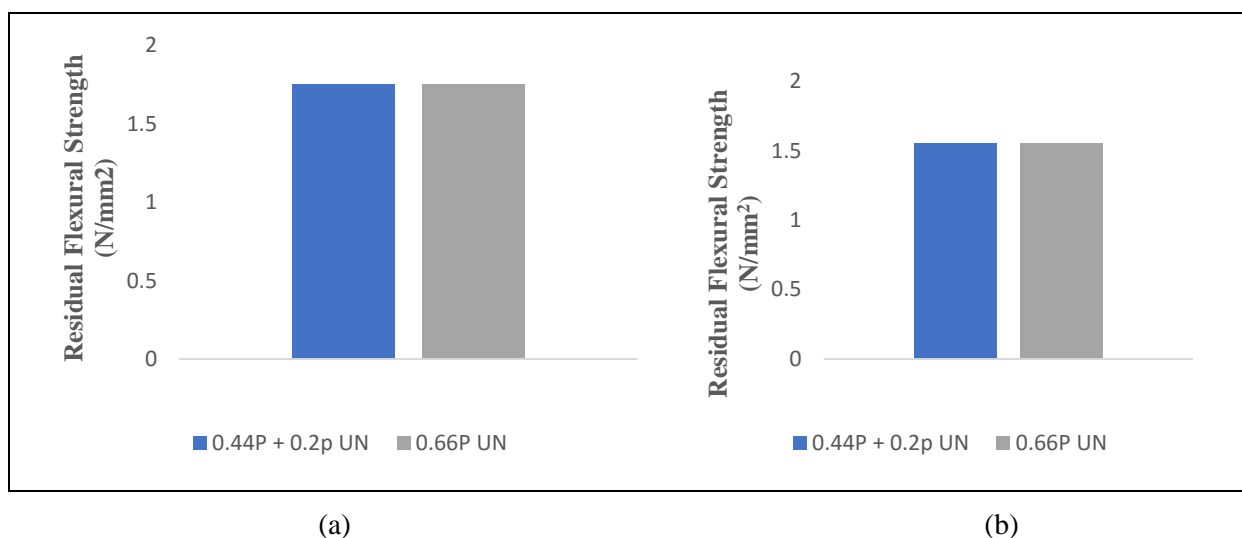


Fig 4.5.5 Residual Strength at 28 days as per ASTM C 1609 (a) L/600 (b) L/150

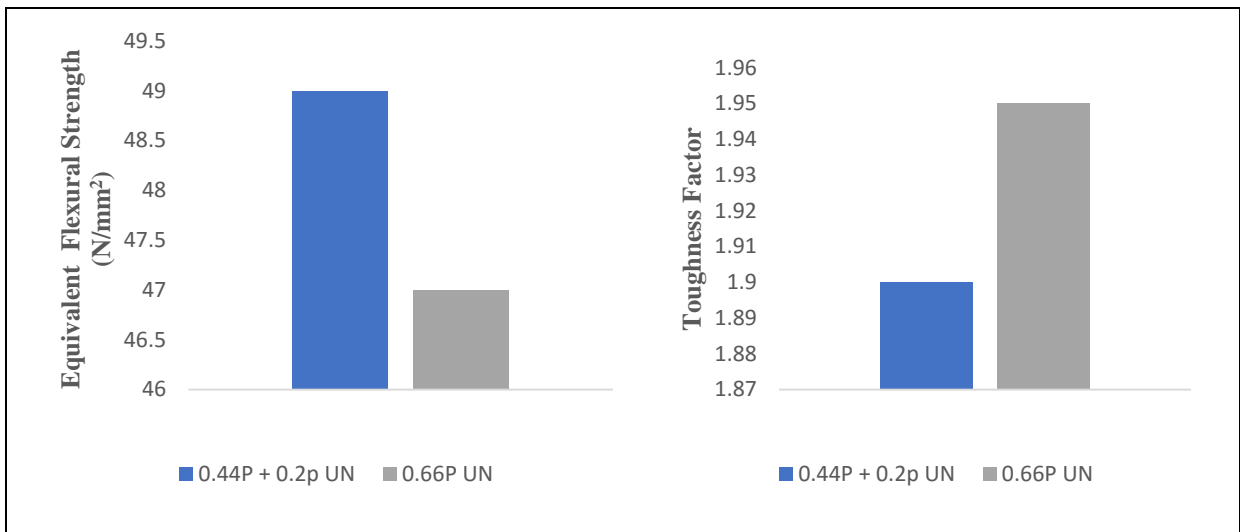


Fig 4.5.6 (a) Equivalent Flexural strength Ratio as per ASTM C 1609 (b) Toughness factor as per JSCE 1609 at 28 days

The response of the SFRC and HFRC beams under flexure were analyzed at early age (3 days and 7 days) and are plotted in Figs 4.5.7 through Fig 4.5.10. Hybrid fiber reinforced concrete (HFRC) shows higher flexural strength and toughness factor than Synthetic Fiber reinforced Concrete (SFRC) at early age.

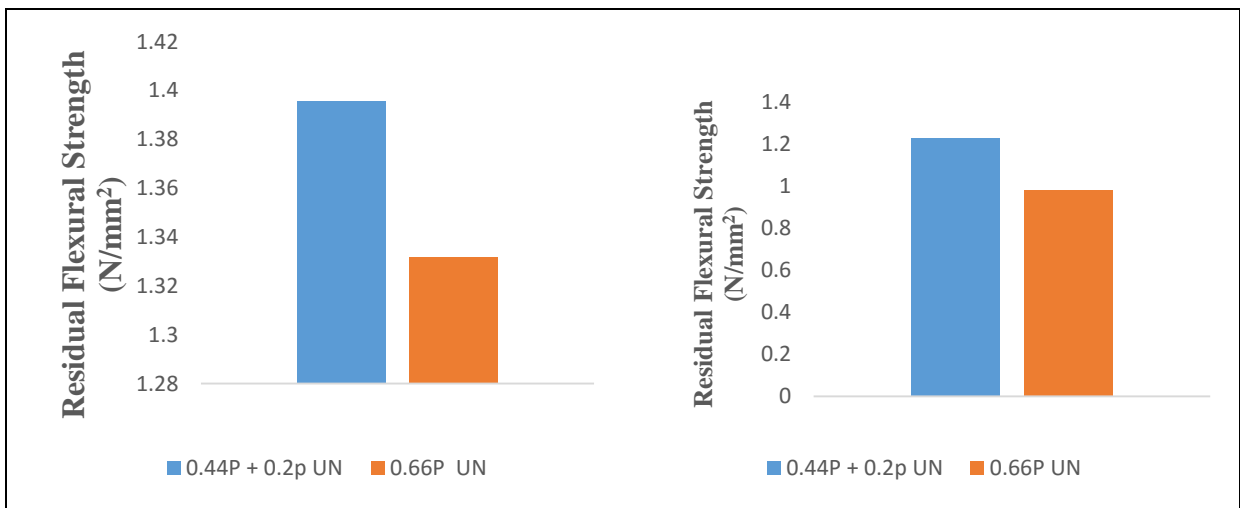


Fig 4.5.7 Residual Strength as per ASTM C 1609 at 3 days (a) L/600 (b) L/150

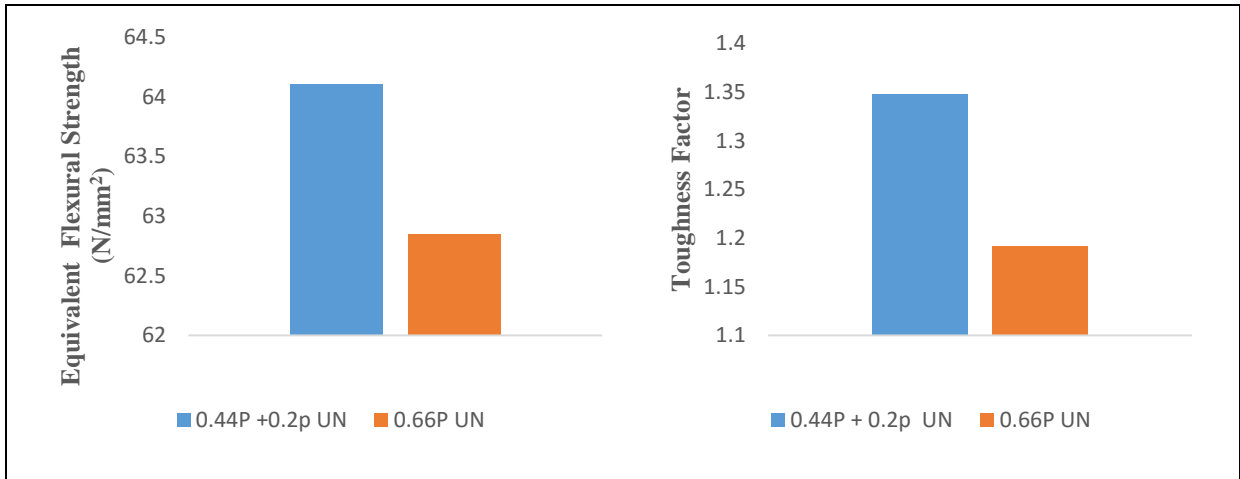


Fig 4.5.8 (a) Equivalent Flexural strength Ratio as per ASTM C 1609 at 3 days (b) Toughness factor as per JSCE 1609

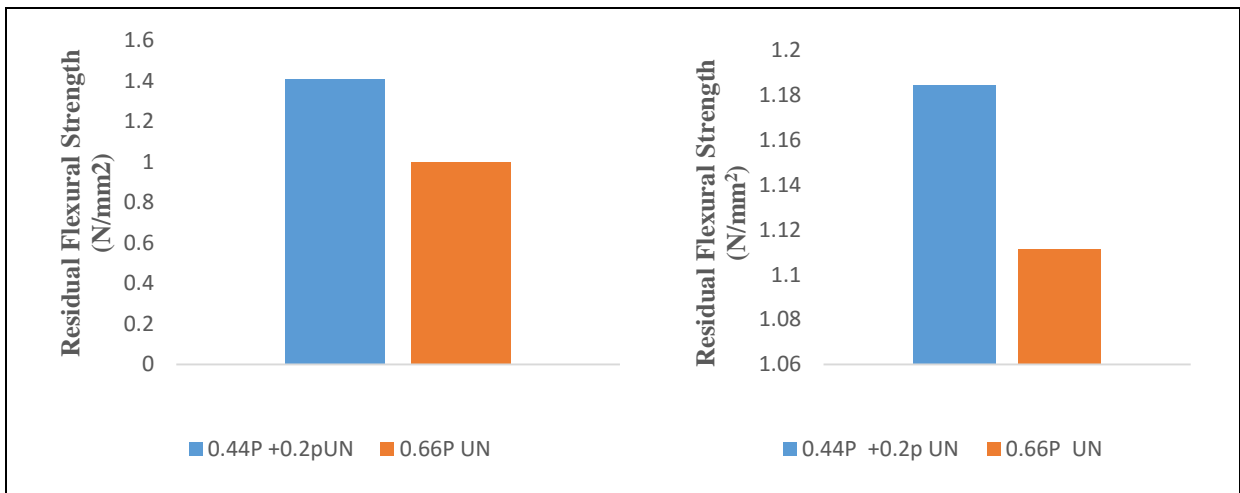


Fig 4.5.9 Residual Strength as per ASTM C 1609 at 7 days (a) L/600 (b) L/150

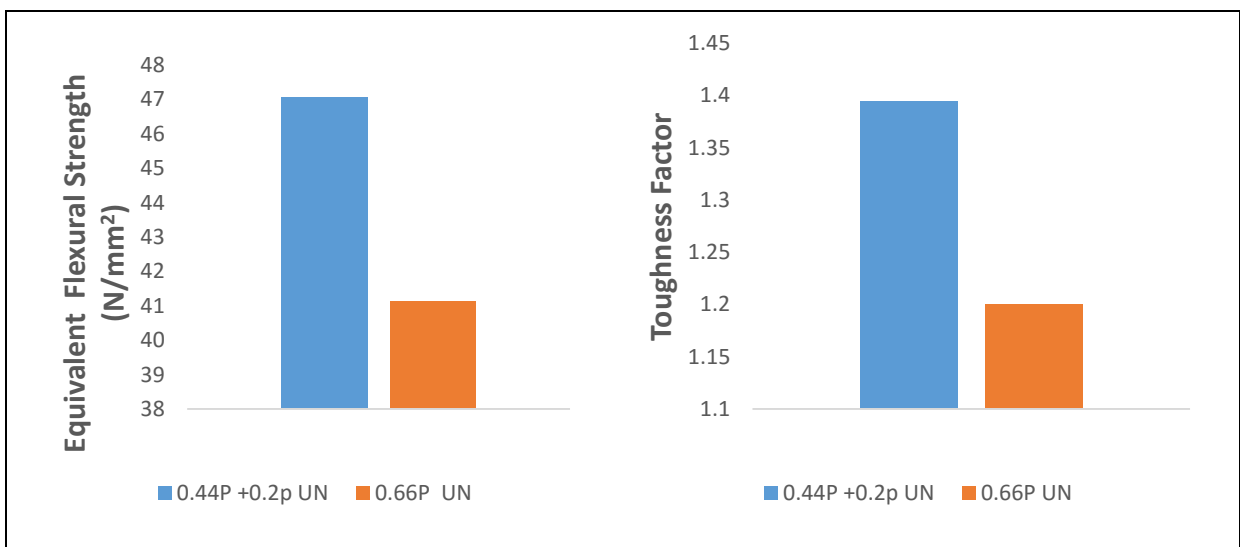


Fig 4.5.10 (a) Equivalent Flexural strength Ratio as per ASTM C 1609 at 7 days (b) Toughness factor as per JSCE 1609

A comparison of the toughness factor for HFRC and SFRC for the fiber volume of 0.66 % is shown in Figure 4.5.11. It is clearly seen that HFRC has a higher toughness than SFRC at early age and almost the same toughness at the later age.

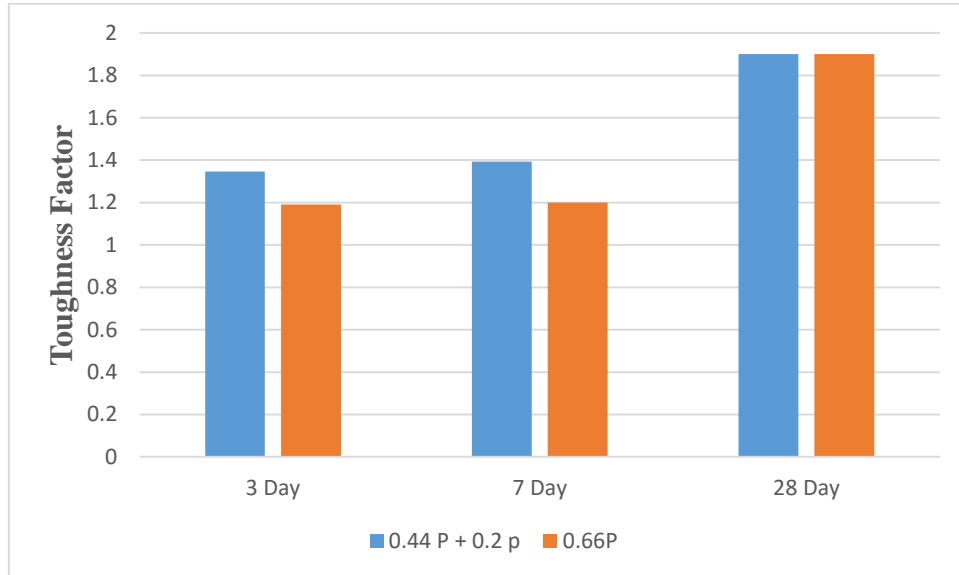
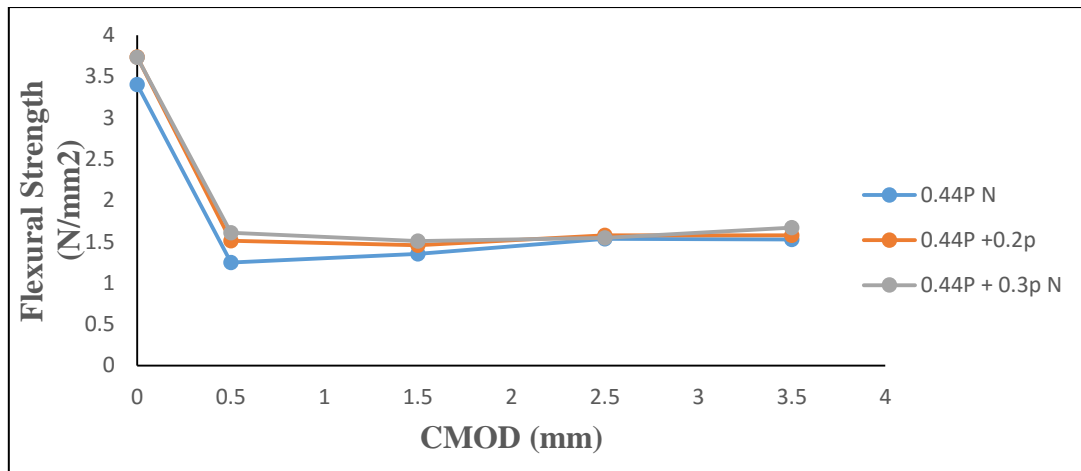
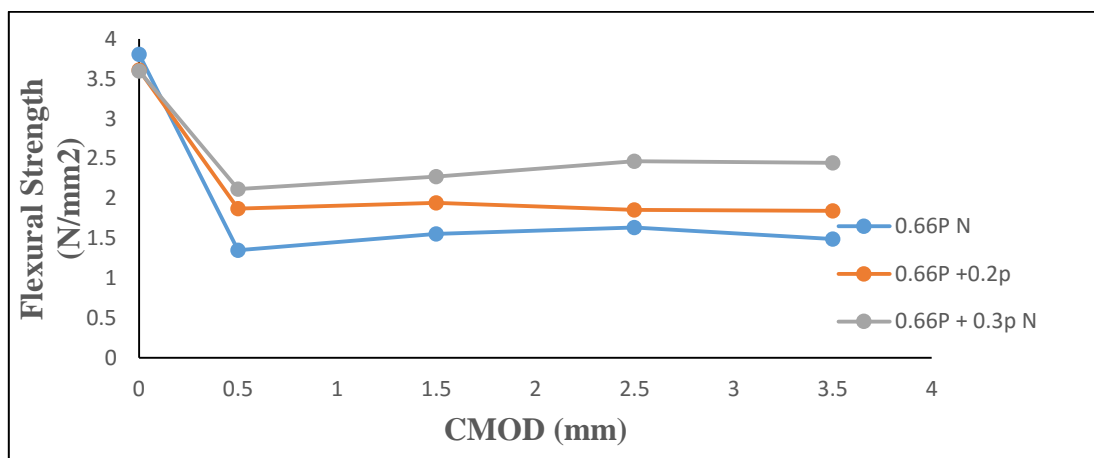


Fig 4.5.11 Comparison of Toughness factor at different ages

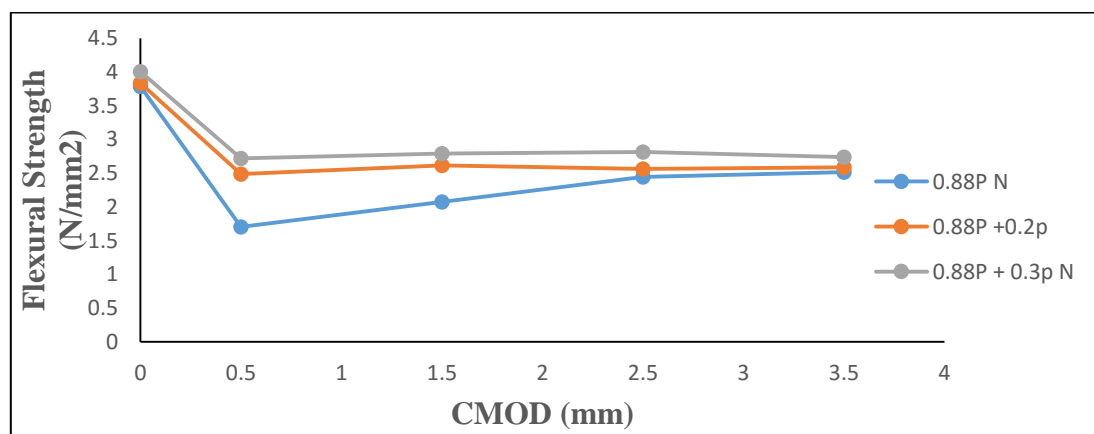
The residual flexural strength calculated as per EN14651 from the test response of notched specimens tested in CMOD control are shown in Fig 4.5.12. The residual flexural strength provides a measure of effectiveness in providing crack closure. Flexural strength remaining constant implies as the crack opens the load carrying capacity of the beam remains constant. In SPFRC beams it can be observed that the Flexural strength increases for all volume fractions with increasing CMOD beyond 0.5 mm. This indicated that the polypropylene fibers are more effective in providing crack closing stresses. At any value of CMOD greater than 0.5 mm the flexural strength increase with an increase in the fiber volume. Significant improvement in the flexural strength was observed on adding 0.2 % of Micro fibers to the SFRC. However the increase in flexural strength beyond a CMOD of 0.5 mm seems to be nominal on adding 0.3% of micro fibers compared to the increase in the flexural strength on adding 0.2 % of micro fibers.



(a)



(b)



(c)

Fig 4.5.12 Residual Flexural Strength of FRC as per EN14651 on adding 0.2 % and 0.3 % Micro fibers to a) 0.44 % P b) 0.66% P c) 0.88% P

The flexural strength was almost the same for HFRC and SFRC at 0.6 % Volume fraction (Fig 4.5.13)

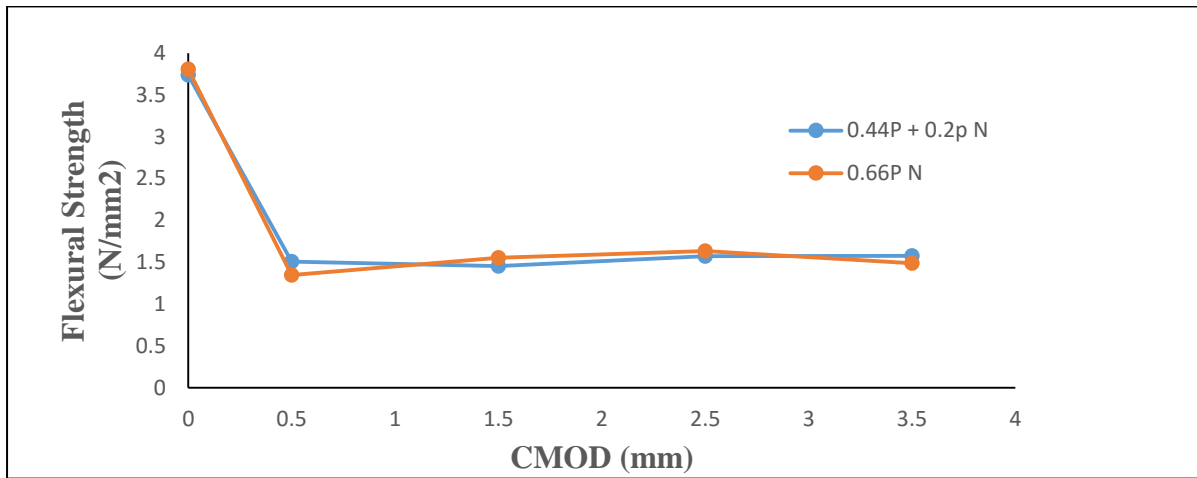
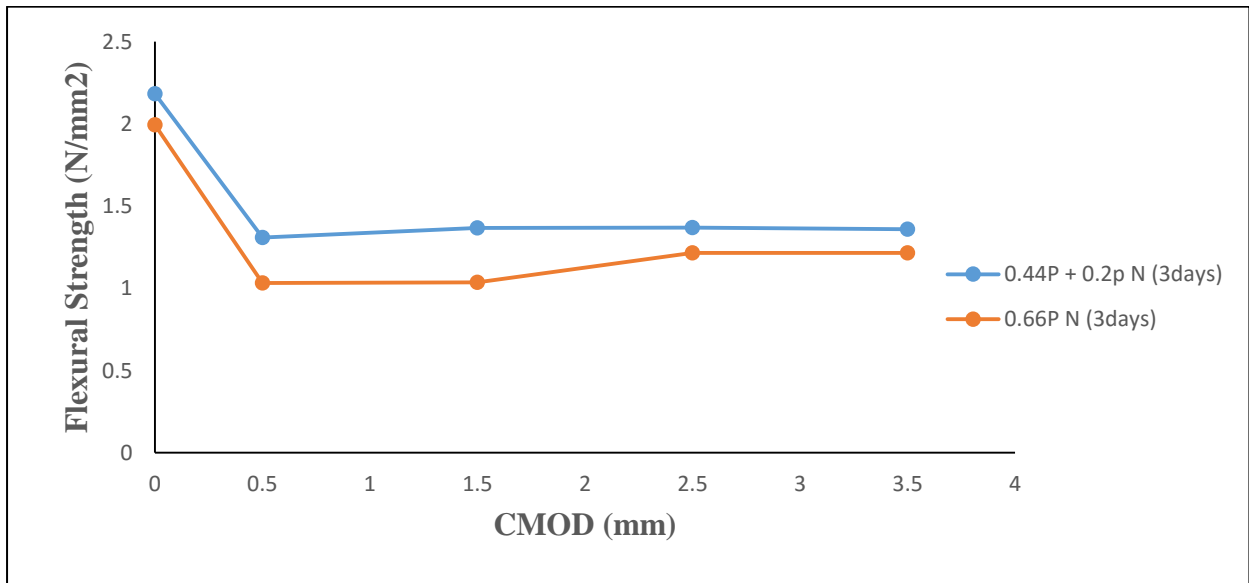
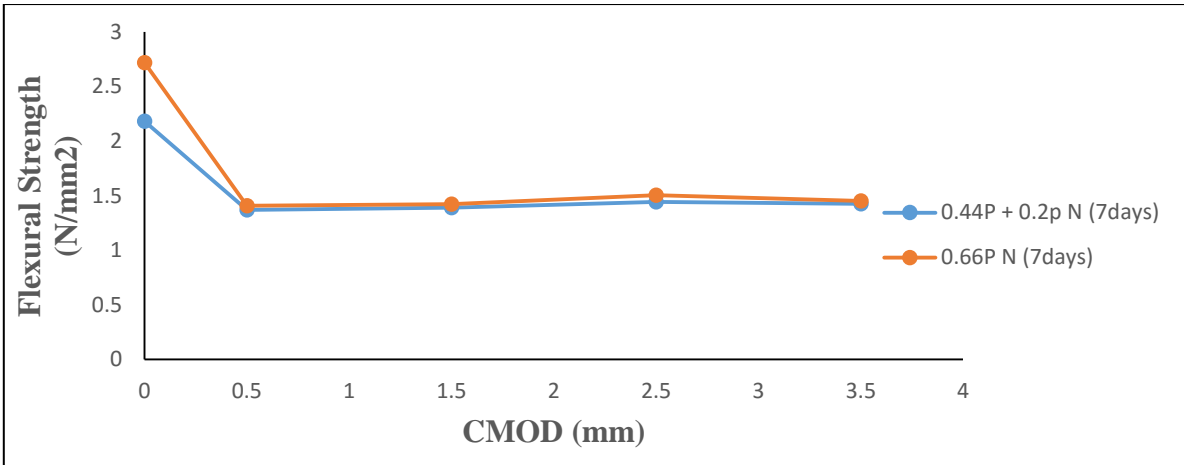


Fig 4.5.13 Residual Flexural Strength of FRC as per EN14651 for 0.66 % Volume fraction of fiber

The flexural strength for HFRC and SFRC at 3 days and 7 days for 0.66 % of fiber volume are shown in Fig 4.5.14 and Fig 4.5.15. It can be clearly seen that first peak load and matrix strength is increasing by age thereby resulting in higher residual flexural strength.



(a)



(b)

Fig 4.5.14 Residual Flexural Strength of FRC as per EN14651 for 0.66 % Volume fraction of fiber at a) 3 days b) 7days

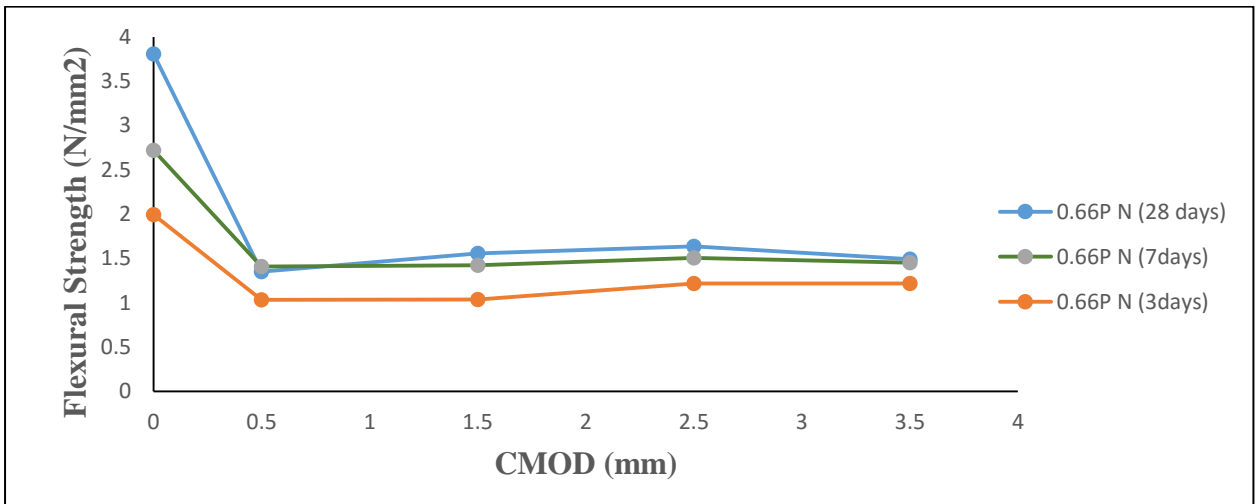


Fig 4.5.15 Residual Flexural Strength of SFRC as per EN14651 at different ages

4.6 Summary of Findings

The results of the experimental investigation reveals that Hybrid polypropylene fiber provide substantial residual load carrying capacity at large deflections. The macro synthetic fibers have an elastic modulus in the range of 10 GPa, while the elastic modulus of mature concrete is expected to be higher than 20 GPa. Therefore, at volumes up to 8 kg/m^3 , which corresponds to approximately 0.9% of the volume, these fibers do not significantly influence the elastic, pre-peak and early part of the load response. The measures obtained from standard tests also do not indicate any significant improvement in the peak strength in flexure tests at 28 days. The micro fibers helped in improving the matrix strength at early age. The failure in both notched and unnotched specimens was observed to be produced by a single crack. Following localization, the crack propagates through the cementitious matrix with little or no resistance from the fibers. The involvement of fibers is seen only at large crack openings. There load drop in the post peak is accompanied with an increasing deflection, which is indicative of increasing compliance produced by the crack propagating along the height of the beam. The influence of the soft fibers is experienced in the post-peak load response after the crack propagates to an extent that the decrease in stiffness of the cracked portion is comparable to the stiffness provided by the fibers. The contribution of the fibers is therefore experienced earlier in the post-peak load response at an early age when the material stiffness of concrete is low and in the later part of the post-peak load response at later ages. The displacement or the crack opening at which the fibers start influencing the load response depends on the volume fraction of the fibers. Following the initial load drop, the load response obtained from the fiber reinforced specimens exhibit a load recovery associated with the crack closing stresses provided by the fibers bridging the crack. The fiber bridging the crack provide a significant load carrying capacity with increasing deflection. Considerable enhancements in the composite fracture energy and toughness are obtained from both macrosynthetic FRC and Hybrid FRC.

For a volume fraction of 0.66%, the Hybrid Synthetic fiber reinforced concrete provides better performance at earlier ages. The Hybrid FRC shows higher flexural strength and toughness factor than Synthetic Fiber reinforced Concrete (SFRC) at early age. At later ages, Hybrid FRC shows a higher resistance in the immediate post-peak softening response than the macrosynthetic FRC. The toughness of both Hybrid and Macrosynthetic FRC are comparable at later ages.

Chapter 5

Digital Image Correlation Results

5.1 Introduction

Digital image correlation (DIC) is a full-field optical technique which provides spatially continuous measurement of displacements across the surface of the specimen. Compared with other optical techniques, DIC is a very robust measurement technique which does not require the use of lasers. It provides reliable measurements without the requirement of any special vibration isolation, which allows the use of this technique during a mechanical test. The technique relies on a random sprayed-on speckle and a digital camera for image acquisition. With the advent of digital cameras, which provide increased resolution, the accuracy obtained from the technique has increased allowing for the use of the technique in applications which required measurements at a higher resolution. DIC has been used to determine the stress concentration produced by a stress riser such as a crack and for stress distribution due to damage. Application of the technique have included determining the stress concentration for evaluating fracture parameters in composite and metallic specimens. [57] [58] [59]. Successful application of DIC in concrete specimens include determination of the strain profile associated with cohesive stress transfer produced with debonding of FRP composite laminates and to derive the cohesive stress-crack separation relationship [60]

DIC measurements were performed on notched specimens tested as per EN 14651. A speckle pattern was created in a region close to the notch. While the available resolution from the technique considering the area of measurement does not allow for determining fracture parameters, the information from the surface displacements and strains obtained using DIC are used for evaluating the crack propagation. The surface displacements and strains were analysed for evaluating the crack growth in concrete in relation to the observed load response in flexure and to compare with measurements obtained from other instrumentation. The observed relationship between crack opening and crack depth as a function of the load supported by the specimen was determined from the DIC results. The effectiveness of fibers in providing crack bridging was evaluated from the observed relationship between crack tip opening and crack depth.

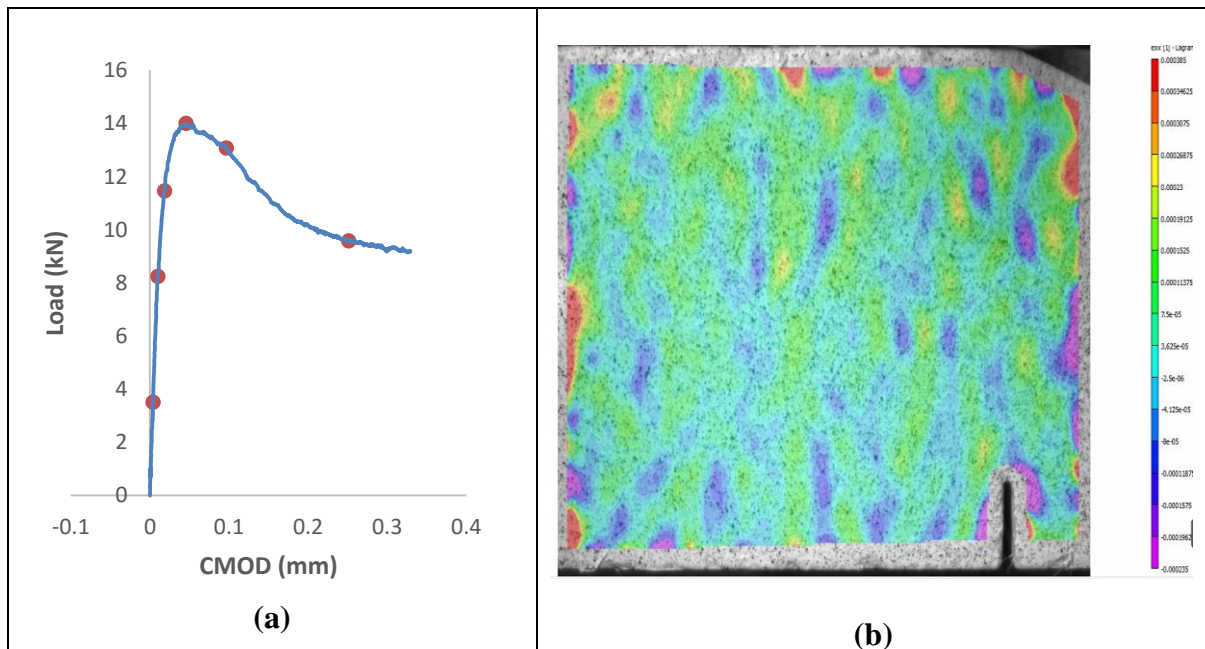
5.2 Background

DIC relies on correlation of the random pattern of speckles between images of the deformed and reference (undeformed) configurations of the specimen within small neighbourhoods called subsets [Sutton et al. (1983,1988)]. The speckle pattern represents a random pattern, which gives a unique distribution of pixel grey level values in each subset. A two-dimensional displacement field was obtained for all points on the surface from cross-correlating the image of the deformed specimen with the image of the specimen in the reference configuration. A subset size equal to 35x35 pixels was used for the correlation. In a given image, the pixel grey value in each subset associated with the random sprayed-on pattern forms a unique grey-level distribution, which differs from grey-level distribution of another subset. In the analysis, positions within the deformed image were mapped on to positions within the reference subsets using second-order, two-dimensional shape functions. Spatial domain cross-

correlation was performed to establish correspondence between matching subsets in images of the reference and deformed states. Quintic B-spline interpolation of the grey values was used to achieve sub-pixel accuracy. The cross correlation analysis of the digital images was performed using the VIC-2D™ software, which maximizes the correlation coefficient between grey levels in the subsets in the reference and deformed images. Surface displacements and displacement gradients at each loading stage were calculated at each subset centre, by evaluating the shape functions and their partial derivatives at the subset centre. For the setup used in this study, the random error in the measured displacement is in the range of 0.002 pixels. Strains were computed from the gradients of the displacements. A conservative estimate of the resolution in strain obtained from the digital correlation was 10^{-5} [Bruck et al (1989), Schreier (2002)].

5.3 Results

Typical load-CMOD response of an HFRC beam with 0.88 % macro polypropylene with 0.2% micro polypropylene tested CMOD control is shown in Fig 5. 1. The strain in the X-direction (ϵ_{xx}) at distinct point on the load response of the specimen (shown marked on the load response) are also plotted. It can be observed that strain localization is initiated close to the peak load and leads to the formation of single crack emanating from the notch. The growth of the crack can clearly be identified with softening in the post peak load response. Correspondingly there is also an increase in the CMOD. The results indicate that the localization close to the peak load, results in an increase in the crack opening. As the crack propagates, there is a steady increase in the crack opening and an associated drop in the load.



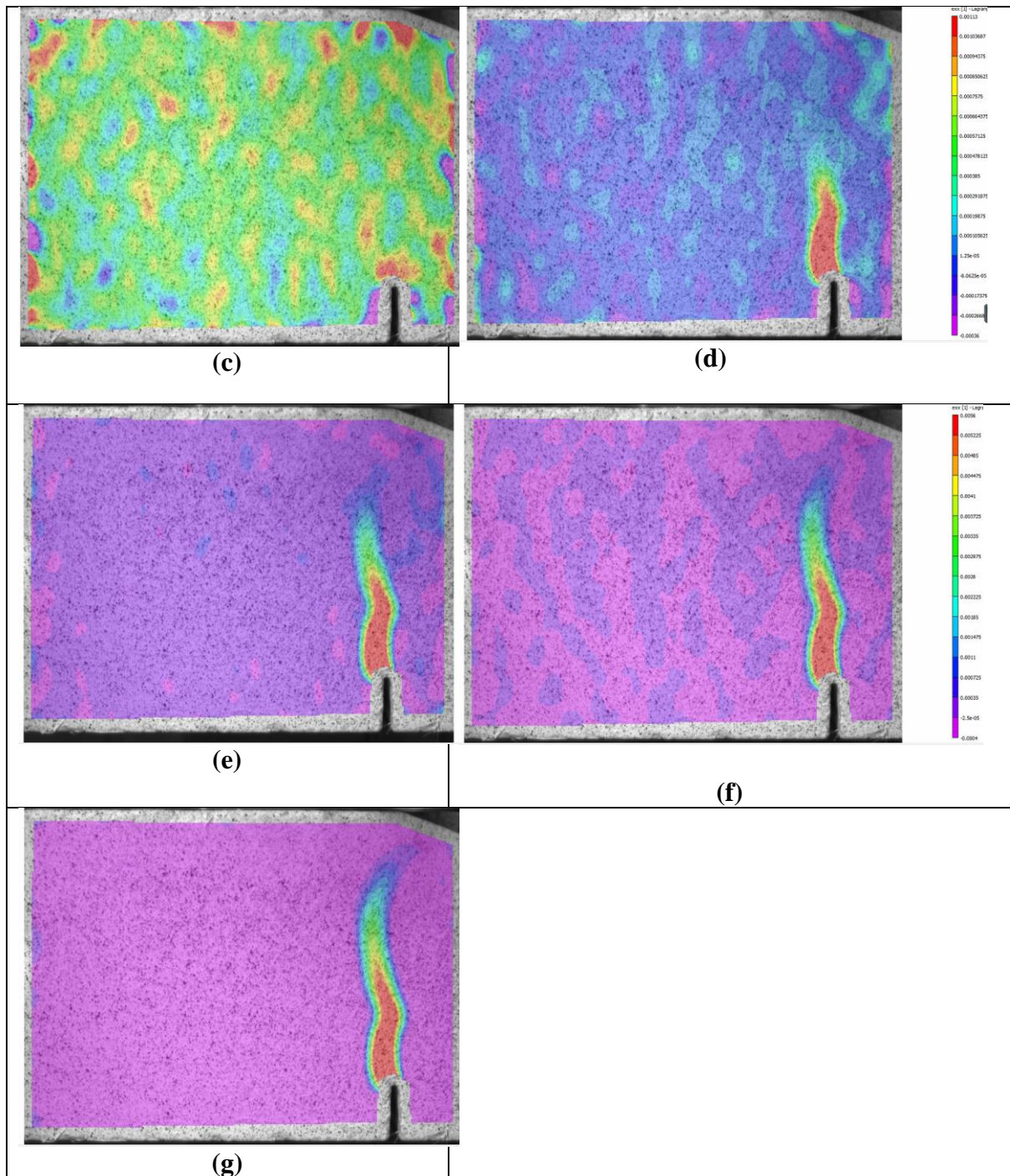


Fig 5. 1: (a) Load-CMOD of plot of HFRC specimen with 0.88 % Macro Polypropylene with 0.2 % Micro Polypropylene fibers. The CMOD measured during the test is also shown in the Figure; (b) ϵ_{xx} at 3.5 kN (pre-peak); (c) ϵ_{xx} at 8.25 kN (prepeak); (d) ϵ_{xx} at 14 (Peak); (e) ϵ_{xx} at 13.07 kN (postpeak); (f) ϵ_{xx} at 11.6 kN (postpeak); and (g) ϵ_{xx} at 9.6 kN (postpeak)

The variation in ϵ_{xx} at different heights along the depth of the beam are analysed at distinct points in the load response for Hybrid fiber reinforced concrete are analysed. Five locations at fixed heights above the notch were selected for evaluating the variation in the strains due to crack propagation. At each location the displacement and strain relative the centreline of the notch was evaluated to determine the variation as a function of depth. The location of the lines are given in

Table 5.1 Locations of lines

and shown in Fig 5.2 The variation in displacement, u and strain ϵ_{xx} along line 1, located just above the notch at distinct point in the load response for all the blend combinations are shown in Fig 5.3, 5.4, 5.5, 5.6, 5.7, 5.8, 5.9 and 5.10

Table 5.1 Locations of lines

Line No	Depth From Crack Tip (mm)
1	12.5
2	25
3	50
4	62.5
5	75

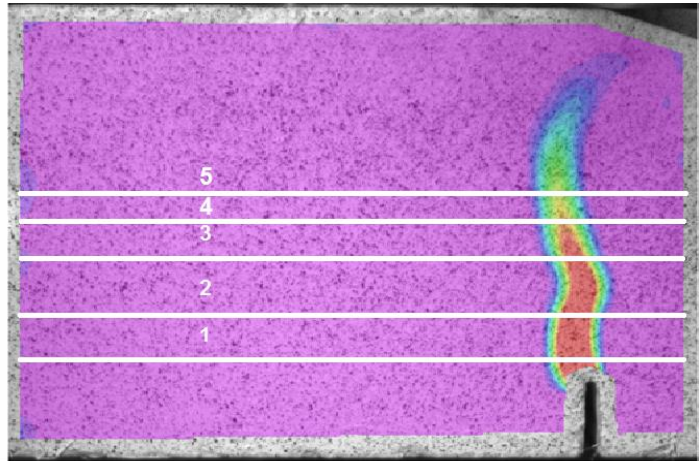


Fig 5.2 Horizontal strips for strain computations

A region of finite length associated with very rapid increase in displacement is observed in the displacement profile along line 1. The region associated with the rapid gradient in displacement is broadly centred on the notch. Within this region, the displacements sharply rise above the linear trend with a gradual slope away from the notch. The size of the region associated with the rapid increase in displacement remains relatively constant with increasing deflection of the beam.

The increase in strain along line 1 close to the notch is indicative of strain localization, which is centred over the notch. The strain localization is noticed over a finite width, along the line. The width associated with localization appears to remain constant during the immediate post peak softening load response following the peak load. This indicates that strains in a finite region close to the crack plane are influenced by the crack. There is no strain localisation till the peak load. The available data indicates that the strain profile in the immediate post-peak is identical for all the specimens.

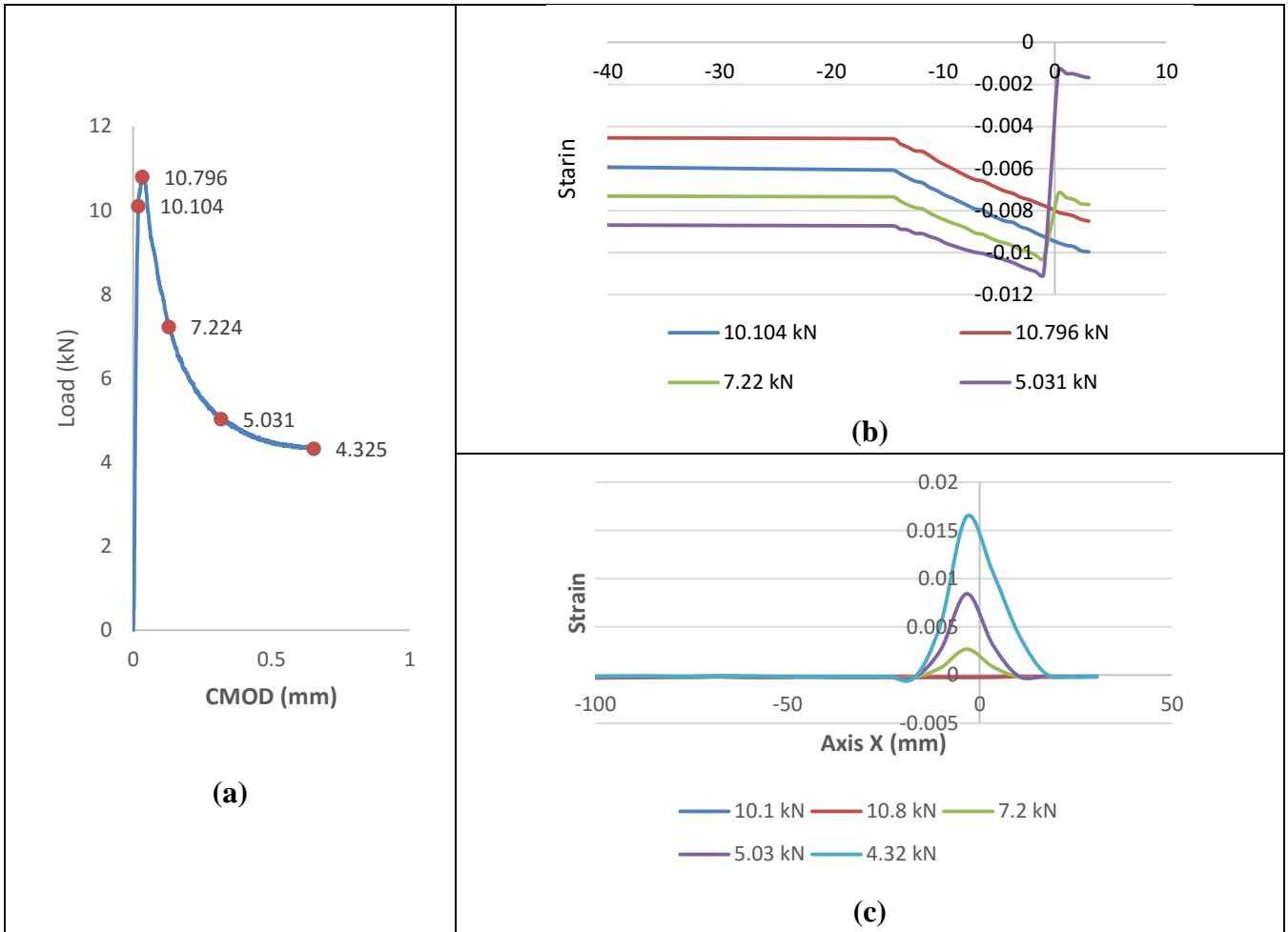


Fig 5.3: (a) Typical load response of 0.44 P + 0.2 %p; (b) displacement profile at line 1; (c) strain profile at line 1 at distinct load points

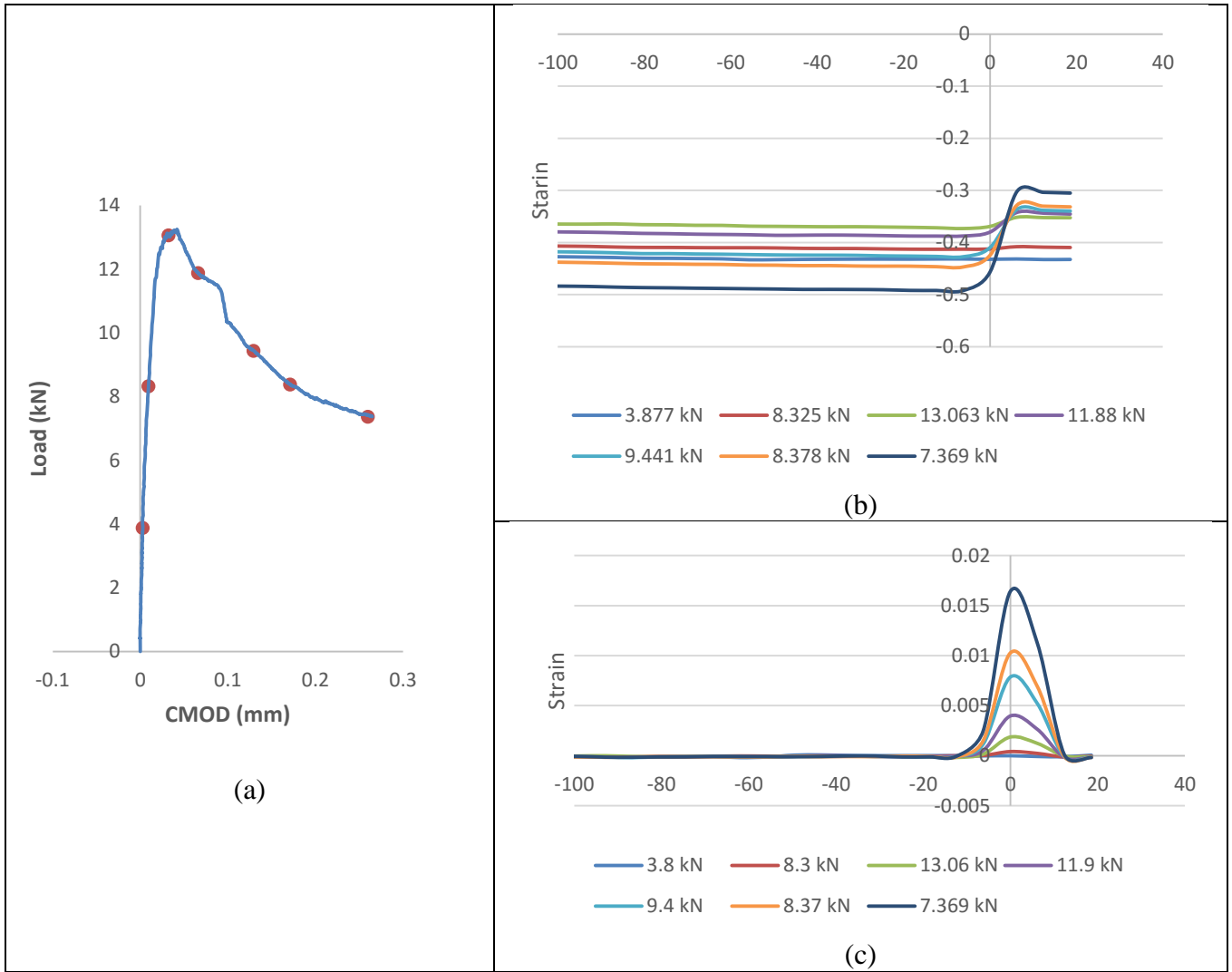


Fig 5.4: (a) Typical load response of 0.44 P +0.3 %p; (b) displacement profile at line 1; (c) strain profile at line 1 at distinct load points

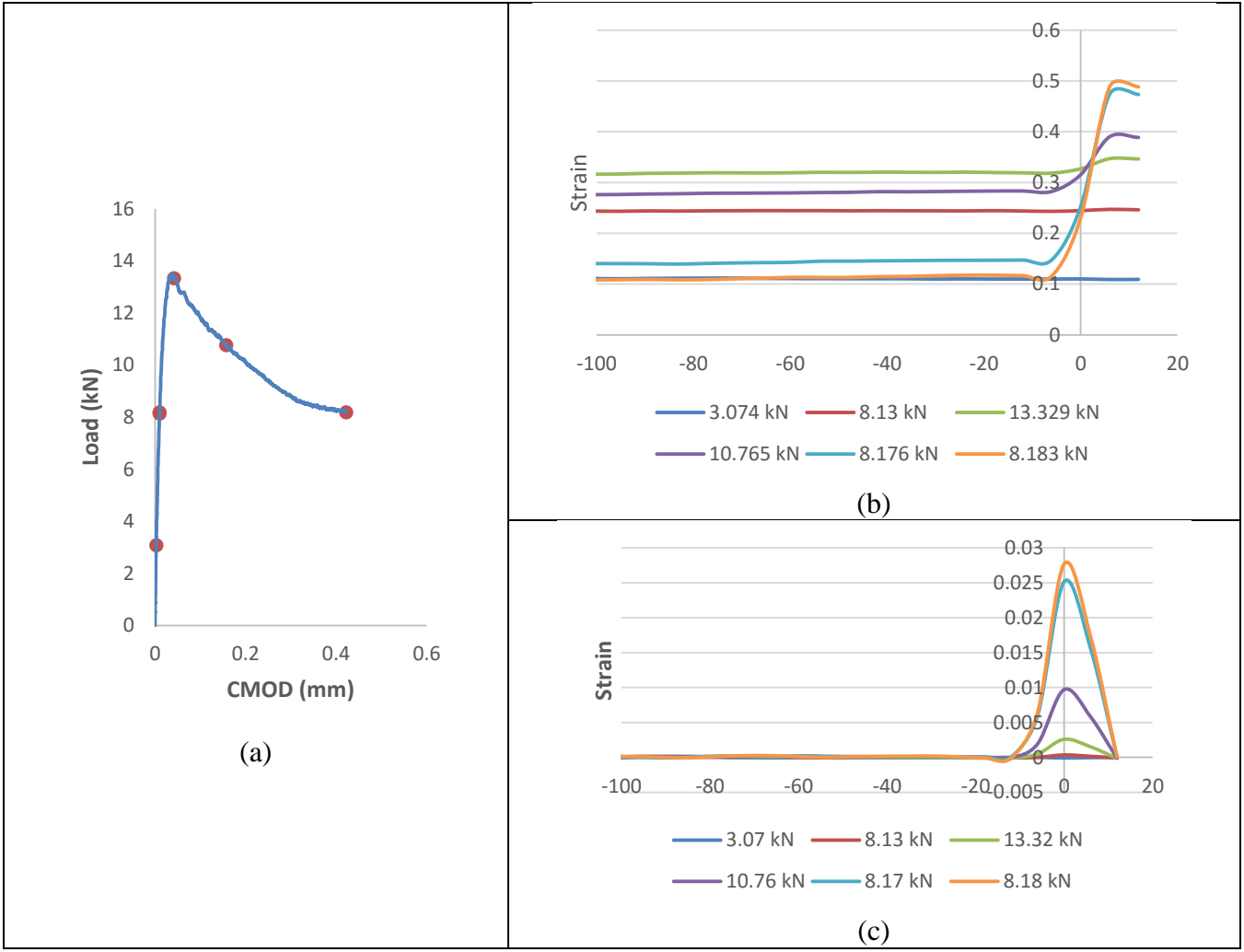


Fig 5.5: (a) Typical load response of 0.6 P +0.3 %p fibers (b) displacement profile at line 1; (c) strain profile at line 1 at distinct load points

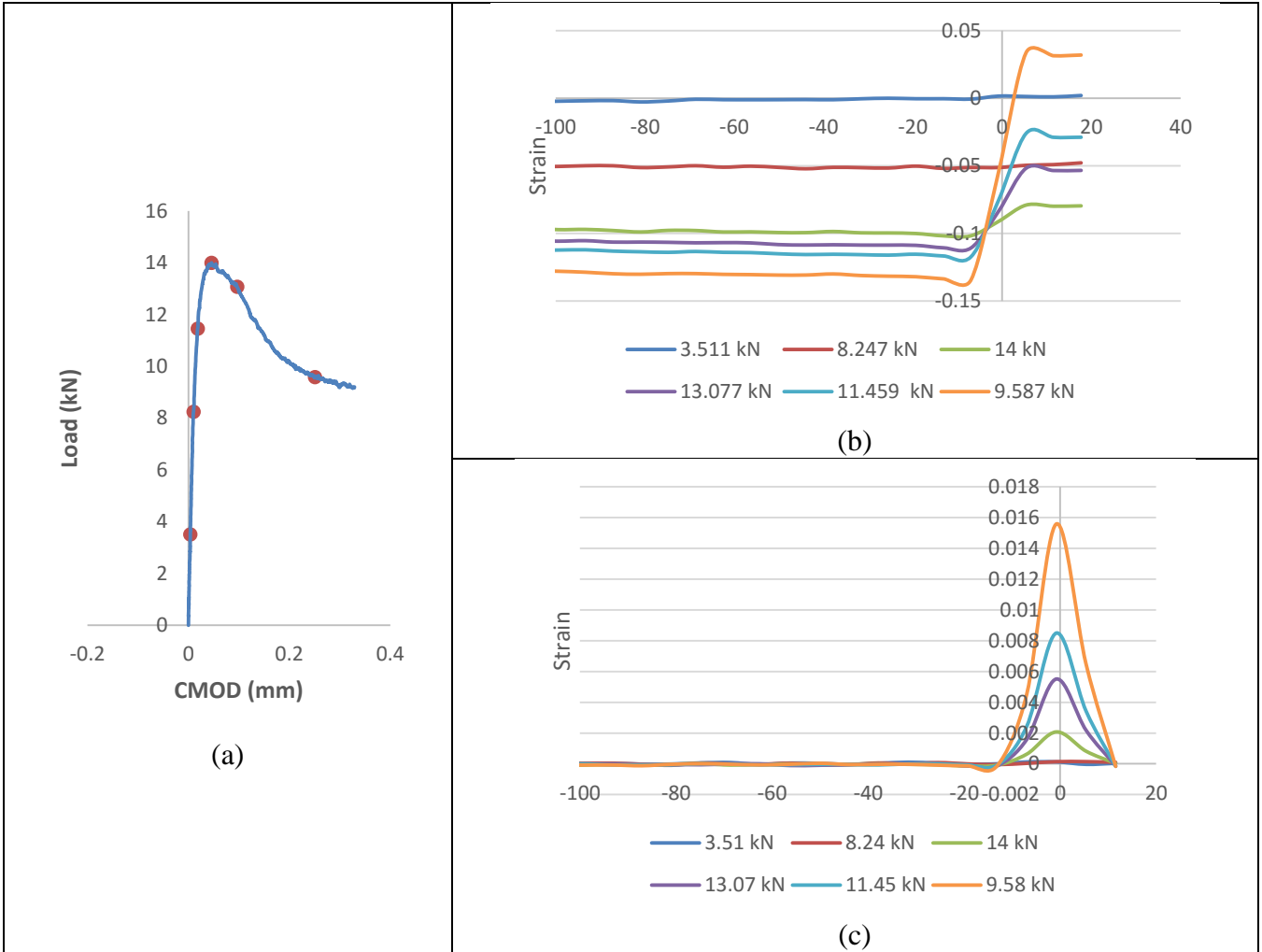


Fig 5.6: (a) Typical load response of 0.88 P + 0.2 %p (b) displacement profile at line 1; (c) strain profile at line 1 at distinct load points

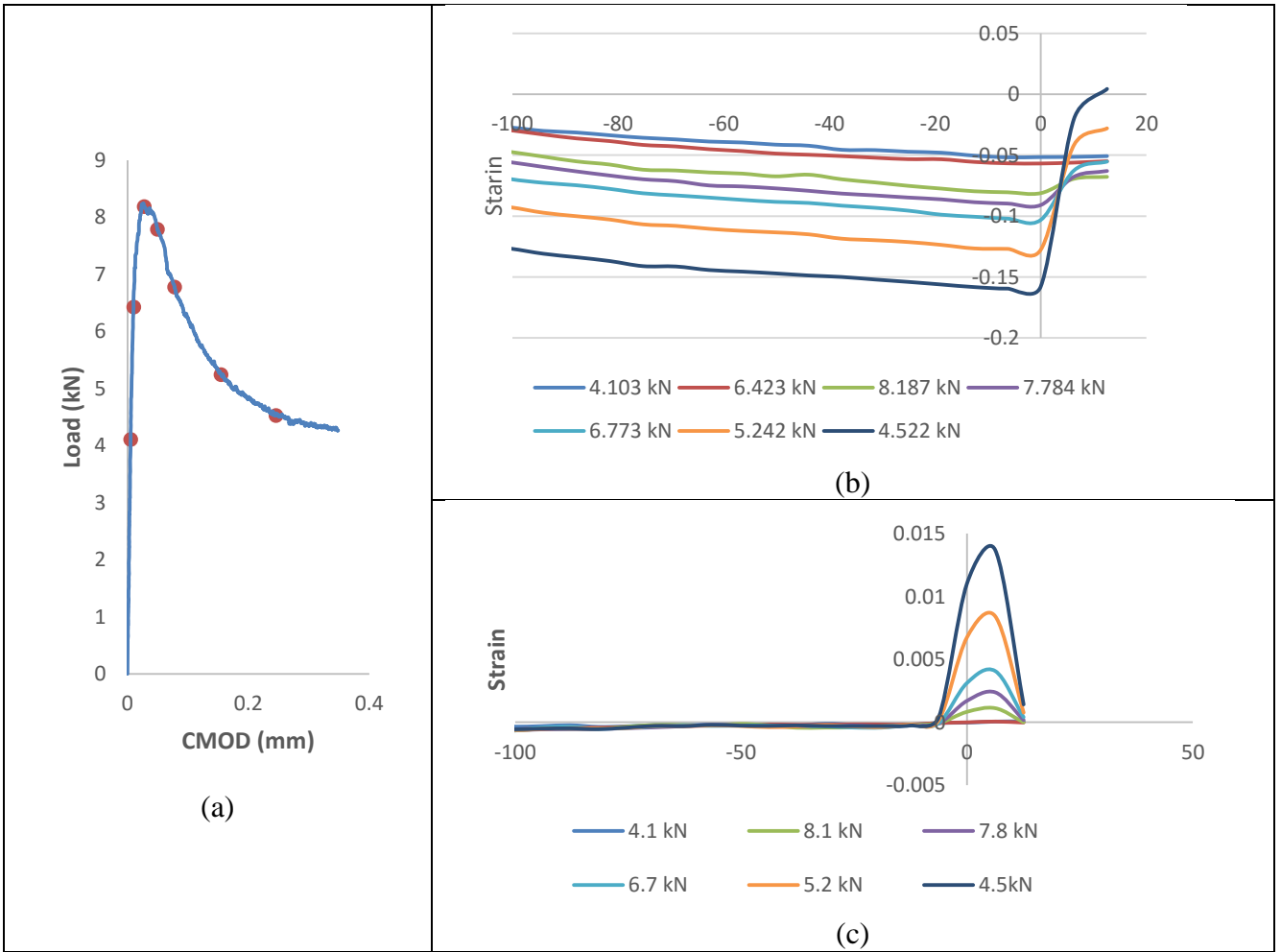


Fig 5.7: (a) Typical load response of 0.44 P +0.2 %p (3day); (b) displacement profile at line 1; (c) strain profile at line 1 at distinct load points

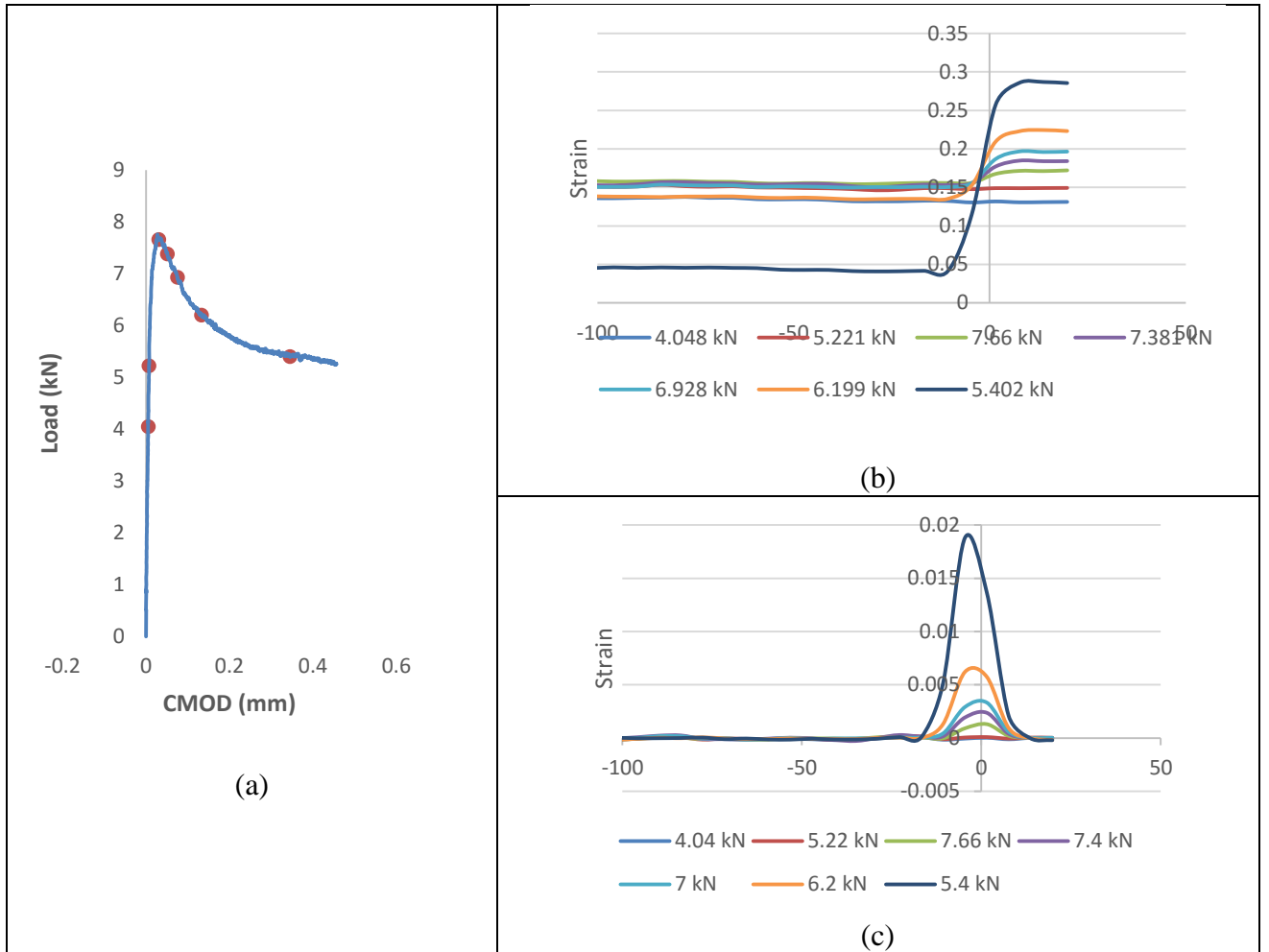


Fig 5.8: (a) Typical load response of 0.66P (3day) (b) displacement profile at line 1; (c) strain profile at line 1 at distinct load points

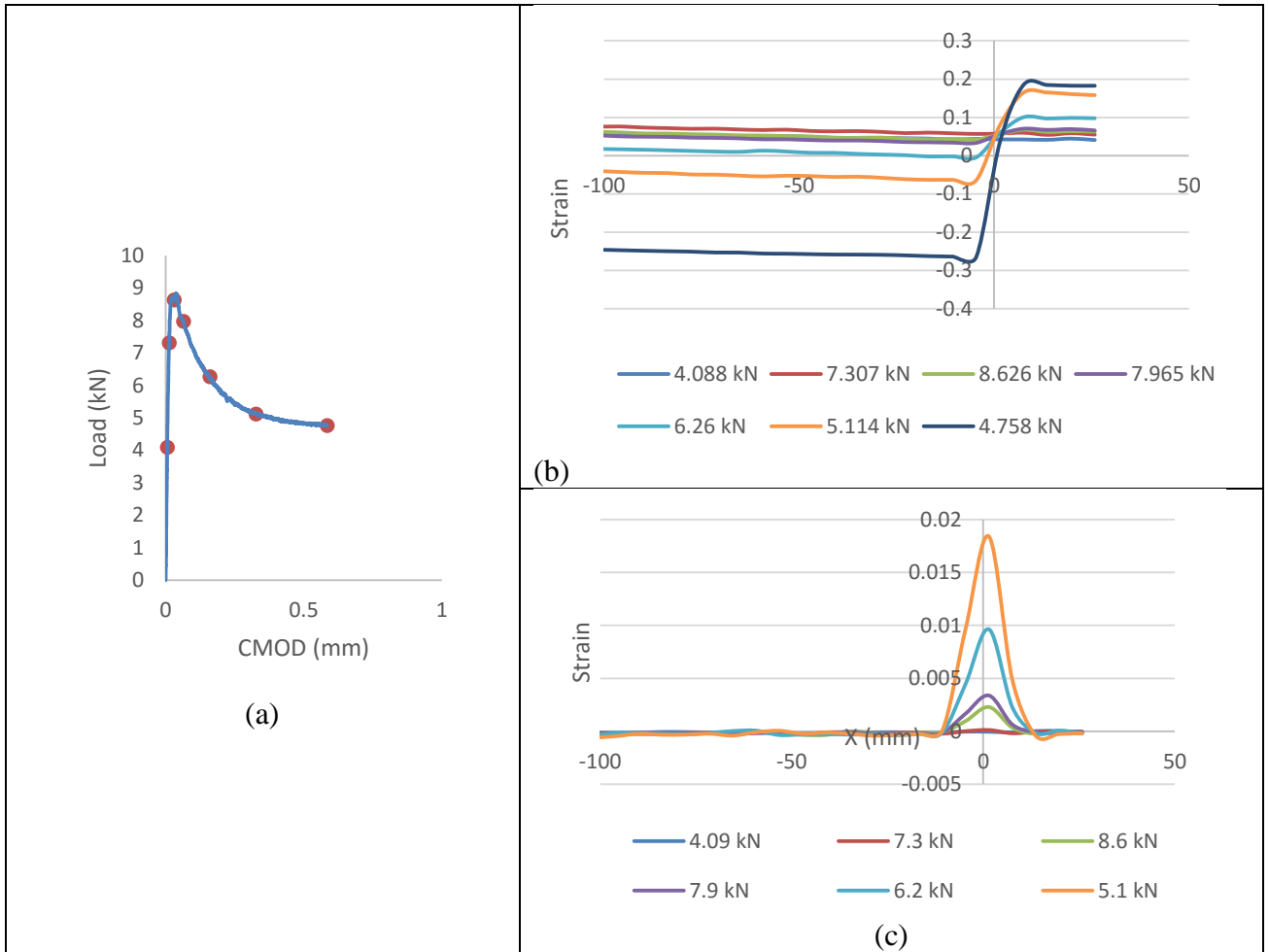


Fig 5.9: (a) Typical load response of 0.44 P +0.2 %p (7day); (b) displacement profile at line 1; (c) strain profile at line 1 at distinct load points

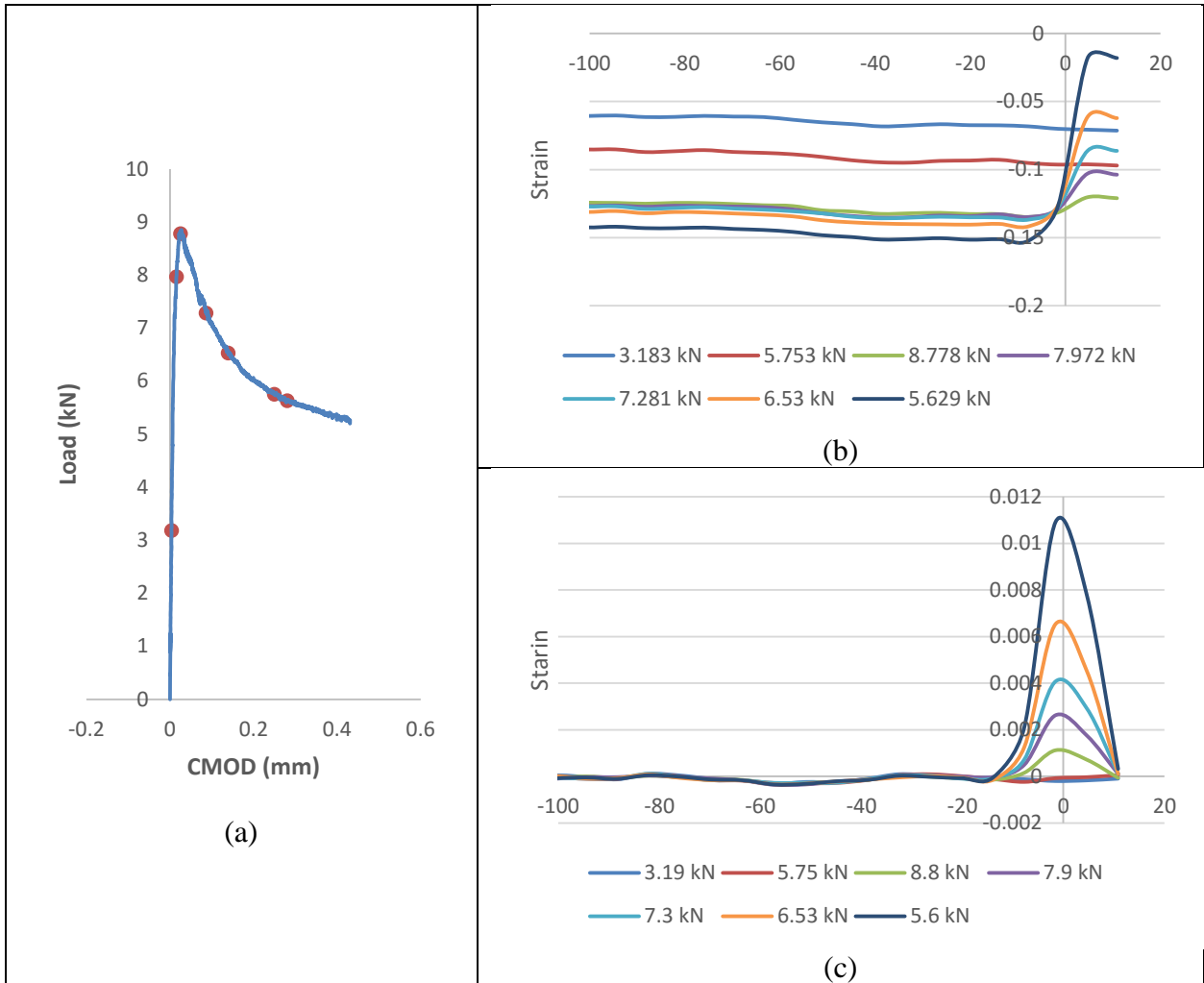
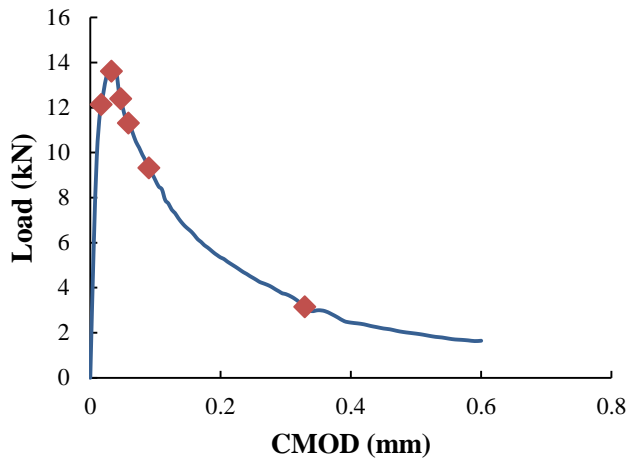


Fig 5.10: (a) Typical load response of 0.66P (7 day) (b) displacement profile at line 1; (c) strain profile at line 1 at distinct load points

Typical result showing strain in the x direction (ϵ_{xx}) at five distinct point on the load response of specimen in the pre peak, close to the peak and in the post peak are shown in Fig 5.11 and 5.12 for 5 lines located at different depths relative to the notch. The respective loads are given in figure for control and specimens with 0.66 % of fibers. The distances of the lines above the bottom face of the beam are tabulated in the figure. The extent of crack propagation and the strain profiles associated with the crack are nominally identical for the control and fiber reinforced concrete. The propagation of crack in the material can be traced from the depth at which strain localization is observed. The results clearly indicate that in both control and synthetic fiber reinforced concrete even in the post peak, when the load drops by about 30-40% of the peak load, the crack does not propagate up to line 5 and the same can be observed in Fig 5.11(e) and Fig 5.12. **Variation of Strain value (ϵ_{xx}) on lines along the depth of section at distinct loads for polypropylene with 0.66% volume** Fig 5.12 (e). The strains at line 5 even at load 5 are very small in magnitude and there is no indication of strain localization along the line. This suggests that the crack propagation in control and fiber reinforced concrete is nominally identical in the immediate post-peak associated with load drop after peak load. There

is no strain localisation at the lower loads before the pre peak even at line 1. Fibres start arresting the crack fast in early days.



Line No	Depth from Crack Tip (mm)
1	7.8
2	40
3	62.5
4	90
5	107

(a) Load CMOD of Control

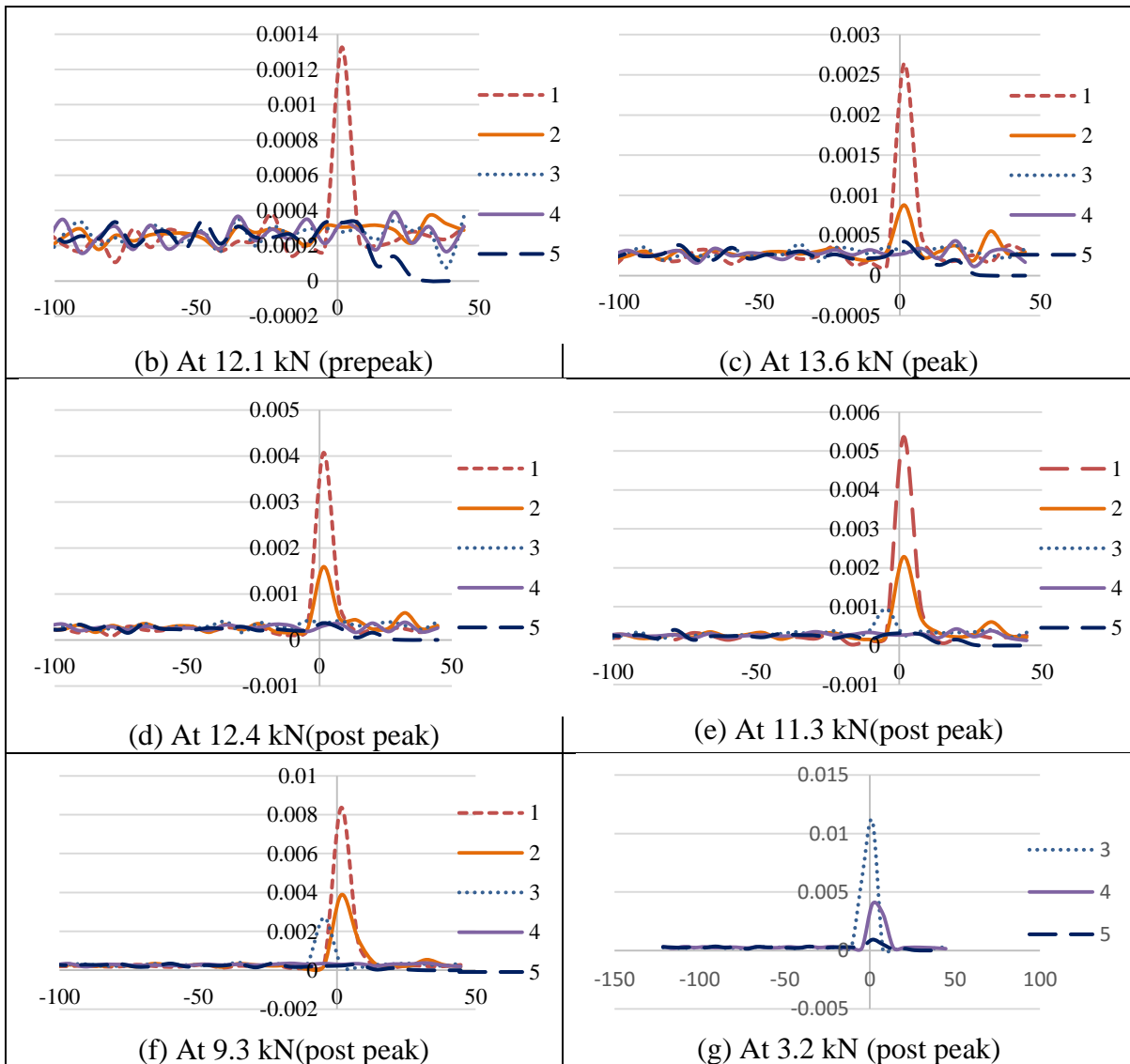
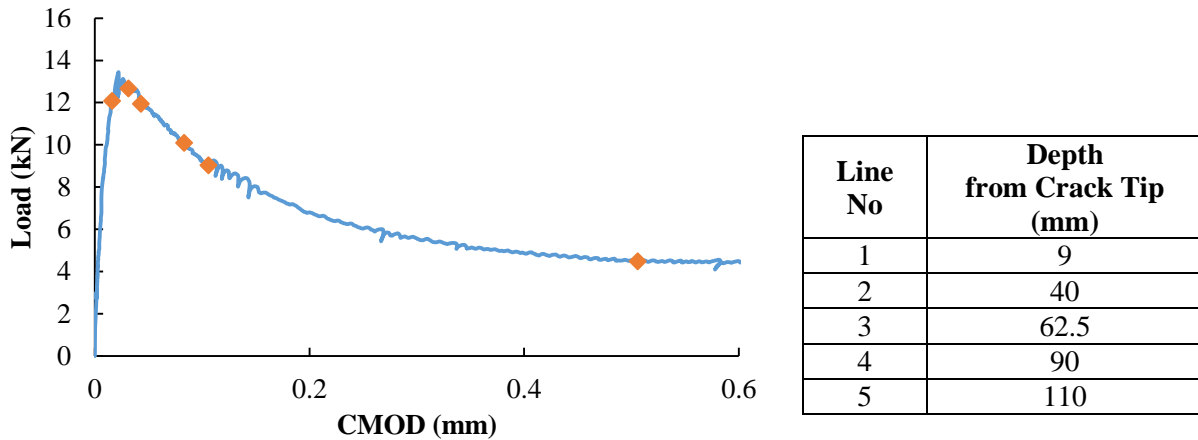


Fig 5.11 Variation of Strain value (ϵ_{xx}) on lines along the depth of section at distinct loads for control Specimen



(a) Load CMOD of 0.66% Polypropylene

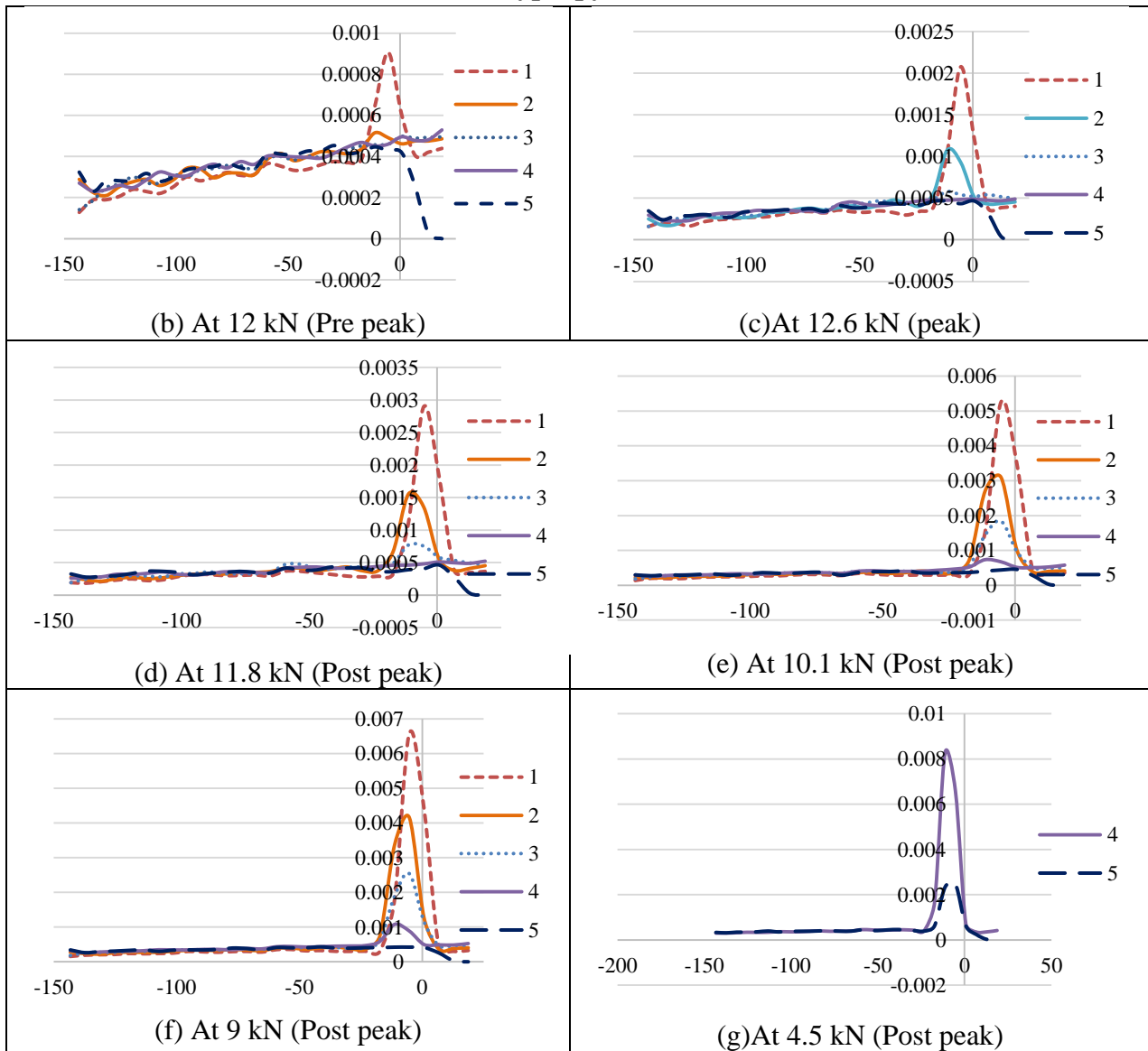
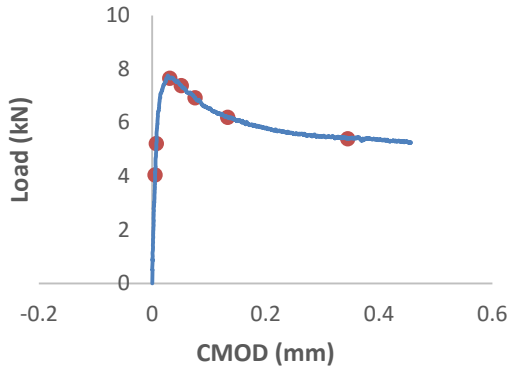
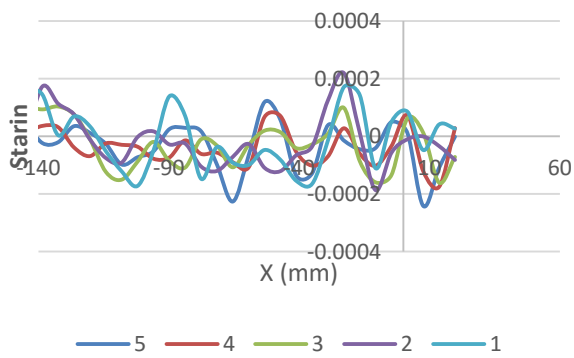


Fig 5.12 Variation of Strain value (ϵ_{xx}) on lines along the depth of section at distinct loads for polypropylene with 0.66% volume at 28 days.

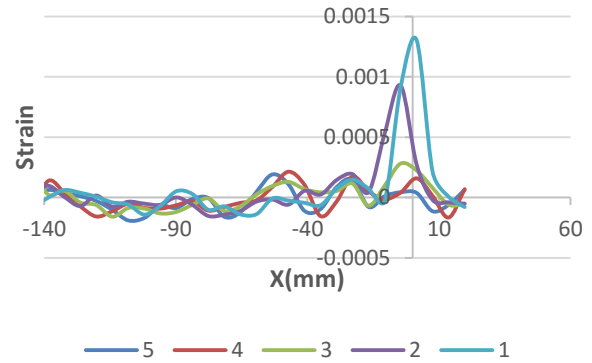


Line No	Depth from Crack Tip (mm)
1	12.5
2	25
3	50
4	62.5
5	75

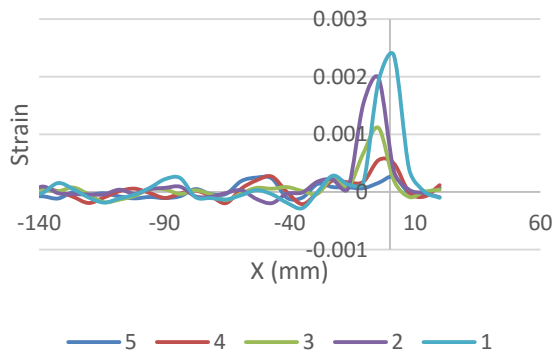
(a) Load CMOD of 0.66% P at 3 days



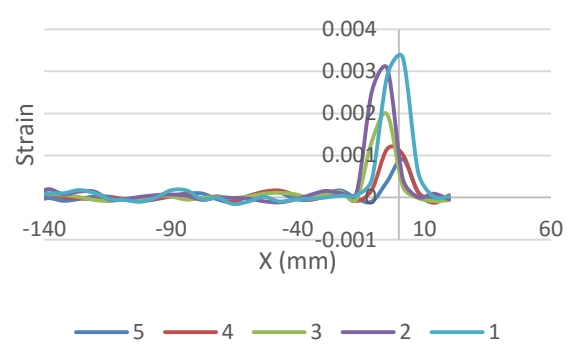
(b) At 5.22 kN (Pre peak)



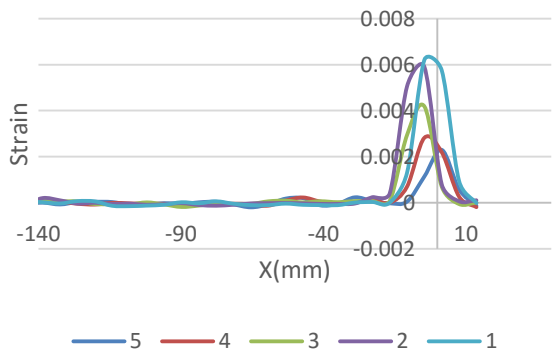
(c) At 7.66 kN (peak)



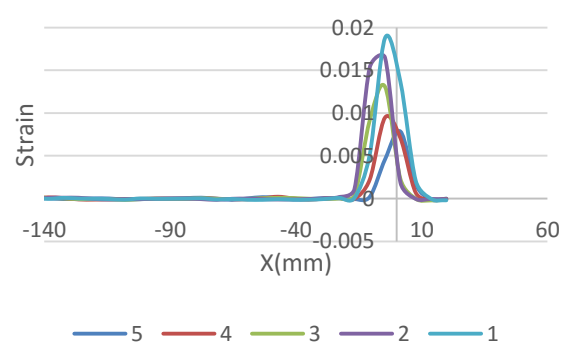
(d) At 7.38 kN (Post peak)



(e) At 6.928 kN (Post peak)

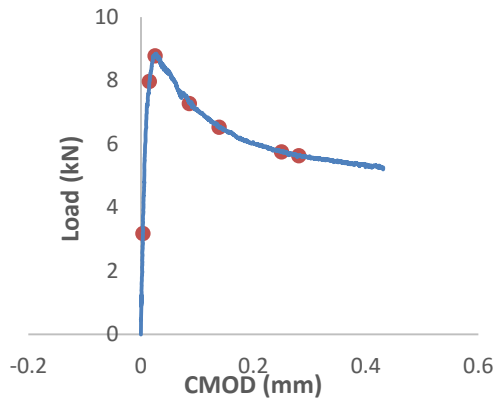


(f) At 6.199 kN (Post peak)



(g) At 5.402 kN (Post peak)

Fig 5.13 Variation of Strain value (ϵ_{xx}) on lines along the depth of section at distinct loads for polypropylene with 0.66% volume at 3 days.



Line No	Depth from Crack Tip (mm)
1	12.5
2	25
3	50
4	62.5
5	75

(a) Load CMOD of 0.66 % P at 7 day

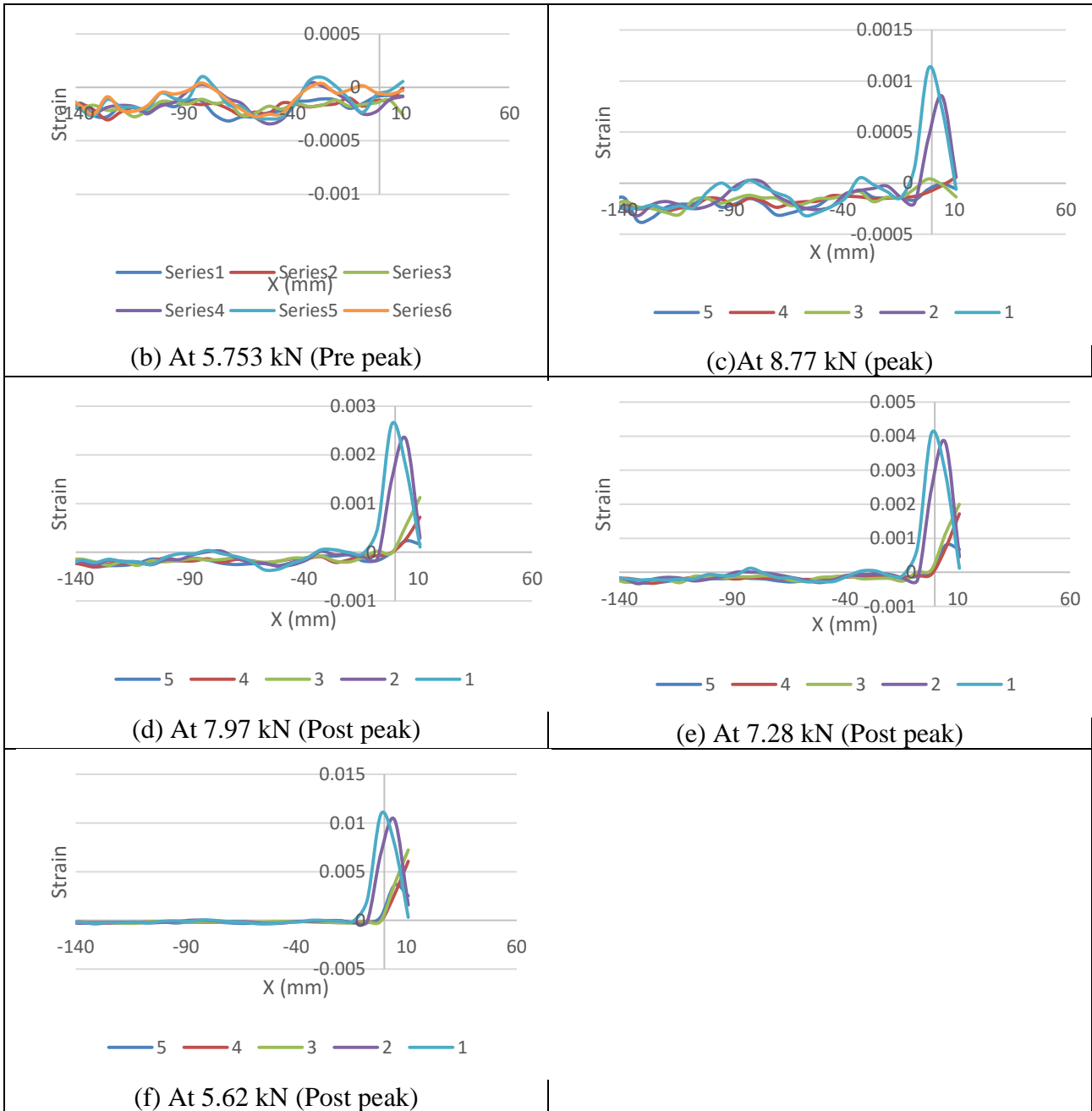


Fig 5.14 Variation of Strain value (ϵ_{xx}) on lines along the depth of section at distinct loads for polypropylene with 0.66 % volume at 7 days.

Differences in the crack propagation between control and FRC specimens are observed at larger CMOD openings. In the fiber reinforced concrete specimens, at a CMOD opening of 0.5 mm, strain localisation is evident at line 5. At the corresponding CMOD, the strain in line 5 in control specimens indicated very high values which were larger than 0.01.

5.4 Analysis of Results

The contribution of fibers result in the load arrest after an initial load drop in the immediate post-peak response. The increase in the total tensile resistance can be attributed to the increased resistance provided by additional fibers across the crack face with an increase in crack length and the additional stress due to increased resistance to crack opening displacement. An analysis of the influence of fibers on providing control of crack opening as the crack propagates into the matrix was performed by combining the results from DIC with the measured crack tip opening displacement (CTOD) obtained from a surface mounted gage at the tip of the notch. The depth of crack at any load was established from an analysis of ϵ_{xx} along horizontal lines located at different heights above the notch. The depth of the crack was established as the line at which the strain deviation produced by the observed localization exceeded by three standard deviations above the background trend. The general trend in crack propagation for increasing crack opening indicates that initially there is very large increase in crack depth for a small increase in CTOD. Subsequently, the crack depth essentially does not increase significantly for large change in CTOD. This indicates that initially there is a crack propagation, while subsequently, there is opening of the crack. There are also significant differences in the crack depth for a given crack opening between control and fiber reinforced concrete. At small values of CTOD, there is significantly higher crack propagation in control specimens than in fiber reinforced specimens. This suggests that fibers influence the propagation of crack, wherein for a given crack opening, there a smaller crack in the fiber reinforced concrete.

The resistance to crack opening comes from either pull out of the fiber from the matrix or fiber extension which could ultimately lead to fiber fracture. The crack opening displacement at which the resistance to crack opening provided by the fibers provides additional crack bridging stresses, depends on the fiber content.

Examination of the failed surface revealed few fibers which exhibited breakage in addition to fibers pulled out from the matrix. Presence of micro fibers leads to better reinforcement of the macro fibers. More macro fibers were found to break in case of HFRC. The post-peak load response at the different volume fractions is associated with both breakage and pullout response of fibers from the concrete matrix averaged over the crack. During crack propagation, debonding and sliding contribute significantly to the pull out resistance of the fibers and hence to the total energy consumption when a large crack develops in the matrix. Fiber breakage is also observed to contribute to the energy dissipated during crack propagation.

5.5 Summary and Findings

The results of the experimental investigation reveals that at low volume fractions, up to 0.88 % of polypropylene, once the matrix has cracked, initial part of the load response is controlled by crack propagation. In the initial softening part of the load response, there is very rapid increase in crack length for a small change in the crack opening. This part of the load response is identical for control and the fiber reinforced concrete specimens and there is little or no influence of fibers. On increasing the deflection, the load response in fiber reinforced beams exhibits a load recovery. The deviation from the softening response of control beams and the load recovery response is influenced by the fiber volume fraction. In the load recovery part of the load response, the crack growth is arrested by the fibers. There is a small increase in crack length as the crack opening continues to increase. The post-cracking resistance is primarily attributed to fiber pull-out.

Chapter 6

Analytical Model

6.1 Introduction

The bending failure of concrete beams may be modeled by the development of a fictitious crack in an elastic layer with a thickness proportional to the beam depth. A brief review about use of various types of stress crack opening (σ - w) relationship was presented in section 2.2. The cracked hinge model proposed by Olesen [14] was used for development of analytical model. The basic idea of the cracked hinge is to model a part of the beam close to the propagating crack as a layer of independent spring elements. These spring elements are formed by incremental horizontal strips, and are attached at each end to a rigid boundary (Fig 6.1). In this way the disturbance of the strain field, caused by the presence of the crack, is confined to take place between the rigid boundaries. Each rigid boundary may translate and rotate such that it may be joined with an uncracked beam modeled according to the classical beam theory. The constitutive relation of the spring layer is the same as that of the FRC, and according to the fictitious crack method, given by

$$\sigma = \begin{cases} E\varepsilon & \text{Precrack State } (w = 0) \\ \sigma_w(w) = g(w) * f_t & \text{cracked State } (w > 0) \end{cases}$$

where E = elastic modulus; ε = elastic strain; $\sigma_w(w)$ denotes the stress-crack opening relationship; and f_t = uniaxial tensile strength. The shape of the stress-crack opening relationship is defined by some function $g(w)$ of the crack opening w , normalized such that $g(0)=1$.

For FRC materials the stress crack open relationship is rather complex. It depends on amount, type of fibers, and age of matrix and pullout of fibers. The hinge model by Olesen starts by adopting a nonlinear hinge with finite length 's' usually a factor of depth as shown in Fig 6.1 within which the stress transfer through fibers is assumed to be taking place.

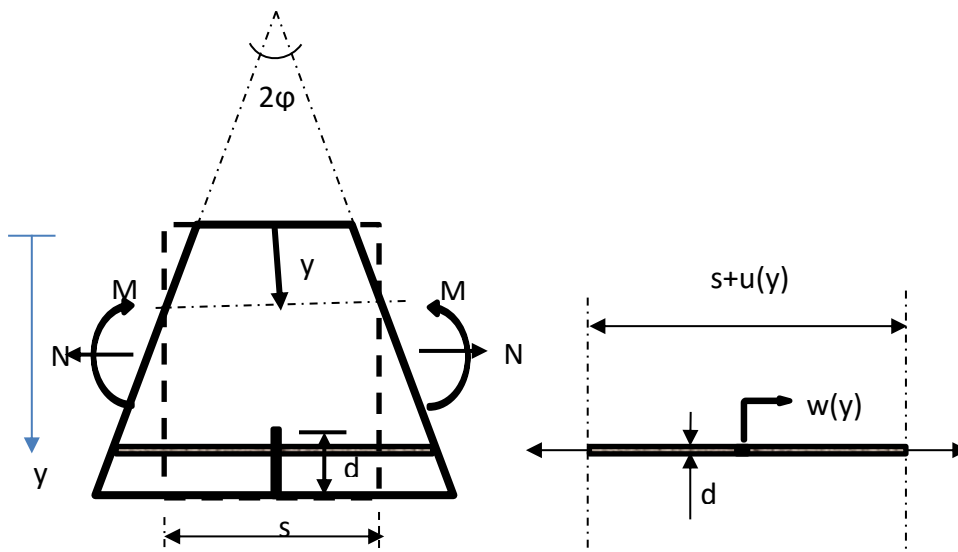


Fig 6.1 Geometry, Loading, and Deformation of Cracked Incremental Horizontal Strip of Hinge

The deformation of the hinge is described by half the angular deformation and the depth of the neutral incremental strip y_0 . It proves convenient to introduce the mean values of the curvature and the distribution of longitudinal strains κ^* and ε^* , respectively given by

$$\kappa^* = 2\phi/s \text{ and } \varepsilon^*(y) = (y-y_0)\kappa^*. \quad (5.1)$$

The deformation of an incremental strip is given by $u(y) = s + \varepsilon^*(y)$, in the case where the strip has cracked the deformation, $u(y)$ may also be obtained as the sum of the elastic deformation of the strip and the crack opening

$$u(y) = s\varepsilon^*(y) = s \frac{\sigma_w(w(y))}{E} + w(y) \quad (5.2)$$

From the equations 5.1 and 5.2 it can written as

$$\sigma_w(w(y)) = (2(y - y_0)\phi - w(y)) \frac{E}{s} \quad (5.3)$$

The bilinear stress crack model assumed by Olesen is shown in Fig 6.2 and the shape of the stress-crack opening relationship is defined by some function $g(w)$ of the crack opening w with slopes of lines and their offsets on ordinate axis which represent normalised tensile strength.

$$g(w) = b_i - a_i w = \begin{cases} b_1 - a_1 w & 0 \leq w < w_1 \\ b_2 - a_2 w & w_1 \leq w \leq w_2 \end{cases} \quad (5.4)$$

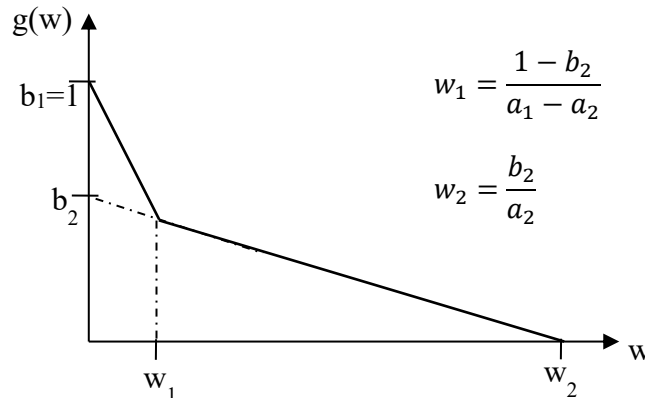


Fig 6.2 Definition of Parameters of Bilinear Stress-Crack opening relationship

From equation 5.3 and 5.4 $w(y)$ and $\sigma_w(w(y))$ for each value of i , the following solutions are obtained:

$$w(y) = \frac{2(y-y_0)\phi - \zeta_i}{1 - \beta_i} \quad (5.5a)$$

$$\sigma_w(w(y)) = \frac{\zeta_i - 2(y-y_0)\phi \beta_i E}{1 - \beta_i} \frac{E}{s} \quad (5.5b)$$

where

$$\beta_i = \frac{f_t a_i s}{E}; \quad \zeta_i = \frac{f_t b_i s}{E} \quad i \in 1, 2$$

The solutions given in (5.5) establish in analytical form the crack opening profile $w(y)$ and the stress distribution in the cracked part of the hinge $\sigma_w(w(y))$ as functions of the hinge deformations w and y_0 . As the crack propagates from the bottom of the hinge, the Stress distribution changes through three distinct phases (Fig 6.3). The crack-opening profile is divided into different intervals of i .

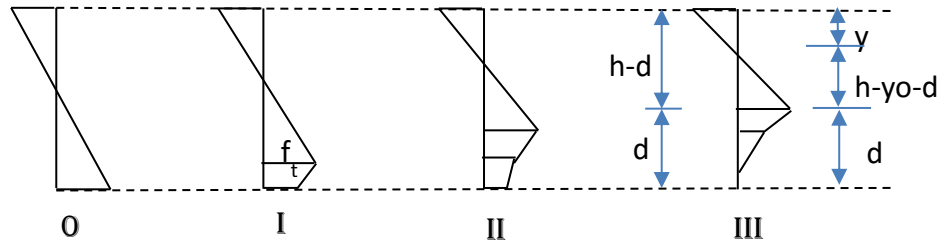


Fig 6.3 Distinct Phases of Stress Distribution during propagation of the crack in the section

Now complete stress distribution for all phases of pre and post cracking was established where phase 0 representing pre crack stress state and others post crack stress states. Now by equating sectional stresses with external applied force N , a relation between moment and curvature was established in the form of closed form equations. To make the derivation simple, following normalisation were introduced.

$$\mu = \frac{6M}{f_t h^2 t} \quad \rho = \frac{N}{f_t h t} \quad \theta = \frac{hE}{s f_t} \varphi \quad \alpha = \frac{d}{h} \quad (5.6 \text{ a-d})$$

The explicit equations for moment rotation with derivations are given in annexure I.

6.2 Load deflection curve from moment curvature analysis

Load-deflection curve can be calculated from given moment rotation relationship. Consider a beam with rectangular cross-section with depth h , width t and span L . The span of the beam is divided into three parts with a centre nonlinear hinge and elastic beam on the either side of the hinge as shown in **Fig 6.4**. The deflection v is calculated as a sum of elastic deflection and crack deflection (i.e. $v = v_e + v_c$)

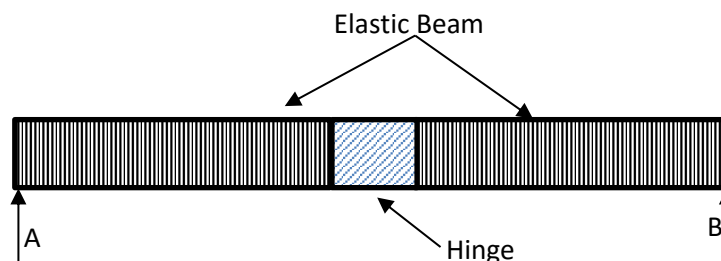


Fig 6.4 Model representation of simply supported beam after cracking

As per classical beam theory, the elastic deflection v_e is given by equation 5.7 (a) and deflection from the nonlinear hinge can be considered as rigid body rotation and is given by equation 5.7(b) but the hinge deflection is sum of deflection due to crack and elastic

deformation of hinge, hence to get deflection from crack only elastic deformation should be subtracted from hinge deflection and is given by equation 5.7(c)

$$v_e = \begin{cases} \frac{ML^2}{12EI} & \text{for centre point loading} \\ \frac{ML^2}{9EI} & \text{for third point loading} \end{cases} \quad (5.7a)$$

$$v_h = \phi * L/2 \quad \text{and} \quad (5.7b)$$

$$\phi_c = \phi - \phi_e \text{ where} \quad (5.7c)$$

Equation (5.7) upon normalisation as shown in Eq (5.8a) the normalised elastic deflection and crack deflection is be given by equations 5.8b and 5.8c

$$\delta = \frac{2\nu hE}{L s f_t} = \frac{2\nu \theta}{L \varphi} = \delta_e + \delta_c \quad (5.8a)$$

$$\delta_e = \begin{cases} \frac{L}{3s} \mu(\theta) & \text{for centre point loading} \\ \frac{4L}{9s} \mu(\theta) & \text{for third point loading} \end{cases} \quad (5.8b)$$

$$(5.8c)$$

$$\delta_c = \theta_c = \theta - \mu(\theta)$$

Total deflection is then given by

$$\delta = \delta_c + \delta_e = \begin{cases} \theta + \left(\frac{L}{3s} - 1\right) \mu(\theta) & \text{for centre point loading} \\ \theta + \left(\frac{4L}{9s} - 1\right) \mu(\theta) & \text{for third point loading} \end{cases} \quad (5.9)$$

Load is calculated for the given loading type from the known moment from equation

$$P(\theta) = \begin{cases} \frac{2}{3} \frac{f_t h^2 t}{L} \mu(\theta) & \text{Centre point loading} \\ \frac{f_t h^2 t}{L} \mu(\theta) & \text{Third point loading} \end{cases} \quad (5.10)$$

The load deflection curve obtained for a beam with adopted parameters (indicated in plot) is shown in figure 5.2.2.

6.3 Proposed Analytical Formulation for multi-linear softening

In order to capture the load recovery and a second peak (or subsequent peak points) after initial post-peak softening, a multi linear stress crack opening is required. Unlike the bi-linear case, the multi-linear stress crack opening relationship may not be readily amenable to deriving closed form solutions. In order to simplify the algorithm, the formulation and definition of stress crack opening relationship has been modified keeping the background mechanism and assumptions identical to the Olesen model. Multi linear Stress crack opening relationship can be described with coordinates as shown in **Fig 6.**, where b axis is described as

a fraction of f_t (such that b values will be always less than 1) and corresponding stress will be b times f_t , the stress distribution for the given relationship is shown in **Fig 6.**

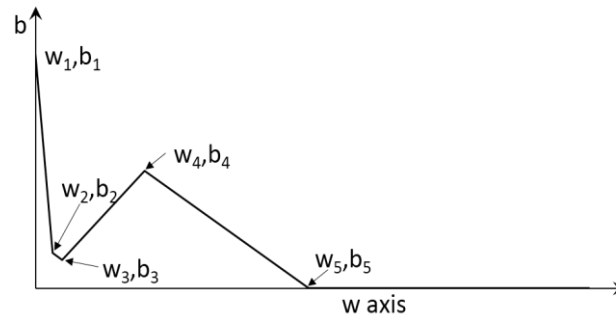


Fig 6.5 Definition of Parameters of Multi linear Stress-Crack relationship

A procedure for obtaining the moment-curvature relationship considering the multi-linear stress-crack opening relationship is presented below. The stress distribution in a section of height h , with crack tip located at a depth d , is shown in Figure 5.3.2. The stress distribution in the cracked portion reflects the multi-linear cohesive stress-crack opening relationship shown in Figure 5.3.1.

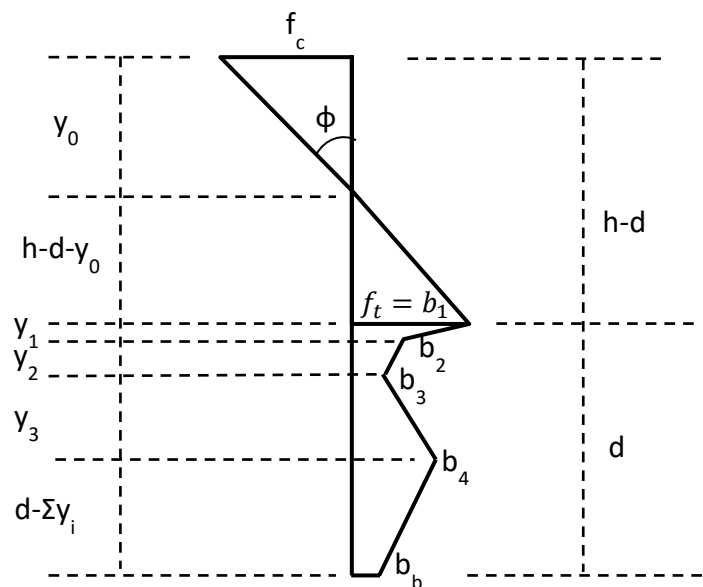


Fig 6.6 General Stress distribution for multi linear case

From compatibility relationship,

$$f_c = \frac{f_t \cdot y_0}{h-d-y_0} \quad (5.9)$$

At the crack tip, the response is elastic (the strain should be elastic) and stress will be equal to tensile strength (i.e. $\sigma_w = f_t$). Therefore, keeping y as $h-d$ and $\sigma_w = f_t$ in equation 5.3 gives

$$d + y_0 = h - \frac{s \cdot ft}{2\phi \cdot E} = h - \frac{h}{2\theta} \quad (5.10)$$

For a given stress crack opening relationship, using equation 5.3 at start point and end point of a line and their difference gives a relation between k_i and normalised rotation as follows. (See Annexure III for detailed derivation).

$$k_i = (b_{i+1} - b_i) + (w_{i+1} - w_i) \frac{E}{s f_t}, \quad (5.11)$$

where $k_i = \frac{2\theta y_i}{h}$

Slope of the lines are given by

$$m_i = \frac{b_{i+1} - b_i}{w_{i+1} - w_i} \in i = 1 \text{ to } n - 1 \quad (5.12)$$

where 'n' represents number of coordinates

In the Equation 5.11, k_i is normalised y_i , which is independent of rotation. Then all transitions rotations (θ_i) are found by force equilibrium as depth, now can be expressed as summation of y_i and is given as in equation 5.12 where transition rotation is rotation at which the slope of line changes.

$$\theta_i = \frac{1}{2} \left[\left(1 + \sum k_i \right) + \left(1 + \sum (k_i (b_{i+1} + b_i)) \right)^{1/2} \right] \quad (5.13)$$

After evaluating transitions the normalized rotation is gradually increased, when $\theta < 1$ (pre crack state), $\mu = \theta$ and for $\theta > 1$, if we observe **Fig 6**. for a given rotation, stresses distribution above the crack can be expressed in terms of α using equations 5.9 and 5.10. Stress distribution below the crack is known except in the bottom $d - \sum y_i$ portion. Stress at bottom (b_b) is expressed in terms of α using equation 5.3 by substituting $y=h$ and calculating width at bottom by using slope of the corresponding line given by equation 5.12.

$$b_b = \frac{(1+2\alpha\theta) + j_i(b_i - m_i w_i)}{1 + j_i} \quad \text{where } j_i = \frac{E}{m_i s f_t} \quad (5.14)$$

The requirement of force equilibrium (the total force on the section is zero) results in a quadratic equation in terms of α , the depth of crack. The depth of neutral axis is obtained from equation 5.10. Moment of stresses is used to calculate the normalised moment. The moment curvature relationship is obtained by repeating the exercise for different values of curvature. (See Annexure II for detailed derivation).

6.4 Inverse analysis

The crack hinge model provides a conceptual framework to interpret the flexural response of a beam in terms of a propagating crack with the crack closing stresses provided by

fibers bridging the crack. In the previous sections the forward analysis for predicting the flexural load response using the crack hinge model with known cohesive stress-crack opening relationship has been performed. The cohesive crack closing stresses on the load response has been shown to have a significant influence on flexural the load response, from the peak load to the shape of the post-peak load response. It is established that the tensile strength and the initial slope of the cohesive stress-crack opening relationship influence the peak strength in flexure. Further, the load recovery portion of the post-peak load response has been shown to be totally the contribution of fibers bridging the crack. The measured response in flexure therefore provides a means for determining the cohesive stress-crack opening relationship.

To determine the cohesive stress-crack opening relationship from the measured flexural response an inverse analysis algorithm has been developed in which the experimentally obtained load deflection response was given as input and the difference with the predicted load response using the hinged crack is minimized. The difference between the two responses was minimized in the least squares sense. An objective function of the normalized squares of residuals for the peak load and the load response was developed.

$$Norm = \frac{1}{n} \sqrt{\sum_{i=1}^n (P_i^{exp} - P_i^{theoretical})^2}$$

where P_i^{exp} and $P_i^{theoretical}$ are the i^{th} loads in the experimental and numerically predicted load responses at corresponding values of deflection, respectively.

A multilinear cohesive stress-crack opening relation of the form shown in Figure 6.8 was assumed. The parameters of the cohesive relationship were optimized to minimize the least square residual. A two-step inversion strategy was developed to separately optimize the tensile strength and the initial softening part of the cohesive behaviour. As the initial part of load deflection response is highly dependent on matrix properties, it was found to be highly sensitive to f_t and initial slope of stress crack relation and hence this part of load response was optimized separately by considering load deflection relationship up to a deflection of 0.3 mm. In first step the tensile strength (f_t) and slope of initial line of stress crack opening relationship by changing b_2 using the load response including the initial softening up to a displacement of $_mm$. In the next step, the value of f_t obtained in th previous step was kept fixed while the other cohesive values at predefined crack openings were optimized.

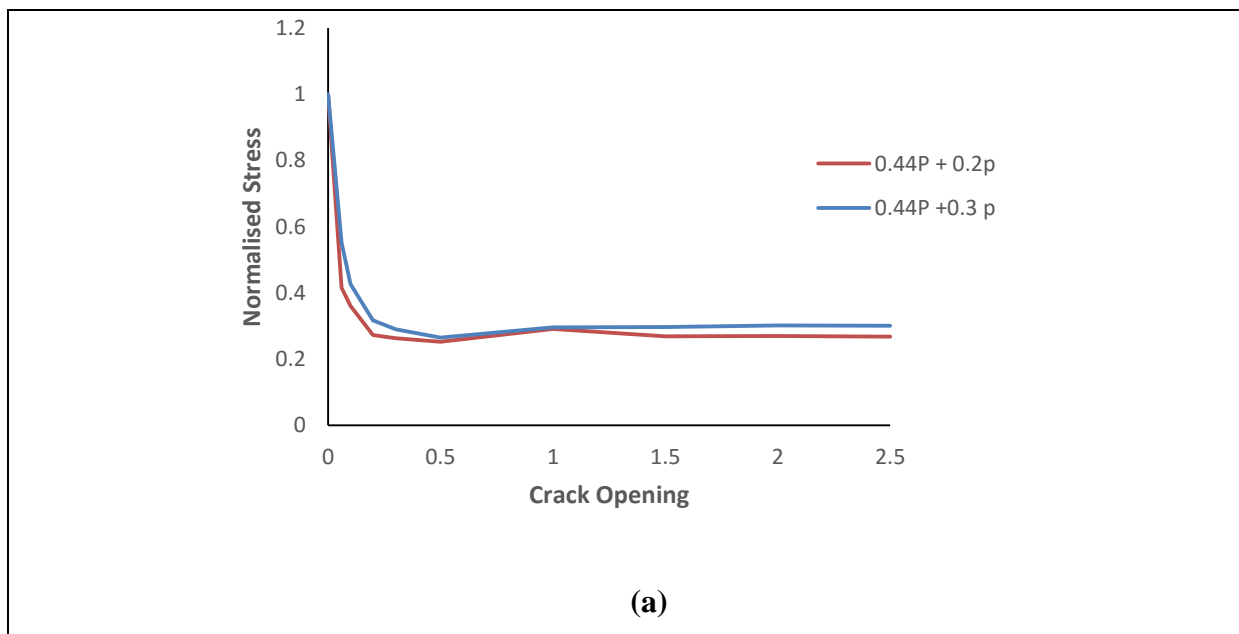
The inversion procedure was implemented numerically in Matlab®. In Matalb®, constrained function minimization algorithm was used in which, constraints were applied on crack opening parameters and tensile strength of concrete. In the first step of optimization, considering the load deflection response up to 0.3 mm, the value of a_2 was fixed at 0.06 mm as it is observed that the peak is attained before an opening of 0.06 mm. The tensile strength f_t was kept fixed and the value of b_2 obtained in the first step was used as an initial guess in the next step. Value of b_2 was not fixed in the second step as it was observed to have an influence on the point of load recovery in the post-peak load response. In second step the crack opening values are predefined with a regular interval considering the sensitivity of load deflection diagram and corresponding stress values were found so as to get good match and predefining

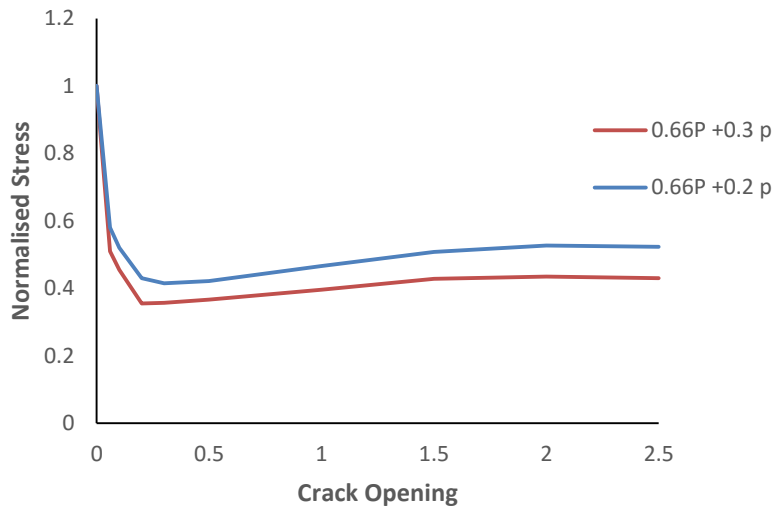
opening values also makes it easy to compare the crack bridging stresses developed by different fiber volumes.

The match between experimental and analytically developed load deflection response and corresponding stress crack opening relation for HFRC beams with 0.66 % of macro polypropylene with 0.3 % micro polypropylene are shown in Figure 6.8. It can be seen that a very close match between the experimental and the predicted load response is obtained. While the cohesive stress-crack opening relationships for the control specimen exhibits a monotonic decrease in stress with crack opening, the FRC exhibits a hardening type behaviour with increasing crack opening after an initial decrease following the initial post-peak softening.

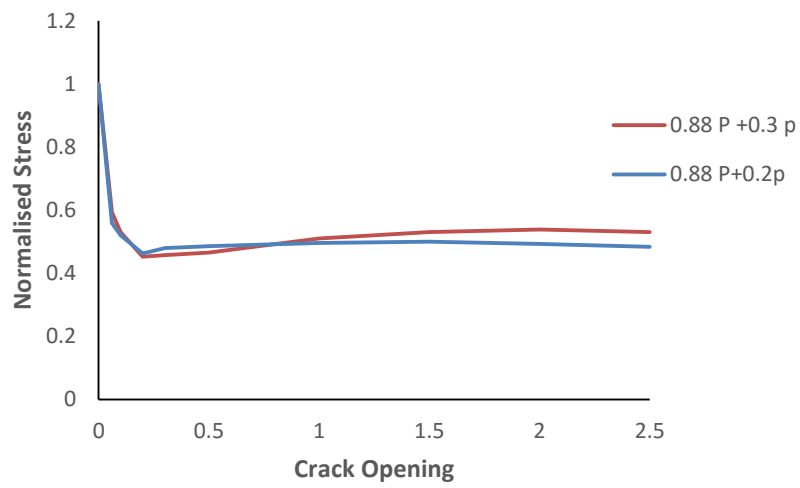
The cohesive stress-crack opening relationships obtained from the inversion analysis are also plotted in Fig 6.7. A comparison of the distinctive points of the cohesive stress response obtained from the control, SFRC and HFRC is shown in

Table 6.2. It can be observed that the stress crack opening relation is not affected up to an opening of 0.1 mm and there is deviation in the stress response after a crack opening of 0.1 mm due to crack closing stresses provided by fibers. Crack closing stresses increase after a crack opening of about 0.1 mm and the increase is in proportion with micro fiber volume for both HFRC. HFRC exhibits a clear trend in an increase in closing stresses with micro fiber volume.

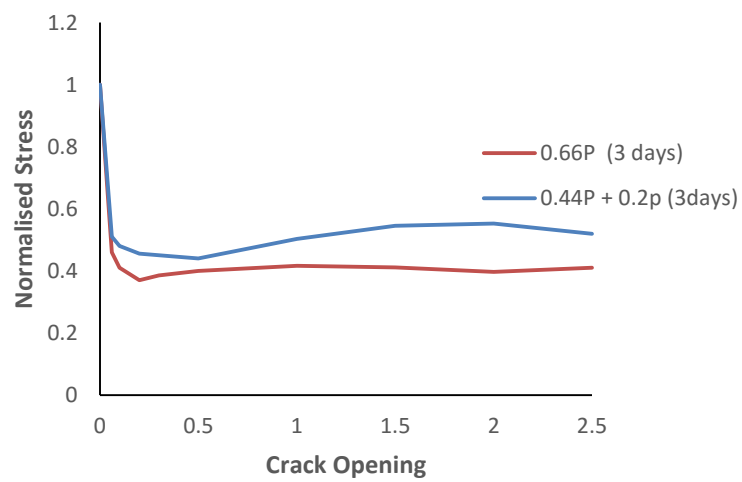




(b)



(c)



(d)

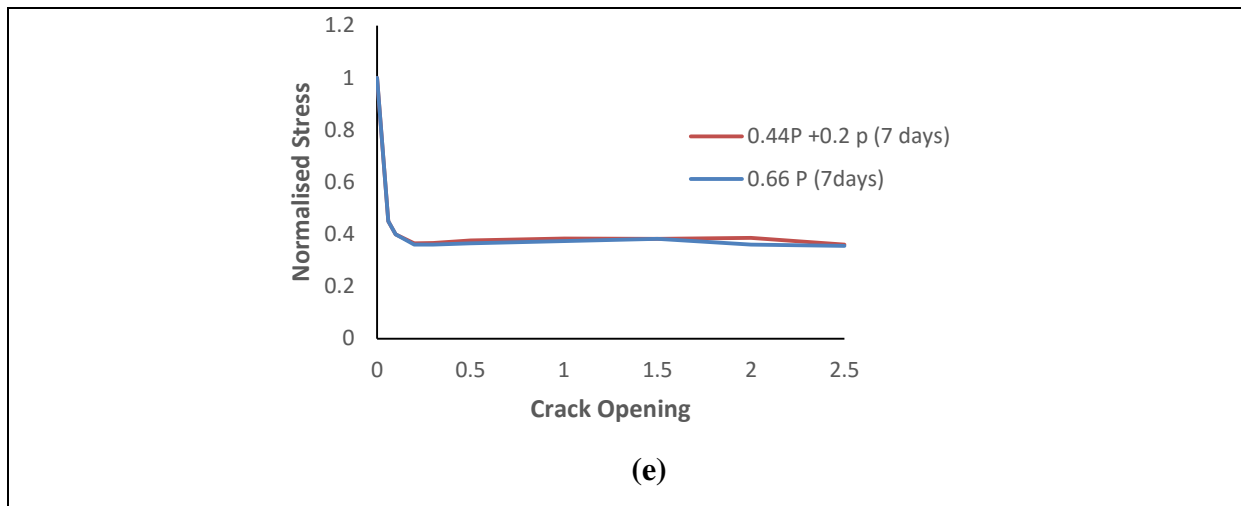


Fig 6.7 Stress Crack opening relationship of HFRC beams by adding 0.2 and 0.3 % micro fibers to a) 0.44 P b) 0.66% P c) 0.88% P d) 3 day specimens e) 7 day Specimens

Table 6.2 Mean Values Of crack opening parameters of SPFRC Beam

Days	Crack opening (mm)	1	0.06	0.1	0.3	1	2	2.5	f_t
3	0.44 % P + 0.2%p	1	0.51	0.48	0.47	0.50	0.55	0.52	1.34
	0.66 % P	1	0.46	0.41	0.39	0.42	0.40	0.41	1.21
7	0.44 % P + 0.2%p	1	0.45	0.4	0.37	0.38	0.39	0.36	1.27
	0.66 % P	1	0.45	0.40	0.36	0.37	0.36	0.36	1.35
28	Control	1	0.26	0.22	0.01				1.97
	0.44 % P	1	0.35	0.33	0.22	0.34	0.34	0.28	1.69
	0.44 % P + 0.2%p	1	0.42	0.36	0.26	0.29	0.18	0.29	1.77
	0.44 % P + 0.3%p	1	0.55	0.43	0.29	0.30	0.30	0.30	1.85
	0.66 % P	1	0.19	0.22	0.18	0.29	0.30	0.35	2.24
	0.66 % P + 0.2%p	1	0.51	0.45	0.36	0.40	0.43	0.43	1.73
	0.66 % P + 0.3%p	1	0.58	0.52	0.41	0.47	0.53	0.52	1.71
	0.88 % P	1	0.27	0.26	0.26	0.38	0.43	0.45	2.15
	0.88 % P + 0.2%p	1	0.56	0.52	0.48	0.50	0.49	0.48	1.91
0.88 % P + 0.3%p	1	0.59	0.63	0.46	0.51	0.54	0.53	1.80	

A comparison of the experimental and the numerically predicted load deflection responses of beams is shown in **Fig 6.** It can be seen that there is a good match between experimental and theoretical curves for all HFRC beams. The difference in the area under curve between the experimental and the numerically predicted responses was mostly less than 1 percent. The model is able to capture the non-linearity prior to peak load, the load recovery point and also load recovery portion. But there is a small deviation in the immediate post peak response after peak where the model is unable to capture the steep load drop. This may be improved by changing predefined crack opening values which are used in the calculation of the norm.

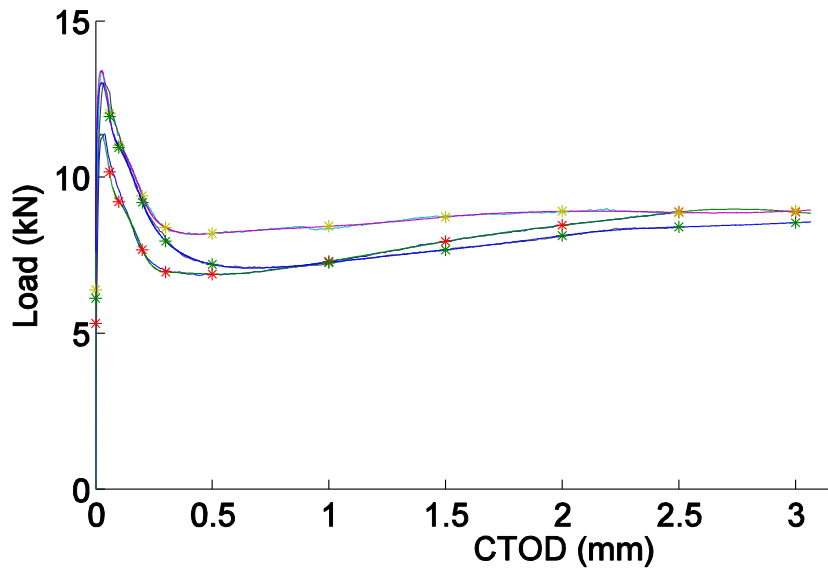


Fig 6.8 Experimental and matched theoretical curves of HFRC 0.66 P+ 0.3 p beams.

Using the results of the inversion analysis, the relationship between the crack length and the crack opening are obtained. The crack length in the hinged crack model is defined by the depth at which the stress is equal to the tensile strength, f_t . Similarly, the crack opening is the crack opening displacement at the lowest portion of the beam. The relationship between the crack length and the crack opening displacement is plotted in Fig 6.9 and 6.10 for HFRC at later age and early age respectively. The results indicate that initially for a small increase in crack opening there is a large increase in the crack length. However, later there is a smaller increase in the crack length and the response is dominated by the opening of the crack. The results also indicate that crack propagation along the depth of section is significantly affected by tensile strength. For a given crack opening, the crack length in specimens with a higher f_t are smaller

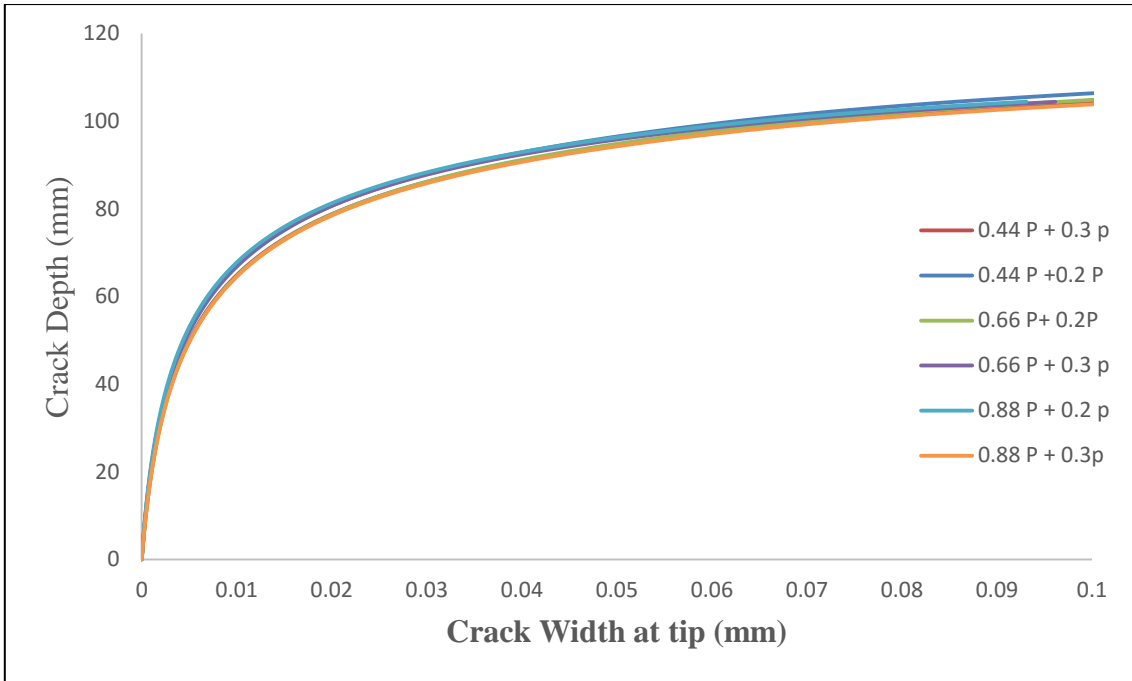


Fig 6.9 Crack depth vs Crack width for mean Crack opening parameters of HFRC

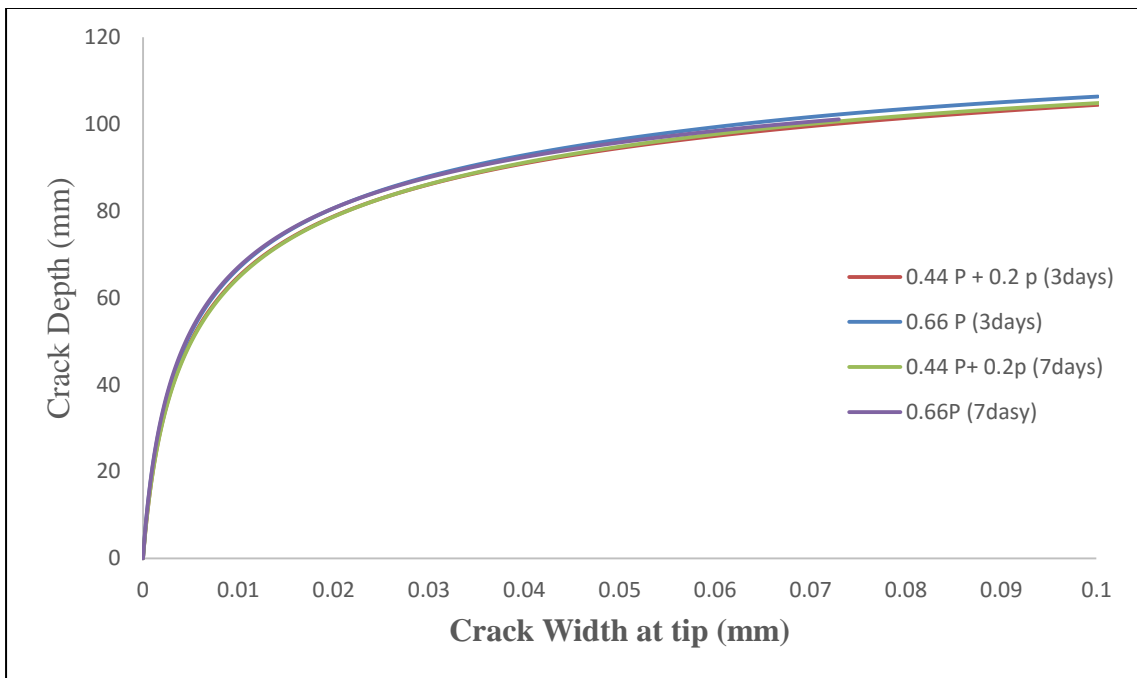


Fig 6.10 Crack depth vs Crack width for mean Crack opening parameters of HFRC (early age)

Chapter 7

Summary of findings and Future Works

The results of the experimental investigation reveals that at low volume fractions, up to 0.88 % by volume, once the matrix has cracked, initial part of the load response is controlled by crack propagation. In the initial softening part of the load response, there is very rapid increase in crack length for a small change in the crack opening. This part of the load response is identical for control and the fiber reinforced concrete specimens and there is little or no influence of fibers. On increasing the deflection, the load response in fiber reinforced beams exhibits a load recovery. The deviation from the softening response of control beams and the load recovery response is influenced by the fiber volume fraction. In the load recovery part of the load response, the crack growth is arrested by the fibers. There is a small increase in crack length as the crack opening continues to increase. The crack closing stresses provided by the fibers also increase with increasing crack opening allowing the composite beam to carry increasing load. The post-cracking resistance is primarily attributed to fiber pull-out. While no significant increase in composite strength is observed, considerable enhancement of the composite fracture energy and toughness is obtained. The presence of micro fibers along with macro fibers resulted in synergy. The matrix strength was improved and provided more reinforcement to the macro fibers thereby resulting in higher pull out resistance.

The implications of the observed post-peak load carrying ability with fibers are discussed below

The increase in toughness obtained from the use of fibers allows cracks in indeterminate structures to work as hinges and to redistribute loads. In this way, the failure load of the structure may be substantially higher than for the unreinforced structure although the flexural strength of the plain concrete, tested on beams, is not increased.

Polypropylene fibers are not expected to bond chemically in a concrete matrix, but bonding has been shown to occur by mechanical interaction. The elastic modulus of the fiber is 10 GPa while the elastic modulus of mature concrete is expected to be higher than 20 GPa. The synthetic fibers were found effective at early ages where the improvement in the fracture behaviour would be significant relative to cracking load. Synthetic fibers have been shown to be effective in the early lifetime of the composite when the matrix is itself weak, brittle, and of low modulus. Considering this, synthetic fibers have great potential for replacement for shrinkage steel in concrete. And Hybrid (Macro with Micro fibers) was found more effective than the macro synthetic FRC at early ages.

Directions for future research that emerge from the findings of this study are:

1. Study the plastic shrinkage at early age with Hybrid fibers.
2. Investigate the fracture behaviour of the beams with macro Steel, macro polypropylene and micro polypropylene fibers.

References

- [1] R. F. Zollo, "Fiber-reinforced concrete: an overview after 30 years of development," *Cement and Concrete Composites*, vol. 19, no. 2, pp. 107-122, 1997.
- [2] B. Belletti, R. Cerioni, A. Meda and G. Plizzari, "Design Aspects on Steel Fiber-Reinforced Concrete Pavements," *Journal of Materials in Civil Engineering*, vol. 20, no. 9, pp. 599-607, 2008.
- [3] G. L. Sorelli, A. Meda and A. G. Plizzari, "Steel Fiber Concrete Slabs on Ground: A Structural Matter," *ACI Structural Journal*, vol. 103, no. 4, pp. 551-558, 2006.
- [4] L. Ferrara and A. Meda, "Relationships between fibre distribution, workability and the mechanical properties of SFRC applied to precast roof elements.," *Materials and Structures*, vol. 39, no. 4, pp. 411-420, 2006.
- [5] G. Ravindra, B. Bryan, G. Tomas, O. Jorge and J. Rolando, "Fiber Concrete Tunnel Lining: Construction of a Subway Line in Barcelona," *Concrete International*, vol. 28, no. 8, pp. 63-69, August 2006.
- [6] L. Taerwe and A. Van Gysel, "Influence of Steel Fibers on Design Stress-Strain Curve for High-Strength Concrete," *Journal of Engineering Mechanics*, vol. 122, no. 8, pp. 695-704, 1996.
- [7] A. C. 544, "State-of-the-Art Report on Fiber Reinforced Concrete," American Concrete Institute, 1996.
- [8] A. 544.3R-93, "Guide for Specifying, Proportioning, Mixing, Placing, and Finishing Steel Fiber Reinforced Concrete," American Concrete Institute, 1993.
- [9] Z. Bayasi and M. McIntyre, "Application of Fibrillated Polypropylene Fibers for Restraint of Plastic Shrinkage Cracking in Silica Fume Concrete," *Materials Journal*, vol. 99, no. 4, pp. 337-344, 7 1 2002.
- [10] V. S. Gopalaratnam and G. Ravindra , "On the characterization of flexural toughness in fiber reinforced concretes," *Cement and Concrete Composites*, vol. 17, no. 3, pp. 239-254, 1995.
- [11] L. Oostergaard, D. Lange and H. Stang, "Early-age stress-crack opening relationship for high performance concrete," *Cement and Concrete Composites*, vol. 26, no. 5, pp. 563-572, 2004.

- [12] H. K. Seung , Z. Zhifang and S. P. Shah, “Effect of specimen size on fracture energy and softening curve of concrete: Part II. Inverse analysis and softening curve,” *Cement and Concrete research*, vol. 38, no. 8-9, pp. 1061-1069, 2008.
- [13] U. 11039-2, “Steel Fibre Reinforced Concrete - Test Method For Determination Of First Crack Strength And Ductility Indexes,” 2003.
- [14] J. F. Olesen, “Fictitious Crack Propagation in Fiber-Reinforced Concrete Beams,” *Journal of Engineering Mechanics*, vol. 127, no. 3, pp. 272-280, 01 March 2001.
- [15] R. T. 162_TDF, “Test and design methods for steel fibre reinforced concrete, “Design of steel fibre reinforced concrete using the (σ -w method: principles and applications),” *Materials and Structures*, vol. 35, pp. 262-278, 2002.
- [16] A. Hillerborg, “Analysis of fracture by means of the fictitious crack model, particularly for fibre reinforced concrete,” *International Journal of Cement Composites*, vol. 2, no. 4, pp. 177-184, 1980.
- [17] R. Evans and M. Marathe, “Microcracking and stress-strain curves for concrete in tension,” *Materials and Structures, Matériaux et Construction*, vol. 1, no. 1, pp. 61-64, 1968.
- [18] P. Petersson, “Fracture energy of concrete: Practical performance and experimental results,” *Cement and Concrete Research*, vol. 10, no. 1, pp. 91-101, 1980.
- [19] H. Reinhardt, “Fracture Mechanics of an Elastic Softening Material like Concrete,” pp. 5-41, 01 01 1984.
- [20] K. Visalvanich and A. E. Naaman, “Fracture Model for Fiber Reinforced Concrete,” *ACI Journal*, vol. 80, no. 2, pp. 128-138, 1983.
- [21] M. Wecharatana and S. P. Shah, “A Model for Predicting Fracture Resistance of Fiber Reinforced Concrete,” *Cement and Concrete Research*, vol. 13, no. 6, pp. 819-829, Novemeber 1983.
- [22] V. S. Gopalaratnam and S. P. Shah, “Post-Cracking Characteristics of Concrete in Uniaxial Tension,” in *Engineering Mechanics in Civil Engineering*, New York, 1984.
- [23] A. R. Ingraffea and W. H. Gerstle, “Non-Linear Fracture Models for Discrete Crack Propagation,” in *Application of Fracture Mechanics to Cementitious Composites, NATO ASI series*, 1985.
- [24] S. P. Shah and C. Ouyang, “Mechanical Behavior of Fiber-Reinforced Cement-Based

Composites,” *Journal of the American Ceramic Society*, vol. 74, no. 11, pp. 2727-38,2947-53, November 2005.

- [25] G. R. Williamson, “The Effect of Steel Fibers on the Compressive Strength of Concrete,” *Fiber Reinforced Concrete, SP-44*, vol. 44, pp. 195-208, 1974.
- [26] C. D. Johnston, “Steel Fiber Reinforced Mortar and Concrete: A Review of Mechanical Properties,” *Fiber Reinforced Concrete SP-44*, vol. 44, pp. 127-142, 1974.
- [27] C. D. Johnston and R. J. Gray, “Uniaxial Tension Testing of Steel Fibre Reinforced Cementitious Composites,” in *Proceedings, International Symposium on Testing and Test Methods of Fibre-Cement Composites.*, 1978.
- [28] J. N. Kar and A. K. Pal, “Strength of Fiber-Reinforced Concrete,” *Journal of the Structural Division, ASCE*, vol. 98, no. 5, pp. 1053-1068, 1972.
- [29] J. P. Romualdi and J. A. Mandel, “Tensile Strength of Concrete Affected by Uniformly Distributed and Closely Spaced Short Lengths of Wire Reinforcement,” *ACI Journal Proceedings*, vol. 61, no. 6, pp. 657-672, 1964.
- [30] C. D. Johnston and R. A. Coleman, “Strength and Deformation of Steel Fiber Reinforced Mortar in Uniaxial Tension,” *Fiber Reinforced Concrete, SP-44 American Concrete Institute*, vol. 44, pp. 177-194, 1974.
- [31] C. D. Johnston, “Definition and Measurement of Flexural Toughness Parameters for Fiber Reinforced Concrete,” *ASTM- Cement, Concrete and Aggregates*, vol. 4, no. 2, pp. 53-60, 1982.
- [32] V. Ramakrishnan, T. Brandshaug, W. V. Coyle and E. K. Schrader, “Comparative Evaluation of Concrete Reinforced with Straight Steel Fibers and Fibers with Deformed Ends Glued Together into Bundles,” *American Concrete Institute*, vol. 77, no. 3, pp. 135-143, 1980.
- [33] C. D. Johnston and R. J. Gray, “Flexural Toughness First-Crack Strength of Fibre-Reinforced-Concrete Using ASTM Standard C 1018,” in *Proceedings, Third International Symposium on Developments in Fibre Reinforced Cement Concrete, RILEM*, , Sheffield, 1986.
- [34] P. J. Hannant, “FIBRE CEMENTS AND FIBRE CONCRETES,” Wiley(John) & Sons, Limited, Chichester, United Kingdom, 1978.
- [35] H. Cifuentes, F. Garcia, O. Maeso and F. Medina, “Influence of the properties of polypropylene fibres on the fracture behaviour of low-, normal- and high-strength FRC,”

Construction and Building Materials, vol. 45, pp. 130-137, August 2013.

- [36] B. H. Oh, J. C. Kim and C. Y. Choi, "Fracture behavior of concrete members reinforced with structural synthetic fibers," *Engineering Fracture Mechanics*, vol. 74, no. 1-2, pp. 243-257, January 2007.
- [37] M. N. Soutsos, T. T. Le and A. P. Lampropoulos, "Flexural performance of fibre reinforced concrete made with steel and synthetic fibres," *Construction and Building Materials*, vol. 36, pp. 704-710, November 2012.
- [38] S. Singh, A. Shukla and R. Brown, "Pullout behavior of polypropylene fibers from cementitious matrix," *Cement and Concrete Research*, vol. 34, no. 10, pp. 1919-1925, October 2004.
- [39] F. Benacardino, L. Rizzuti, G. Spadea and R. N. Swamy, "Experimental evaluation of fiber reinforced concrete fracture properties," *Composites Part B: Engineering*, vol. 41, no. 1, pp. 17-24, January 2010.
- [40] A. Hillerborg, M. Modeer and P. E. Petersson, "Analysis of crack formation and crack growth in concrete by means of fracture mechanics and finite elements," *Cement and Concrete Research*, vol. 6, no. 6, pp. 773-781, November 1976.
- [41] N. Buratti, C. Mazzotti and M. Savoia, "Post-cracking behaviour of steel and macro-synthetic fibre-reinforced concretes," *Construction and Building Materials*, vol. 25, no. 5, pp. 2713-2722, May 2011.
- [42] J. Barros, V. Cunha, A. F. Ribeiro and J. A. B. Antunes, "Post-cracking behaviour of steel fibre reinforced concrete," *Materials and Structures*, vol. 38, no. 1, pp. 47-56, January-February 2005.
- [43] Larson ES, Krenchel H. "Durability of FRC –materials" . Mater Res Soc Symp proc Vol.211,pp 119-124, 1991
- [44] Dorel Feldman and Zhihong Zheng " Synthetic Fibres for Fibre Concrete Composites." MRS Proceedings, 305, 123 doi:10.1557/PROC-305-123, 1993
- [45] Horiguchi T, Sakai K. " Hybrid effects of fiber reinforced concrete on fracture toughness" : Third ACI Int. Conf. (SP-172), Malaysia; 1997. p. 535–48
- [46] Qian CX, Stroeven P. Development of hybrid polypropylene-steel fiber reinforced concrete. *Cem Concr Res* 2000;30:63–9.

- [47] Ramanalingam N, Paramasivam P, Mansur MA, Maalej M. Flexural behaviour of hybrid fiber-reinforced cement composites containing high-volume fly ash. *ACI SP 199 2001*:147–62.
- [48] Lawler J, Zampini D, Shah SP. Permeability of cracked hybrid fiber reinforced mortar under load. *ACI Mater J 2002*(July–August):379–85.
- [49] Wu Yaa, Jie Lib, Keru Wua : Mechanical properties of hybrid fiber-reinforced concrete at low fiber volume fraction, *Cement and Concrete Research* (2003) 27–30
- [50] N. Banthia and R. Gupta Hybrid fiber reinforced concrete (HyFRC): fiber synergy in high strength matrices *MATERIALS AND STRUCTURES*. Vol. 37, 2004, pp 707-716
- [51] Lawler, Davide Zampini, Surendra P. Shah, *Microfiber and Macrofiber Hybrid Fiber Reinforced Concrete*, *Journal of Materials in Civil Engineering*. ASCE (2005) 595–694.
- [52] Banthia N, Soleimani SM. Flexural response of hybrid fiber reinforced cementitious composites. *ACI Mater J 2005*;102(5):382–9.
- [53] S.F Uddin Ahmed , M. Maalej , P. Paramasivam, Flexural responses of hybrid steel polyethylene fiber reinforced cement composites containing high volume fly ash. *Construction and bulding materials*. 2006
- [54] Banthia N, Sappakittipakorn M. Toughness enhancement in steel fiber reinforced concrete through fiber hybridization. *Cem Concr Res 2007*;37(9):1366–72
- [55] Machine Hsie, Chijen Tu, P.S. Song : Mechanical properties of polypropylene hybrid fiber-reinforced concrete, *Materials Science and Engineering A 494* (2008) 153–157
- [56] N. Banthia , F. Majdzadeh, J.Wu, V. Bindiganavile, “Fiber synergy in Hybrid Fiber Reinforced Concrete (HyFRC) in flexure and direct shear”. / *Cement & Concrete Composites 48* (2014) 91–97
- [57] T. C. Chu, W. F. Ranson, M. A. Sutton and W. H. Peters, “Applications of Digital Image correlation technique to Experimental Mechanics,” *Exp. Mech*, vol. 25, pp. 232-244, 1985
- [58] A. Kobayashi, *Handbook on Experimental Mechanics*, Indiana: Prentice Hall / Society for Experimental Mechanics, Inc., Lebanon, 1993.
- [59] f. Pierron , B. Green, Wisnom MR and S. R. Hallet, “Full-field assessment of the damage process of laminated composite open-hole tensile specimens. Part I: methodology,” *Compsites*, vol. 38, pp. 2307-2320, 2007
- [60]] K. V. Subramaniam, C. Carloni and L. Nobile, “Interface Fracture and Debonding in the FRP-Concrete Interface: Influence of the FRP Laminate width on Load Capacity,” *Engineering Fracture Mechanics*, vol. 74, no. 4, pp. 578-594, 2007.

Appendix I

Fiber Count Data

0.44 P + 0.2 p (28 days)

Unnotched 0.44P + 0.2p-1						
1	0	1	0	2	4	8
3	4	1	1	5	7	21
0	1	0	0	2	3	6
0	1	0	0	2	3	6
0	0	1	0	0	1	2
0	0	0	4	1	3	8
4	6	3	5	12	21	51

Unnotched 0.44P + 0.2p-2						
1	0	5	1	2	1	10
3	4	1	1	3	0	12
0	1	2	2	1	2	8
0	0	0	2	1	1	4
0	3	0	1	1	0	5
1	1	5	1	1	0	9
5	9	13	8	9	4	48

Unnotched 0.44P + 0.2p-3						
1	0	1	0	2	4	8
3	4	1	1	5	7	21
0	1	0	0	2	3	6
0	1	0	0	2	3	6
0	0	1	0	0	1	2
0	0	0	4	1	3	8
4	6	3	5	12	21	51

Unnotched 0.44P + 0.2p-4						
1	0	2	3	2	0	8
3	0	1	0	1	1	6
1	0	1	0	1	1	4
2	2	3	2	0	1	10
1	1	1	3	2	1	9
0	0	3	5	0	0	8
8	3	11	13	6	4	45

Notched 0.44P + 0.2p-1						
1	0	0	1	2	1	5
0	1	1	0	0	2	4
0	1	1	0	0	0	2
1	1	2	0	2	3	9
1	1	3	2	0	3	10
0	0	0	0	0	0	0
3	4	7	3	4	9	30

Notched 0.44P + 0.2p-2						
0	2	2	0	2	0	6
0	2	1	0	2	0	5
0	0	0	0	0	0	0
1	0	0	0	1	2	4
0	1	1	0	3	2	7
0	0	0	0	0	0	0
1	5	4	0	8	4	22

Notched 0.44P + 0.2p-3						
0	6	1	1	2	0	10
3	1	0	3	1	1	9
1	0	0	1	2	1	5
1	1	2	0	5	2	11
2	2	4	4	1	1	14
0	0	0	0	0	0	0
7	10	7	9	11	5	49

Notched 0.44P + 0.2p-4						
0	2	3	3	1	2	11
2	2	2	1	1	1	9
1	0	1	2	0	0	4
0	1	1	1	0	1	4
1	2	0	0	1	2	6
0	0	0	0	0	0	0
4	7	7	7	3	6	34

0.44 P +0.3 p (28 days)

Unnotched 0.44P + 0.3p-1						
1	1	2	1	1	2	8
0	0	1	3	0	0	4
2	2	0	3	1	1	9
4	2	3	1	0	1	11
1	5	4	1	1	2	14
2	2	2	2	2	2	12
10	12	12	11	5	8	58

Unnotched 0.44P + 0.3p-2						
1	1	2	0	0	0	4
4	1	0	1	0	0	6
3	0	1	0	0	2	6
2	1	1	1	0	1	6
1	0	2	3	1	2	9
3	2	4	0	2	1	12
14	5	10	5	3	6	43

Unnotched 0.44P + 0.3p-3						
3	3	0	0	0	0	6
2	0	1	1	0	0	4
0	2	4	3	1	1	11
1	0	3	1	0	1	6
1	0	3	2	1	1	8
0	0	2	0	5	4	11
7	5	13	7	7	7	46

Unnotched 0.44P + 0.3p-4						
1	0	3	2	0	0	6
0	0	3	0	0	1	4
2	2	0	2	0	0	6
2	0	4	1	2	1	10
3	1	0	3	2	3	12
0	3	2	3	0	5	13
8	6	12	11	4	10	51

Notched 0.44P + 0.3p-1						
1	1	2	2	1	3	10
0	3	2	2	2	3	12
1	0	0	3	1	2	7
1	5	1	2	3	1	13
0	3	0	0	1	1	5
0	0	0	0	0	0	0
3	12	5	9	8	10	47

Notched 0.44P + 0.3p-2						
0	0	3	0	3	1	7
0	0	4	1	1	0	6
1	0	2	0	0	2	5
2	1	2	2	1	0	8
0	2	1	3	0	0	6
0	0	0	0	0	0	0
3	3	12	6	5	3	32

Notched 0.44P + 0.3p-3						
2	2	1	0	2	0	7
0	0	0	1	0	0	1
3	0	0	0	1	1	5
3	0	0	0	1	1	5
1	2	1	0	1	0	5
0	0	0	1	2	0	3
9	4	2	2	7	2	26

Notched 0.44P + 0.3p-4						
0	2	0	1	3	4	10
1	4	0	2	2	1	10
0	0	2	2	0	1	5
0	0	2	2	0	1	5
0	1	0	0	0	2	3
0	0	0	0	3	3	6
1	7	4	7	8	12	39

0.66 P + 0.2 p (28 days)

Unnotched 0.66P + 0.2p-1						
0	4	1	0	2	1	8
3	2	0	0	3	2	10
0	4	2	1	0	0	7
1	2	0	2	0	1	6
0	1	1	2	0	3	7
2	2	2	1	0	2	9
6	15	6	6	5	9	47

Unnotched 0.66P + 0.2p-2						
3	0	1	1	3	1	14
1	2	4	3	1	1	12
0	1	7	2	1	3	14
2	0	0	4	0	3	9
3	1	1	2	3	2	12
1	1	0	1	2	3	8
10	5	13	18	10	13	69

Unnotched 0.66P + 0.2p-3						
0	5	2	3	0	5	15
1	3	5	2	3	4	18
2	2	2	2	1	0	9
2	1	3	0	0	1	7
0	0	1	3	4	0	8
0	4	4	2	4	2	16
5	15	17	12	12	12	73

Unnotched 0.66P + 0.2p-4						
2	6	2	1	0	0	11
7	3	1	3	4	2	20
1	5	0	1	2	2	11
0	6	3	5	1	1	16
1	0	3	1	1	1	17
2	2	2	0	3	3	12
13	2	1	11	11	9	87

Notched 0.66P + 0.2p-1						
0	6	7	5	5	6	29
3	5	2	7	3	0	20
1	3	1	2	1	3	11
1	4	1	0	0	6	12
2	2	1	2	1	2	10
0	0	0	0	0	0	0
7	20	12	16	10	17	82

Notched 0.66P + 0.2p-2						
1	2	3	2	2	2	12
1	3	3	3	3	2	15
0	0	1	1	2	2	6
2	3	2	0	2	4	13
2	2	1	1	0	2	8
2	2	1	1	0	2	8
8	2	1	8	9	14	62

Notched 0.66P + 0.2p-3						
3	2	3	3	4	1	16
1	1	0	1	1	3	7
5	0	1	1	3	1	11
1	0	2	0	0	1	4
0	0	2	3	3	0	8
0	0	0	0	0	0	0
10	3	8	8	11	6	46

0.66 P +0.3 p (28 days)

Unnotched 0.66P + 0.3p-2						
1	0	1	0	3	8	13
1	0	2	3	1	5	12
0	1	1	0	2	0	4
0	1	3	4	1	2	11
1	4	1	2	1	1	10
3	4	3	1	1	3	15
6	10	11	10	9	19	65

Unnotched 0.66P + 0.3p-3						
0	0	0	1	1	2	4
4	0	2	2	2	1	11
0	2	0	1	0	2	5
2	1	1	2	1	2	9
0	0	4	3	2	1	10
5	3	4	2	1	5	20
11	6	11	11	7	13	59

Unnotched 0.66P + 0.3p-4						
3	1	3	3	2	1	13
1	5	2	1	4	1	14
0	0	0	4	1	1	6
2	1	1	3	6	2	15
3	0	2	3	1	4	13
1	3	0	1	4	0	9
10	10	8	15	18	9	70

Notched 0.66P + 0.3p-1						
0	7	6	1	2	3	19
0	0	2	2	4	1	9
0	1	3	1	2	1	8
3	1	1	1	4	1	11
4	2	4	1	0	5	16
0	0	0	0	0	0	0
7	11	16	6	12	11	63

Notched 0.66P + 0.3p-2						
2	2	5	0	0	0	9
2	5	4	1	2	2	16
5	0	4	2	0	3	14
2	4	0	0	3	3	12
0	5	0	8	2	0	15
0	0	0	0	0	0	0
11	16	13	11	7	8	66

Notched $0.66P + 0.3p-3$						
2	0	1	2	5	0	10
2	4	3	0	0	1	10
0	0	2	2	6	2	12
3	0	3	5	2	3	16
0	0	1	4	4	1	10
0	0	0	0	0	0	0
7	4	10	13	17	7	58

Notched $0.66P + 0.3p-4$						
0	3	2	1	1	1	8
3	0	4	4	0	4	15
2	1	3	2	1	3	12
1	1	2	0	5	2	11
1	0	2	1	2	1	7
0	0	0	0	0	0	0
7	5	13	8	9	11	53

0.88 P + 0.2 p (28 days)

Unnotched $0.88P+0.2p-1$						
3	2	5	6	1	4	21
2	10	3	3	1	2	21
1	4	4	2	3	1	15
1	3	1	3	8	1	17
1	2	2	4	4	1	14
5	3	3	5	1	5	22
13	24	18	23	18	14	110

Unnotched $0.88P+0.2p-2$						
1	3	0	0	0	0	4
1	2	4	1	2	17	27
0	7	0	1	5	3	16
1	2	2	1	2	2	10
2	5	2	0	2	2	13
4	5	4	5	5	3	26
9	24	12	8	16	27	96

Unnotched $0.88P+0.2p-3$						
2	7	1	7	2	0	19
7	6	3	1	1	1	19
4	3	4	1	3	4	19
3	4	2	2	0	2	13
1	2	0	2	2	4	11
1	1	3	4	3	3	15
18	23	13	17	11	14	96

Unnotched $0.88P+0.2p-4$						
3	2	4	1	0	2	12
6	5	0	1	1	6	19
3	0	3	1	2	7	16
2	0	1	5	0	4	12
1	2	0	3	1	3	10
5	0	1	4	5	5	20
20	9	9	15	9	27	89

Notched 0.88P+0.2p-1						
3	0	3	2	7	0	15
2	1	1	0	5	2	11
1	1	0	2	2	6	12
5	3	1	2	1	4	16
1	2	5	5	6	2	21
0	0	0	0	0	0	0
12	7	10	11	21	14	75

Notched 0.88P+0.2p-2						
3	9	0	4	3	3	22
6	1	5	3	0	0	15
3	4	9	1	4	2	23
0	3	3	2	1	1	10
2	0	3	4	1	1	11
0	0	0	0	0	0	0
14	17	20	14	9	7	81

Notched 0.88P+0.2p-3						
2	1	2	2	3	3	13
1	0	4	3	3	0	11
2	0	0	0	1	2	5
1	4	4	4	0	0	13
2	2	15	2	3	1	25
0	0	0	0	0	0	0
8	7	25	11	10	6	67

0.88 P +0.3 p (28 days)

Unnotched 0.88P+0.3p-1						
1	3	3	1	0	5	13
3	3	1	2	0	3	12
1	6	3	1	2	2	15
4	3	3	1	1	0	12
8	2	3	1	1	4	19
3	1	1	4	0	2	11
20	18	14	10	4	16	82

Unnotched 0.88P+0.3p-2						
0	5	2	1	4	1	13
2	3	4	3	6	3	21
7	6	4	1	1	0	19
5	6	7	1	2	1	22
0	10	4	2	3	0	19
4	3	2	5	6	3	23
18	33	23	13	22	8	117

Unnotched 0.88P+0.3p-3						
2	3	1	6	6	3	21
5	2	1	2	4	0	14
1	3	3	1	4	0	12
3	3	3	0	1	2	12
2	2	3	4	2	2	15
9	5	5	4	2	1	26
22	18	16	17	19	8	100

Unnotched 0.88P+0.3p-4						
9	3	6	9	1	3	31
7	3	2	1	3	5	21
4	4	3	1	8	3	23
1	1	3	4	3	4	16
3	5	2	2	1	2	15
0	0	0	5	3	4	12
24	16	16	22	19	21	118

Notched 0.88P+0.3p-1						
1	2	0	1	2	8	14
3	2	2	4	3	4	18
1	1	0	3	0	4	9
1	0	7	3	1	2	14
2	3	3	2	3	2	15
0	0	0	0	0	0	0
8	8	12	13	9	20	70

Notched 0.88P+0.3p-2						
2	0	6	2	0	3	13
3	0	0	0	2	0	5
5	0	2	1	2	4	14
5	2	1	0	2	4	14
5	2	1	1	1	11	21
0	0	0	0	0	0	0
20	4	10	4	7	22	67

Notched 0.88P+0.3p-3						
3	3	1	8	2	3	20
3	1	3	8	1	2	18
4	2	0	2	3	8	19
4	2	5	2	2	2	17
2	0	2	0	7	7	18
0	0	0	0	0	0	0
16	8	11	20	15	22	92

Notched 0.88P+0.3p-4						
4	5	6	1	9	6	31
3	3	2	3	2	2	15
7	3	3	2	0	2	17
3	2	4	2	7	3	21
1	3	2	1	1	1	9
0	0	0	0	0	0	0
18	16	17	9	19	14	93

0.44 P + 0.2 p (3 days)

Unnotched 0.44P + 0.2p-1						
1	2	0	2	0	3	8
3	0	1	3	0	1	8
0	0	0	0	0	1	1
1	2	4	2	1	6	16
0	0	2	0	2	2	6
0	2	3	0	2	2	9
5	6	10	7	5	15	48
Unnotched 0.44P + 0.2p-3						
1	0	1	0	2	4	8
3	4	1	1	5	7	21
0	1	0	0	2	3	6
0	1	0	0	2	3	6
0	0	1	0	0	1	2
0	0	0	4	1	3	8
4	6	3	5	12	21	51

Unnotched 0.44P + 0.2p-2						
2	1	1	3	0	2	9
2	1	1	0	0	1	5
1	0	1	0	0	1	3
2	0	1	0	0	0	3
3	0	0	1	0	1	5
3	0	1	4	1	1	10
13	2	5	8	1	6	35

Notched 0.44P + 0.2p-1						
0	2	4	2	0	1	9
0	1	3	0	0	1	5
0	0	2	1	0	2	5
0	0	1	0	1	1	3
0	1	6	3	1	0	11
0	0	0	0	0	0	0
0	4	16	6	2	5	33

Notched 0.44P + 0.2p-2						
0	0	0	1	1	1	3
1	0	3	3	0	0	7
0	2	4	0	0	0	6
1	1	3	1	1	2	9
1	0	1	1	1	0	4
0	0	0	0	0	0	0
3	3	11	6	3	3	29

Notched 0.44P + 0.2p-3						
0	6	1	1	2	0	10
3	1	0	3	1	1	9
1	0	0	1	2	1	5
1	1	2	0	5	2	11
2	2	4	4	1	1	14
0	0	0	0	0	0	0
7	10	7	9	11	5	49

0.66 P (3 days)

Unnotched 0.66P -1						
3	4	1	3	0	2	13
2	0	1	0	1	1	5
2	1	1	1	0	8	13
0	0	0	0	0	5	5
3	1	3	1	0	9	17
0	0	4	6	0	4	14
10	6	10	11	1	29	67

Unnotched 0.66P -2						
6	0	3	2	2	0	13
0	0	1	0	3	2	6
2	0	1	0	3	2	8
2	1	2	0	1	0	6
6	0	1	1	0	1	9
1	2	0	3	3	3	12
17	3	8	6	12	8	54

Unnotched 0.66P -3						
4	0	4	1	0	1	10
5	2	2	4	3	2	18
3	0	1	0	0	0	4
2	0	1	8	2	0	13
3	1	1	0	4	1	10
2	0	3	1	4	6	16
19	3	12	14	13	10	71

Notched 0.66P -1						
0	1	3	1	3	3	11
0	2	0	0	2	0	4
0	1	0	3	0	1	5
0	1	0	0	0	2	3
3	2	0	0	3	1	9
0	0	0	0	0	0	0
3	7	3	4	8	7	32
Notched 0.66P -3						
1	0	3	2	2	0	8
0	0	0	1	4	2	7
0	1	4	0	1	1	7
3	0	0	0	1	0	4
1	1	1	2	5	1	11
0	0	0	0	0	0	0
5	2	8	5	13	4	37

Notched 0.66P -2						
3	1	1	5	1	1	12
0	3	0	0	3	2	8
2	0	0	2	0	2	6
0	1	0	0	1	2	4
2	2	0	1	0	4	9
0	0	0	0	0	0	0
7	7	1	8	5	11	39

0.44 P +0.2 p (7 days)

Unnotched 0.44P + 0.2p-1						
1	2	0	2	0	3	8
3	0	1	3	0	1	8
0	0	0	0	0	1	1
1	2	4	2	1	6	16
0	0	2	0	2	2	6
0	2	3	0	2	2	9
5	6	10	7	5	15	48

Unnotched 0.44P + 0.2p-2						
1	0	5	1	2	1	10
3	4	1	1	3	0	12
0	1	2	2	1	2	8
0	0	0	2	1	1	4
0	3	0	1	1	0	5
1	1	5	1	1	0	9
5	9	13	8	9	4	48

Unnotched $0.44P + 0.2p-3$						
1	0	1	0	2	4	8
3	4	1	1	5	7	21
0	1	0	0	2	3	6
0	1	0	0	2	3	6
0	0	1	0	0	1	2
0	0	0	4	1	3	8
4	6	3	5	12	21	51
Notched $0.44P + 0.2p-1$						
4	1	4	1	2	0	12
1	0	0	0	1	0	2
1	0	0	0	3	0	4
4	2	1	0	0	0	7
1	4	0	3	0	0	8
0	0	0	0	0	0	0
11	7	5	4	6	0	33

Notched $0.44P + 0.2p-2$						
1	1	0	0	4	0	6
0	1	0	0	0	2	3
0	4	0	0	2	4	10
0	0	1	1	3	7	12
0	0	0	3	1	0	4
0	0	0	0	0	0	0
1	6	1	4	10	13	35

Notched $0.44P + 0.2p-3$						
3	1	4	3	0	0	11
0	0	2	3	3	1	9
1	0	4	0	0	0	5
0	2	1	2	0	3	8
0	1	0	1	1	1	4
0	0	0	0	0	0	0
4	4	11	9	4	5	37

0.66 P (7 days)

Unnotched 0.66P -1						
2	2	0	5	5	2	16
1	1	2	5	1	3	13
0	0	2	3	2	1	8
3	0	0	0	2	2	7
0	0	1	2	1	1	5
1	0	0	3	2	3	9
7	3	5	18	13	12	58
Unnotched 0.66P -3						
0	1	1	0	2	1	5
0	0	3	0	1	6	10
3	2	1	3	3	2	14
2	2	1	0	3	0	8
3	0	0	0	0	3	6
1	1	3	0	0	0	5
9	6	9	3	9	12	48
Notched 0.66P -1						
2	2	3	0	5	2	14
1	0	2	2	0	2	7
3	2	1	1	1	0	8
0	4	2	0	0	0	6
8	0	2	4	2	1	17
0	0	0	0	0	0	0
14	8	10	7	8	5	52
Notched 0.66P -3						
3	2	3	2	3	8	21
0	0	0	0	0	4	4
2	0	0	0	0	2	4
2	0	0	0	3	2	7
3	2	2	2	2	3	14
0	0	0	0	0	0	0
10	4	5	4	8	19	50

Unnotched 0.66P -2						
2	1	2	0	2	1	8
1	0	2	1	1	2	7
2	1	0	0	1	0	4
0	1	1	1	1	1	5
1	0	0	1	0	0	2
1	2	2	0	0	3	8
7	5	7	3	5	7	34

Notched 0.66P -2						
1	3	2	0	0	4	10
3	6	2	3	1	0	15
5	5	0	1	2	1	14
0	3	2	1	0	1	7
1	3	2	1	1	0	8
0	0	0	0	0	0	0
10	20	8	6	4	6	54

